THE UNIVERSITY OF CHICAGO

CELL FATE SPECIFICATION, SIGNALING, AND MORPHOGENESIS IN THE ZEBRAFISH GASTRULA

A DISSERTATION SUBMITTED TO
THE FACULTY OF THE DIVISION OF THE BIOLOGICAL SCIENCES
AND THE PRITZKER SCHOOL OF MEDICINE
IN CANDIDACY FOR THE DEGREE OF
DOCTOR OF PHILOSOPHY

COMMITTEE ON DEVELOPMENT, REGENERATION, AND STEM CELL BIOLOGY

BY
ELAINE ELIZABETH KUSHKOWSKI

CHICAGO, ILLINOIS
DECEMBER 2026

© 2026 by Elaine Elizabeth Kushkowski

All Rights Reserved

To my parents, for teaching me to be curious and persistent.

I've lived a life that's full

I traveled each and every highway

And more, much more than this

I did it my way

...

To think I did all that

And may I say not in a shy way

Oh no, oh no, not me

I did it my way

Frank Sinatra, "My Way"

CONTENTS

LIST OF FIGURES viii

ACKNOWLEDGMENTS ix

ABSTRACT xi

1 INTRODUCTION 1
1.1 Preface 1
1.2 Development of the vertebrate body plan 1
1.3 Zebrafish as a model of vertebrate development 2
1.4 Developmental stages between fertilization and pharyngula 4
1.4.1 Fertilization to gastrula 4
1.4.2 Gastrula to neurula 5
1.4.3 Neurula to pharyngula 6
1.5 Signaling generates positional information in the gastrula 7
1.5.1 Maternally deposited factors drive initial symmetry breaking in the early embryo 7
1.5.2 Zygotic genes establish and enforce gradients 8
1.5.3 Organizer genes and BMP establish the dorsal-ventral axis 9
1.5.4 Nodals establish the animal-vegetal axis 9
1.5.5 The whole gastrula margin organizes the AP axis 11
1.5.6 Wnt and FGF modulate DV and AP axis formation 12
1.6 Fate maps reveal the spatial organization of the early embryo 13
1.7 Overview of the dissertation 14

2 FATE MAP OF THE ZEBRAFISH VENTRAL GASTRULA 16
2.1 Preface 16
2.2 Abstract 16
2.3 Introduction 17
2.4 Results 22
2.4.1 A region-based strategy for fate mapping the zebrafish ventral gastrula 22
2.4.2 Overall organization of fates within the ventral gastrula 24
2.4.3 The ventral gastrula fate map 30
2.4.4 Organization within the neural crest progenitor domain 33
2.4.5 Cranial neural crest and cranial placodes arise from a shared progenitor domain 36
2.4.6 Cranial neural crest and neural tube arise from partially overlapping progenitor domains 37
2.4.7 Multiple cell types arise with neural crest at all axial levels 37
2.4.8 Differential AP distribution of major cell fates 42
2.5 Discussion 45

2.5.1 The ventral fate map reveals progenitor domain organization 45
2.5.2 Orderly arrangement within the neural crest progenitor domain . . . 47
2.5.3 Developmental relationships between neural crest and neural tube . . 48
2.5.4 Cranial cell fate relationships across vertebrates 50
2.5.5 Signatures of morphogenesis within the fate map 51
2.5.6 Implications of the ventral gastrula fate map 53
2.6 Supplemental Figures 54

3 SIGNALING AND MORPHOGENESIS DURING GASTRULATION 65
3.1 Abstract 65
3.2 Contributions 66
3.3 Introduction 66
3.4 Results 68
3.4.1 Methodological considerations for interpreting the effects of SU5402 treatment 68
3.4.2 Defining experimental conditions for FGF signaling inhibition in the gastrula 69
3.4.3 FGF signaling inhibition at the onset of gastrulation causes abnormal morphology at 30 hpf 72
3.4.4 Loss of FGF signaling causes defects in neurulation and somitogenesis at 24 hpf 73
3.4.5 Wildtype ventral gastrula morphogenesis and formation of posterior structures 80
3.4.6 Loss of FGF signaling accelerates formation of the evacuation zone and disrupts posterior development 82
3.4.7 FGF signaling controls ventral/posterior morphogenesis and tail formation 86
3.4.8 FGF inhibition shifts axial marker expression 89
3.4.9 Spatial dynamics of downstream FGF signaling marker *etv4* and early neural patterning genes 92
3.5 Discussion 98
3.5.1 FGF signaling controls the rate of epiboly and response to positional cues 98
3.5.2 Early FGF signaling influences formation of the neural plate border . 99
3.5.3 Temporal effects of SU5402 treatment on FGF signaling centers . . . 100
3.5.4 Posterior development phenotypes and self-organization within the vegetal extension 101

4 DISCUSSION AND FUTURE DIRECTIONS 103
4.1 Development of the fate map methodology 103
4.2 Future Directions 106
4.2.1 Transplants into the ventral gastrula 106
4.2.2 Lineage relationships across the neural crest progenitor domain . . . 107

4.2.3 Morphogenesis of the cranial neural crest progenitor domain and neural plate border . . . 108
4.2.4 Morphogenesis of the posterior body . . . 109
4.2.5 Developmental disorders of the neural crest . . . 110
4.2.6 Uncovering the earliest influences on cell type specification . . . 110

5 MATERIALS AND METHODS . . . 112
5.1 Zebrafish husbandry . . . 112
5.2 Fate Map Methods . . . 112
5.2.1 Overview of fate mapping strategy . . . 112
5.2.2 Agarose embryo molds . . . 113
5.2.3 mKaede microinjection and embryo screening . . . 114
5.2.4 Photoconversion of regions in gastrula-stage specimens . . . 114
5.2.5 Measurement of photoconverted region positions at 6 hpf . . . 115
5.2.6 Sample fixation and immunohistochemistry . . . 116
5.2.7 Imaging of fixed 30 hpf specimens . . . 116
5.2.8 Identification of cell fates and positions at 30 hpf . . . 117
5.2.9 Analysis and data visualization . . . 118
5.3 FGF Signaling Methods . . . 119
5.3.1 Pharmacological manipulation . . . 119
5.3.2 Timelapse microscopy . . . 119
5.3.3 Hybridization chain reaction . . . 120
5.3.4 Immunolabeling . . . 120

BIBLIOGRAPHY . . . 121

LIST OF FIGURES

1.1 Rapid morphogenesis during early embryonic development. 3

2.1 Embryonic body plan and fate map schematics. 18
2.2 Strategy to generate a new ventral gastrula fate map 23
2.3 Photoconversions and cell type identification 25
2.4 Cell type identification criteria 27
2.5 Axial coverage and overview of the ventral fate map 28
2.6 Cell type-specific ventral gastrula fate maps 31
2.7 Neural crest progenitor domain relationships 34
2.8 Cell fate data from all regions that produced cranial neural crest 38
2.9 Cell fate data from all regions that produced post-cranial neural crest 41
2.10 AP position and axial spread of cell fates 43
2.11 Summary of the ventral fate map 46
2.12 Spreadplots for all 86 specimens 54
2.13 Abundance of major cell types 64

3.1 Gross morphological consequences of inhibiting FGF signaling at gastrulation onset 71
3.2 Loss of FGF signaling at the onset of gastrulation affects axial patterning and cell type specification 74
3.3 DAPI single channel images from Fig. 3.2 76
3.4 Sox10 single channel images from Fig. 3.2 78
3.5 Myosin heavy chain single channel images from Fig. 3.2 79
3.6 Gastrulation and tailbud formation in untreated embryos 81
3.7 Disruptions in development caused by inhibition of FGF signaling at gastrulation onset 83
3.8 Timelapse analysis of gastrulation and posterior morphogenesis in SU5402-treated embryos 87
3.9 Expression of axial markers *otx2*, *hoxb1b*, and *eve1* in SU5402-treated embryos . 90
3.10 Wildtype expression of FGF signaling activity reporter *etv4* and neural plate border markers *foxd3* and *ap2a*. 93
3.11 Expression of *etv4*, *foxd3*, and *ap2a* in FGF signaling-deficient specimens 95

ACKNOWLEDGMENTS

I would like to thank Victoria Prince for her mentorship and support over many years. Vicky, thank you for the opportunity to work on a project that would not have been possible anywhere else. It has been a privilege to ask and answer fundamental developmental questions under your guidance. Our fate map paper writing sessions were a highlight of our work together. Your training will be invaluable for my ongoing development as a developmental biologist and educator. To my thesis committee - Sally Horne-Badovinac, Robert Ho, Ellie Heckscher, and Urs Schmidt-Ott - thank you for your insights, questions, challenges, and mentorship. I appreciate how you helped to develop my project, encouraged me to keep asking questions, and pushed me to think about the bigger picture.

To my scientific collaborators, I have enjoyed your company and appreciated your support, which improved many aspects of this project. I am so thankful for your contributions to this work, especially Vish for helping me think about all the structures in an organism, Adam for showing me how to do photoconversions and listening to many complaints about spreadplots, and Patrick for his collaboration on the FGF project. I am grateful to my Prince Lab colleagues for their company and conversations. Ana and Manny helped me through in the beginning, and learning cell transplantation with Manny inspired what eventually became the fate map project. Vish and I worked together through the pandemic, and I appreciate our fascinating evo-devo conversations. Michael and Sarah, thank you for bringing new energy to the lab. My time in the lab was greatly enhanced by working with the many wonderful undergraduates, including Ruby, Clare, Lindsey, Noel, Theresa, Alex, Rachel, and Caroline. I would like to thank Noor, Vanity, Adam, Zach, and Ethan for supporting the zebrafish that made this work possible. A special thanks to Ethan, for curiosity, perceptiveness, and encouragement in the final stretch of my PhD.

I am thankful for the many opportunities I had to engage in teaching and science at the University of Chicago and beyond. The Chicago Center for Teaching and Learning provided

a second home for me throughout graduate school. The conversations I had with Teaching Fellows keep me hopeful about the future of higher education. To my students, thank you for asking thoughtful questions and inspiring me to look for deeper answers. My scientific and professional thinking was shaped through an alphabet soup of conferences, including SDB, MWSBD, MWZFC, NWSDB, GRC, SCDB, SICB, and POD. Many visits to the Marine Biological Laboratory, for both teaching and research, inspired and invigorated my curiosity as an embryologist. I am especially grateful for the UChicago Microscopy course, where I learned the patience necessary to collect the data for the final fate map project.

Many, many thanks to my family and friends for their generous support and patience. Rachel, Sarah, Guananí, and Anya, our visits and trips kept me grounded. I appreciate that you make me feel seen and loved, and are only a phone call away. Shreya, I cannot imagine a better person to have lived with through the pandemic. Thank you for the goofy times and even better coffee. Tristan, our weekly teaching-turned-beer meetings have been a constant source of joy, comfort, and support as we navigated the final years of graduate school and beyond. A special thanks to Puddles, my canine compatriot, for always being excited when I get home and snoring gently during Zoom calls. I am glad you picked me and that we have gotten to be pals for many years.

Finally, I could not have done this without my parents. Mom and Dad, I love you and I am incredibly grateful for three decades of your love and encouragement. The funny photos, long-distance hugs, country house visits, and sleepy science phone calls kept me going and got me to where I am today. Thank you for believing in me.

ABSTRACT

During early embryonic development, all vertebrates share common features at the pharyngula stage. However, patterning the pharyngula body plan begins much earlier in development. Gastrulation is a critical period for establishing the organization of essential tissues and initiating key processes that generate the vertebrate body plan. Using the zebrafish as a model of vertebrate development, I have investigated aspects of cell fate specification, signaling and morphogenesis between gastrula and pharyngula stages. In this thesis, I present a fate map of the ventral gastrula that describes the early embryonic organization of 15 cell fates in the pharyngula, including the neural crest, cranial placodes, and posterior somites and spinal cord. The fate map reveals the relationship between early position in the gastrula and later contribution to cell fates along the anteroposterior axis. I demonstrate that the cranial neural crest and placodes arise from a ventral domain that is largely separate from the neural domain, while trunk neural crest and neural tissues always arise together. I have also investigated the role of FGF signaling in patterning the pharyngula body plan. I show that disruption of FGF signaling at the onset of gastrulation results in axial patterning defects and changes in morphogenesis that disrupt specification of ventral gastrula fates. In the context of newly defined organization and patterning of progenitor domains within the ventral gastrula, my findings provide insight into how spatial organization and patterning during gastrulation generate complex tissues and structures within the pharyngula body plan.

CHAPTER 1

INTRODUCTION

1.1 Preface

This thesis focuses on three key aspects of early embryonic organization that occur between the onset of gastrulation and the establishment of the pharyngula stage body plan. Cell fate specification is the process by which cellular identity changes over time to take on the characteristics of a distinct cell fate. Signaling is the molecular process by which cells produce, recognize, and respond to environmental cues (including morphogens) by regulating gene expression, cell morphology, and molecular identity. Morphogenesis, meaning the origin of form, is the process by which an embryo changes shape to produce all of the tissues and structures within the body plan. Together, these developmental processes act in concert within the early embryo to produce complexity within the body plan of a developing organism. In this chapter, I begin with an overview of vertebrate body plan development and the zebrafish as a model for studying early embryogenesis. Next, I introduce the morphogenetic processes that occur between gastrulation and pharyngula stages. I summarize our current understanding of how signaling establishes positional information prior to gastrulation, setting up the molecular context for the developmental processes I investigate in the dissertation. Finally, I introduce fate mapping and the key cell types in vertebrate development that feature prominently in this dissertation, highlighting gaps in knowledge about their developmental origins.

1.2 Development of the vertebrate body plan

Multicellular organisms take a variety of developmental paths to generate the diversity of body plans across the tree of life. There are many aspects of development that vary between species, from the size of the early embryo to the timescale within which development oc-

curs. During early embryogenesis in vertebrates, embryos develop a variety of morphologies ranging from spheres to cups to flat discs, with or without a yolk. Shared developmental processes guide disparate vertebrate embryos to converge toward the fundamental vertebrate body plan at the phylotypic or pharyngula stage, when embryos across the phylum share a variety of features (Levin et al. 2016). At this stage, the vertebrate embryo has a defined anterior to posterior axis (head to tail), and dorsal to ventral axis (back to belly). The body plan includes a cranium with expanded neural structures, rudiments of the cranial sensory systems, and distinct pharyngeal arches, from which the term 'pharyngula' derives. Limb buds are present, with the forelimb buds typically lying posterior to the pharyngeal arches, near the transition between head and trunk. The trunk and tail contain a dorsal neural tube and underlying notochord (a rod of axial mesoderm), flanked by muscle blocks known as somites, but the most posterior aspect of the embryo has not yet formed completely at this stage. All vertebrate embryos share the conserved morphological features of the pharyngula body plan at some point during normal development. After the phylotypic stage, vertebrate development diverges again to elaborate on a wide array of features, including crania and appendages, and ultimately produce diverse adult forms. However, the developmental processes that pattern the vertebrate body plan begin much earlier, during a transformational developmental window called gastrulation.

1.3 Zebrafish as a model of vertebrate development

Rapid early development, which occurs external to the mother, makes the zebrafish an ideal model for studying vertebrate development. Under standard temperature conditions, the zebrafish embryo undergoes rapid cell divisions, begins to form the germ layers at 6 hours post fertilization (hpf), completes gastrulation around 10 hpf, and by 30 hpf the pharyngula body plan is established (Figure 1.1). Young zebrafish hatch out of their protective chorion at 2-3 days post fertilization (dpf) and continue developing into free-swimming, free-feeding

larvae by 5 dpf (Kimmel, Ballard, et al. 1995). Large clutch size allows for higher-throughput studies than are possible in many other vertebrate model systems.

The zebrafish offers an array of benefits for studying early developmental processes, especially between gastrula and pharyngula stages. Zebrafish embryos are easily accessible for observation and manipulation of the earliest events in vertebrate embryogenesis. The embryos are optically clear, permitting microscopic observation of molecular, cellular, and morphogenetic processes without disrupting embryonic development. Zebrafish are amenable to embryological, pharmacological, and genetic manipulation, and can be observed using a variety of microscopy approaches. Since zebrafish was established as a developmental model system over 40 years ago, a wide variety of experimental approaches have been developed that allow for interrogation of early embryonic processes on molecular to organismal scales.

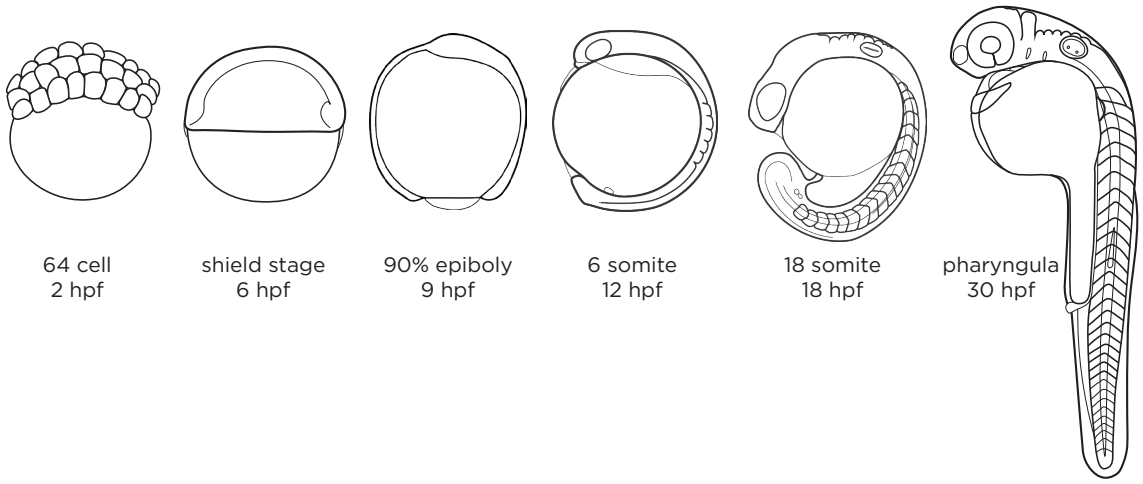

Figure 1.1: **Rapid morphogenesis during early embryonic development.** Schematics of a zebrafish embryo at 64 cell, shield, 90% epiboly, 6 somite, 18 somite, and pharyngula stages. The embryo undergoes dramatic shape change as the germ layers, body axes, and rudimentary organs form during early development.

1.4 Developmental stages between fertilization and pharyngula

1.4.1 Fertilization to gastrula

Shortly after fertilization, the first cell rises above the yolk and prepares for the first cell division. Cells divide synchronously, producing a collection of blastomeres on top of the yolk. The maternal to zygotic transition occurs around 3 hpf, when the zygote switches from translating maternally-deposited RNA to transcription and translation of the zygotic genome. The early cell divisions are synchronous, followed by a period of asynchronous division and mixing of the blastoderm. At 4 hpf, the blastoderm begins to thin and descend vegetally over the yolk in a process called epiboly (Warga and Kimmel 1990).

At blastula stage, position in the embryo can be correlated with a likely germ layer contribution in later development. As in many other organisms, cell fates within the zebrafish develop from indeterminate lineages, such that later cell fates are correlated with position and signaling environments at particular stages in development (Kimmel and Warga 1987). This is in contrast with organisms that display a determinate mode of development, such as *C. elegans*, in which the progeny and fates of each cell can be traced back to specific cell divisions in early development (Sulston et al. 1983). In zebrafish, cells closer to the margin are more likely to give rise to mesodermal fates later in development, while cells closer to the animal pole are more likely to give rise to ectodermal, including neural, fates. This allows for blastula-to-blastula transplantation of cells into broad mesodermal or ectodermal domains. However, without a molecular or morphological marker for the future dorsal side, it is not possible to target more specific cell fates in the zebrafish blastula.

By 5.3 hpf, a germ ring is visible at the margin, where some cells begin to internalize under the blastoderm. As epiboly proceeds, a thickening of cells on the dorsal side of the embryo becomes visible around 6 hpf (Kimmel, Ballard, et al. 1995). This is the embryonic shield, a structure equivalent to the organizer in other species. At this stage, major signaling

pathways interact with one another to provide positional information across the blastoderm, patterning the embryo prior to the dramatic rearrangement that follows during gastrulation. In the early gastrula, the shield is the first morphological feature to define the early embryonic axes, though the molecular basis for axis specification was initiated through maternal factors at fertilization, a topic I explore below. In the gastrula, cell position relative to the shield reliably correlates with later cell fates due to molecular patterning of the blastoderm. However, transplantation experiments show that with the exception of the outer enveloping layer cells (EVL), and the marginally localized endoderm progenitors, cells are not yet committed to specific fates at this time point, as transplanted cells assume fates appropriate to their new position within the gastrula (Ho and Kimmel 1993).

1.4.2 Gastrula to neurula

Gastrulation is a fundamental developmental process that organizes cells into germ layers and rearranges the embryo along a primary anteroposterior body axis. Between 6 hpf and 10 hpf, dramatic transformation occurs throughout the embryo that generates the basic axial organization of the pharyngula body plan. Between 6 hpf and 8 hpf, the blastoderm moves vegetally and mesendoderm begins to internalize around the margin, forming the ectodermal epiblast and mesendodermal hypoblast. Differential cell movements of internalization, epiboly, convergence and extension drive elongation of the primary body axis. By 8 hpf, cells on the ventral side of the embryo move rapidly toward the animal, dorsal, or marginal domains, leaving behind an area of reduced cell density known as the evacuation zone. During formation of the evacuation zone, cells that move toward the animal pole will generate the cranium, while cells that converge toward the dorsal midline or undergo epiboly toward the margin will generate more posterior structures. Gastrulation movements distribute cells from the ventral side of the gastrula along the length of the body, contributing to formation of both the cranium and posterior body in zebrafish.

Specific forms of gastrulation vary widely between species, but the general mechanisms and outcomes of this developmental process are broadly conserved and form the basis for later development of unique morphologies across animals. Embryo morphology has significant consequences for the types of cell movement and patterning events that occur during gastrulation. Species that gastrulate as flat embryos (chick, human), cups (mouse), or spheres (*Xenopus*), have organizers that move during gastrulation to induce germ layer specification (Lila Solnica-Krezel and Sepich 2012). Zebrafish gastrulate around a spherical yolk, posing a spatial challenge for organizing tissues further away from the dorsal organizer. It has been shown that the entire zebrafish margin acts as an organizer for body axis formation due to signaling activity from this domain (Fauny, B. Thisse, and C. Thisse 2009). Marginal domains at increasing distances from the shield are capable of inducing increasingly posterior tissues, further patterning the axial organization of the embryo at the onset of gastrulation (B. Thisse and C. Thisse 2015). In general, the ectoderm arises furthest from the margin and is patterned by competing signals across the dorsoventral and animal-marginal axes.

1.4.3 Neurula to pharyngula

The neurula stage is defined by rapid convergence of neural tissue in the newly formed anterior aspect of the embryo. During neurulation, the ectoderm is further divided into neural ectoderm, which forms the brain and spinal cord, and non-neural ectoderm, which is further subdivided into epidermis and neural crest, as well as placodes in the cranial region. The neural plate border forms at the interface of these major ectodermal domains in response to integrated Wnt, BMP, and FGF signals (Garnett, Square, and Medeiros 2012). The neural plate border becomes genetically encoded through activation of a highly conserved gene regulatory network (Martik, Gandhi, et al. 2019; Martik and Bronner 2021; Rocha, Beiriger, et al. 2020). In the developing cranium, the neural plate border gives rise to both neural crest and the cranial placodes, two tissues of significant importance for

vertebrate evolution and development, a topic that has been reviewed extensively and is discussed below (Schlosser 2014; Thawani and Groves 2020; Stundl and Bronner 2025).

During segmentation and tail extension, organization and patterning of the neural tube occurs in a progressive fashion from anterior to posterior. During this period, development continues along the AP axis as the neural plate condenses to form the neural keel. Neural crest specification continues in tandem with neural development. The paraxial mesoderm condenses and segregates into somites adjacent to the notochord. The tailbud extends away from the yolk due to progressive expansion of the notochord and addition of neural and mesodermal structures from progenitor pool in the tailbud (Kanki and Ho 1997; Wymeersch et al. 2016; McLaren and B. J. Steventon 2021; Sambasivan and Benjamin Steventon 2021).

1.5 Signaling generates positional information in the gastrula

1.5.1 Maternally deposited factors drive initial symmetry breaking in the early embryo

Symmetry breaking sets up formation of the primary body axis during early embryogenesis. At a molecular level, this process is initiated by spatially localized maternal effector molecules in the zygote and early blastula. Maternally deposited transcripts establish the animal/vegetal axis in the oocyte, regulate the Wnt/β-catenin pathway, and ultimately allow β-catenin to enter the nuclei of future dorsal cells. This process prefigures establishment of the dorsal organizer (Schneider et al. 1996). Wnt8a is a particularly strong candidate for dorsal determination in zebrafish because it induces expression of known dorsal marker Chordin (Lu, C. Thisse, and B. Thisse 2011). Mutation or loss of Wnt8a results in progressive expansion of axial mesoderm and posterior neural markers at the expense of paraxial mesoderm around the embryo margin, providing additional evidence that Wnt8a promotes dorsal determination (Hino et al. 2018). Simultaneously, expression of maternally deposited

frizzled related protein (Frzb) and secreted frizzled-related protein 1a (Sfrp1a) block Wnts and restrict nuclear localization of β-catenin to the dorsal organizer (Lu, C. Thisse, and B. Thisse 2011). A recently identified symmetry breaking factor that functions independent of Wnt ligand/receptor binding is Huluwa, a membrane-bound protein that promotes degradation of Axin (a protein that targets β-catenin for degradation) and therefore allows β-catenin to enter the nucleus (Yan et al. 2018). Together, maternal control of Wnt/β-catenin signaling results in stabilization of nuclear localized β-catenin in a small region of the blastula, which drives differential expression of zygotic genes and initiates the formation of the dorsal organizer.

1.5.2 Zygotic genes establish and enforce gradients

Following the maternal-to-zygotic transition, many newly expressed zygotic genes participate in specifying and refining the dorso-ventral axis. One of the earliest expressed genes is *nieuwkoid/dharma/bozozok*, which is expressed in the dorsal organizer and represses expression of *bmp2b* on the ventral side (Koos and Ho 1998; Koos and Ho 1999; Yamanaka et al. 1998). Removal of the dorsal shield results in a similar phenotype to loss of *bozozok* (Saude et al. 2000). The ventral homeobox gene (*vox*) is a direct target of BMP signaling, while ortholog VENT homeobox (*vent*) is indirectly controlled by BMP. Together, these genes act as ventralizing factors that are expressed broadly in the embryo at sphere stage (everywhere but the presumptive dorsal organizer) and become progressively reduced to more ventral regions of the embryo between shield stage and somite formation (Pshennikova, Tereshina, and Voronina 2017). Mutually antagonistic interactions between ventral *vox/vent* and dorsal *bozozok* result in opposing BMP and Wnt gradients in the gastrulating embryo (Melby, Beach, et al. 2000). Goosecoid is also an early marker of the prospective dorsal shield that represses ventral fate signals (BMPs and Vox/Vent) and is itself repressed by Vox/Vent (Langdon and Mullins 2011; Stachel, Grunwald, and P. Z. Myers 1993). Formation of the shield, along

with the unique molecular identity of this dorsal structure, sets the embryo up to pattern the primary body axis during gastrulation.

1.5.3 Organizer genes and BMP establish the dorsal-ventral axis

By 6 hpf, the dorsal organizer of the zebrafish embryo is visible as the embryonic shield, a thickening of cells at the dorsal margin of the embryo. As previously outlined, the shield is a source of factors that interact with other signaling molecules (often through mutual repression) to generate overlapping signaling gradients that further cell fate specification and direct cell movements during gastrulation. Transplantation of superficial or deep shield tissues shows that each gives rise to different derivatives, suggesting that their functions are already segregated by the time the morphological shield appears (Saude et al. 2000). Intriguingly, embryonic development proceeds normally in many embryos with ablated morphological shields, indicating that the presence of just a few cells expressing shield factors (dorsalizing factors) can robustly compensate and direct gastrulation and tissue specification (Saude et al. 2000). Dorsalizing factors (Chordin, Noggin, and Follistatin) act semi-redundantly to antagonize BMP signaling and maintain appropriate signaling gradients for cell specification (Dal-Pra et al. 2006; Langdon and Mullins 2011). Mutually antagonistic interactions between Wnt-initiated dorsal signals (Bozozok, Goosecoid, Chordin, Noggin, Follistatin) and ventral signals (BMPs, Vox/Vent) generate a gradient of high to low BMP signaling from ventral to dorsal, as well as specify expression domains of dorsalizing genes during gastrulation (Melby, Beach, et al. 2000).

1.5.4 Nodals establish the animal-vegetal axis

The margin of the gastrulating embryo acts as a signaling center that patterns the embryo along the animal-vegetal axis. Nodals, including Squint (*sqt*), Cyclops (*cyc*), and Lefty specify mesendoderm and posterior fates, while their inhibition at the animal pole allows

anterior structures to develop. Nodal ligands direct mesodermal and endodermal cell fate decisions, as well as cell sorting and ingression of endodermal cells (Gritsman, Talbot, and Schier 2000; Liu, S. Woo, and Weiner 2018). Expression of Nodals from the gastrula margin drives specification of the mesendoderm in a concentration-dependent manner. Cells closest to the margin receive high levels of these signals, driving endoderm identity, while cells further away from the margin receive lower concentrations of these signals and assume mesoderm and neurectoderm fates.

Expression of *sqt* begins at the dorsal margin in the 3.3 hpf blastula and spreads around the margin of the embryo over the next few hours, where it also activates expression of *cyc* (Dougan et al. 2003). Interestingly, *sqt* and *cyc* expression are activated by β-catenin at the dorsal margin, suggesting that the dorsoventral and animal-vegetal axes are initiated by the same maternally deposited signaling factor. Loss of *sqt* and *cyc* results in aberrant *gsc* expression, with normal *gsc* (a prechordal plate marker) lost in *sqt*-/-;*cyc*+/- individuals and delayed in *sqt*-/-;*cyc*+/+ individuals, which exemplifies the inherent robustness of the axis specification system in vertebrates (Dougan et al. 2003). Further, fate mapping in *sqt* and *cyc* deficient embryos shows that loss of Nodal signaling results in addition of hindbrain and spinal cord derivatives at the expense of mesendoderm derivatives (Dougan et al. 2003). The *one-eyed pinhead (oep)* mutant shows loss of endoderm, mesoderm, and ventral neurectoderm, as well as a posterior shift in AP patterning, due to loss of Crypto, an extracellular protein essential for transduction of Nodal signaling (Gritsman, J. Zhang, et al. 1999; Schier et al. 1997).

Recent studies have clarified some of the mechanisms that underlie Nodal mutant phenotypes through transplantation and mathematical modeling approaches. Nodal signaling from the zebrafish margin has recently become a popular target for modeling of cell signaling dynamics. In a study of Nodal signaling dynamics, pSmad2 was used as a read-out for active Nodal signaling. The timing of Nodal signaling and speed of activation determine the

degree of Smad2 activation and transcription of downstream genes. Delayed transcriptional response to Nodal signaling determined the range of target gene responsiveness to differing levels of Nodal received from the margin (Dubrulle et al. 2015). Another study modeled the Nodal signaling dynamics between cell populations at the dorsal midline and found that duration of contact between Nodal-expressing cells is remembered long after the contacts are lost. Midline cells that were engaged in a positive feedback loop between cell-cell contact and Nodal signaling maintained contact for longer and were more likely to become prechordal plate than cells with shorter contact times, which assumed endoderm fates (Barone et al. 2017). Together, these studies help to explain the complex roles of Nodal signaling in germ layer formation and positional identity, as well as cellular memory of early cell-cell contacts at the onset of gastrulation.

1.5.5 The whole gastrula margin organizes the AP axis

Previous work has shown that the whole gastrula margin acts as an organizer of embryonic patterning, with the ratio of BMPs and Nodals determining the anteroposterior (AP) character of the organized tissue (Agathon, C. Thisse, and B. Thisse 2003; Fauny, B. Thisse, and C. Thisse 2009). In particular, the ventral margin has a high BMP to Nodal ratio (25:1) and acts as the tail organizer (Fauny, B. Thisse, and C. Thisse 2009). Injection of Nodal alone drives formation of an ectopic blastopore, while the ratio and distance between ectopic Nodal and BMP injection sites determine the AP character of the resultant embryonic axis (B. Thisse and C. Thisse 2015). In wildtype embryos, cells all around the margin pattern the primary body axis, with the dorsal shield patterning the most anterior (cranial) tissues and the ventral margin patterning the most posterior (tail) tissues (Agathon, C. Thisse, and B. Thisse 2003; Saude et al. 2000; B. Thisse and C. Thisse 2015). Grafting a dorsal organizer to the animal pole of a host blastula results in an embryo with two sets of anterior tissues, while transplantation of the ventral margin results in embryos with two tails (Saude et al. 2000;

B. Thisse and C. Thisse 2015). Further, loss of dorsal margin tissue just prior to tailbud formation results in loss of axial tissue in the post-anal tail, while lateral tissue structures (e.g. somites) persist and tail formation proceeds relatively normally (Agathon, C. Thisse, and B. Thisse 2003). Further investigation of the contribution of the pre-tailbud gastrula margin to post-anal tail structures is needed to understand the origin of these structures during normal development fully, and especially if or to what degree the gastrula margin contributes to posterior neural crest in the zebrafish.

1.5.6 Wnt and FGF modulate DV and AP axis formation

Maternal Wnt signals act to establish the organizer and induce zygotic FGF expression at the margin. Zygotic FGFs are expressed around the margin and in the dorsal organizer (Langdon and Mullins 2011). As the dorsal organizer matures, Wnt and FGF are excluded from the dorsal margin by organizer-derived antagonists. At the onset of gastrulation, FGF acts as a diffusible morphogen from the margin over a longer range than Wnt (S. R. Yu et al. 2009; Bökel and Brand 2013; Harish et al. 2023). FGF receptors are expressed in slightly different domains in the gastrula, consistent with reports that FGFs can function redundantly at this early stage (Ota et al. 2010). FGF acts directly, as well as indirectly through Chordin, to repress ventral BMP signaling, reinforcing the dorsoventral axis (Fürthauer et al. 2004; Londin, Niemiec, and Sirotkin 2005; Cho, S.-C. Choi, and Han 2013; Pera, Ikeda, and Eivers 2003). In the absence of FGF signaling in the gastrula, neural and tail tissue are depleted (K. Griffin, Patient, and Holder 1995). FGF and Nodal also work together to induce the mesendoderm (K. J. P. Griffin and Kimelman 2003). Injection of a dominant-negative FGF receptor into MZ*oep* mutants (which lack Nodal signaling) leads to a reduction of *otx2*, a neural marker, as well as expansion of the ectoderm marker *gata2*, suggesting that these pathways act together to pattern appropriate allocation of ectodermal cells (Londin, Niemiec, and Sirotkin 2005). Together, FGF, BMP, Wnt, and Nodal pattern the AP axis by acting

as posteriorizing signals that promote posterior development. The breadth of interactions between FGF and other signaling pathways in the gastrula remains to be fully elucidated, as disruptions of one pathway often result in phenotypes that are caused by changes in another. Further investigation of the phenotypes and patterning consequences of FGF and Wnt modulation in the gastrula is needed to uncover the multifaceted functions of these signaling pathways in embryonic patterning.

1.6 Fate maps reveal the spatial organization of the early embryo

For more than a century, fate maps have been providing fundamental insights into the early organization of the body plan across numerous vertebrate and invertebrate species. Fate maps describe the spatial relationship between progenitors at earlier stages of embryogenesis and the differentiated cell fates that arose from their progeny later in development, providing essential information about the early organizing principles of development. In the early 20th century, embryologists characterized developmental processes and generated fate maps in easily accessible embryos. Conklin tracked natural pigmentation variation in ascidian embryos through successive cell divisions (Conklin 1905), while Vogt used vital dye staining of small embryonic regions to generate a comprehensive fate map in amphibians (Vogt 1925; Vogt 1929). Such descriptions of embryonic development allowed researchers to begin to classify cell division patterns, observe cell movements, test hypotheses about cell signaling and lineage relationships, interpret experimental embryology findings, and propose evolutionary relationships based on developmental patterns.

With the advent of modern developmental biology in the late 20th century, there was a renewed interest in describing embryonic patterning through fate mapping, lineage tracing, and clonal analysis, using newly emerging labeling approaches and advanced imaging technologies. Many model organisms were fate mapped during this period, including C. elegans (Sulston et al. 1983), chick (Couly and Le Douarin 1985; Hatada and Stern 1994), mouse

(Tam and Beddington 1987), *Xenopus* (Moody 1987a; Moody 1987b; Dale and Slack 1987), zebrafish (Kimmel, Warga, and Schilling 1990), and sea urchin (Logan and McClay 1999). Subsequent fate mapping studies investigated the origins of specific tissues and organs, further contributing to detailed descriptions of early embryonic organization and supporting rigorous inquiry into the developmental mechanisms driving early embryogenesis. When compared across species, fate maps have the potential to reveal evolutionary patterns across clades and provide insight into the remarkable diversity of forms that arise during embryogenesis.

1.7 Overview of the dissertation

This thesis focuses on understanding how early cell positions, gastrulation movements, and signaling pathway activities contribute to zebrafish development, with a particular emphasis on the origin of the neural crest. In this chapter, I have provided a detailed primer on early zebrafish development and introduced core concepts that are referenced throughout this thesis, including gastrulation, morphogenesis, signaling, cell fate specification, and key cell types in the pharyngula, including the neural crest. While these topics have been studied in depth across a variety of vertebrate systems, this work aims to broaden our understanding of the integrative developmental processes that shape early embryonic organization in the zebrafish.

In Chapter 2, I present a fate map of the ventral gastrula that clarifies the origin of a variety of cell fates in the zebrafish. While previous fate maps described the origins of many cell types in zebrafish, there was not a comprehensive fate map of the ventral gastrula and the origin of the neural crest remained unclear. To address this gap, I developed a photoconvertible labeling approach for labeling small regions of the zebrafish ventral gastrula and visualizing the fates that they contributed to later in development. My methodology built on previous fate mapping techniques by documenting both the cell type contributions

of small regions and their spreads relative to one another along the later embryonic body axis. The resulting fate map clarifies the origin of multiple cell types, including the neural crest and cranial placodes, and defines the overall organization of the ventral gastrula in zebrafish.

In Chapter 3, I investigate the role of FGF signaling in gastrula patterning and morphogenesis. While FGF signaling has been shown to have a variety of roles in early development, the specific effects of FGF signaling at the onset of gastrulation are particularly complicated. I investigated the influence of FGF signaling during gastrulation on subsequent axis formation and cell type specification by taking advantage of pharmacological inhibition of FGF receptor activity. Analysis of overall morphology and gene expression patterns revealed that FGF signaling is necessary for appropriate specification of pharyngeal arch neural crest and cranial placodes. Using live confocal microscopy, I examined the stereotypical cell movements in the ventral gastrula and identified key differences in gastrulation as a result of FGF inhibition. My findings indicate that FGF signaling at the onset of gastrulation is key to directing gastrulation movements, axial patterning, and formation of posterior structures.

Taken together, my findings clarify the organization of the zebrafish gastrula and how embryonic domains contribute to the overall body plan later in development. This dissertation highlights the complex interplay between position, signaling, and movement in early development and provides a foundation for investigating the early embryonic origin of cell types in vertebrates. In Chapter 4, I discuss these findings further and highlight unanswered molecular, morphological, and evolutionary questions to guide further research.

CHAPTER 2

FATE MAP OF THE ZEBRAFISH VENTRAL GASTRULA

2.1 Preface

A version of this chapter was published in Kushkowski EE and Prince VE. Zebrafish ventral gastrula fate map reveals neural crest progenitor domain. Developmental Dynamics. 2026;1-25. doi:10.1002/dvdy.70174. Figures from this publication have been adapted to better reflect the format of this document.

2.2 Abstract

Fate maps relate progenitor cell positions to later fates and locations of their progeny, revealing early embryonic organization. Previous zebrafish fate maps identified the origin of germ layers and derivative cell fates, but ventral gastrula progenitor domains were not fully resolved. In particular, the neural crest, a multipotent cell type central to vertebrate development and evolution, was not characterized in the zebrafish fate map. We generated a region-based fate map to resolve the origin of the neural crest and overall organization of the ventral gastrula. This fate map demonstrates that cranial neural crest and placodes arise from a broadly overlapping progenitor domain. Notably, trunk neural crest and neural tube always arise together, while cranial neural crest and neural tube can arise from segregated progenitor pools. A separate, far-ventral progenitor domain produces somites, spinal cord, neural crest, and epidermis in the posterior tail. We situate the neural crest in the fate map and clarify the early embryonic organization of the zebrafish ventral gastrula. Our fate map establishes multiple mixed-fate domains in the ventral gastrula and their contributions to the overall body plan. This fate map provides information for further investigation of early vertebrate development and neural crest biology.

2.3 Introduction

For over a century, fate maps have provided foundational insights into early embryonic organization across a variety of vertebrate and invertebrate species (Couly and Le Douarin 1985; Dale and Slack 1987; Kimmel, Warga, and Schilling 1990; Logan and McClay 1999; Sulston et al. 1983; Tam and Beddington 1987). Fate maps reveal early embryonic organization by documenting the spatial positions of progenitor cells that give rise to specific differentiated cell fates later in development. While fate maps capture static information from early and late stages, mapping later cell fate and axial position data back onto the early embryo provides insight into the morphogenetic processes and underlying mechanisms that pattern the embryo in space and over time. This information is essential information for investigating how cell fate diversity and organismal complexity arise during development. Deep understanding of early embryonic organization is vital to tackling unresolved developmental and evolutionary questions about morphogenesis, signaling, and cell fate specification.

In zebrafish, the embryonic shield (dorsal organizer) becomes morphologically apparent within the gastrula at 6 hours post fertilization (hpf) (Kimmel, Ballard, et al. 1995; Warga and Kimmel 1990). At this stage, the dorsal-ventral axis is defined relative to the position of the shield, and the animal-marginal axis extends from the animal pole to the margin, where the blastoderm meets the underlying yolk (Fig. 1A). Major signaling pathways, including BMP, Wnt, FGF, and Nodal, provide positional information across the multipotent blastoderm (Tuazon and Mullins 2015; Concha 2025). Morphogenetic movements during gastrulation drive formation of germ layers and extension of the primary body axis, reshaping the spherical embryo into a bilaterally symmetric organism (Rohde and Heisenberg 2007; Concha 2025). Cells arrive in their final positions within the body plan and differentiate into regionalized cell fates during neurulation, segmentation and elongation. By 30 hpf, many of the structures and rudimentary organs of the basic vertebrate body plan are present (Figure 2.1 A).

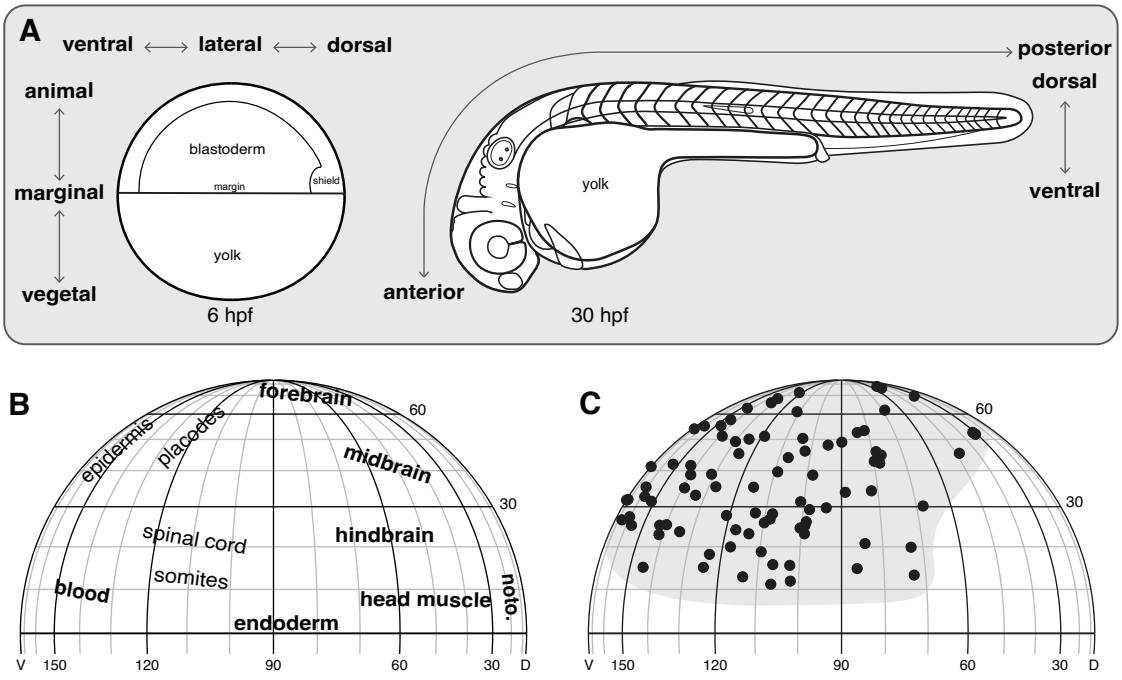

Figure 2.1: **Embryonic body plan and fate map schematics.** (A) Schematics of a 6 hpf gastrula, indicating the animal-vegetal axis and the dorsal-ventral axis (dorsal shield, margin, blastoderm, and yolk are indicated), and a 30 hpf embryo, indicating the anterior-posterior (AP) primary body axis, and the dorsal and ventral sides. (B) Summary of previously published zebrafish gastrula-stage fate maps (Dougan et al. 2003; Kimmel, Warga, and Schilling 1990; Kozlowski et al. 1997; Melby, Warga, and Kimmel 1996; Ward, Warga, and Prince 2007; Warga, Kane, and Ho 2009; Warga and Nüsslein-Volhard 1999; K. Woo and Fraser 1995). Bolded text indicates cell type derivatives where extensive data supports fate classifications, and for which axial position of cell progeny was also collected. Unbolded text indicates cell types supported by fewer data points and with a lack of information about axial position of progeny. D = dorsal; V = ventral; degrees of latitude (relative to the margin) and longitude (relative to the dorsal side) are indicated. (C) Summary of the regions fate mapped in this study. Gray shading indicates the overall area mapped, which focuses on the domain that previously lacked data. Dark gray dots indicate the centers of the 86 individual regions evaluated.

Differentially coordinated morphogenetic movements drive dynamic reorganization of the embryonic body axes during gastrulation. Epiboly directs cells toward the vegetal pole, by thinning and spreading the blastoderm to fully engulf the yolk. Convergence movements direct cells towards the dorsal midline, leading to the extension of the body that produces the anteroposterior (AP) axis. Cells at the margin begin to internalize, forming the germ ring, and migrate beneath the epiblast to ultimately produce endodermal and mesodermal derivatives (M. L. K. Williams and Lilianna Solnica-Krezel 2020). The dorsal-animal blastoderm primarily converges toward the dorsal midline and rotates past the animal pole to form anterior structures (Bronner-Fraser and Fraser 1988). Due to a combination of epiboly and convergence movements, lateral blastoderm becomes widely distributed along the AP axis, contributing to a significant proportion of the body plan. Ventral blastoderm rapidly disperses from the evacuation zone around 8 hpf, spatially segregating cranial and posterior progenitors (Kimmel, Warga, and Schilling 1990; Kimmel, Ballard, et al. 1995). On the far ventral side of the embryo, cells primarily move toward the vegetal pole, where they form the tailbud and contribute to posterior structures during segmentation and elongation (Attardi et al. 2019; Kanki and Ho 1997; Ben Steventon, Duarte, et al. 2016; D. C. Myers, Sepich, and Lilianna Solnica-Krezel 2002). Fate maps help to make sense of how these complex processes influence embryonic organization and cell fate specification.

In zebrafish, several fate maps have been produced at, or approaching, shield stage (6 hpf) that describe early embryonic organization of specific cell fates (summarized in Figure 2.1 B). The first zebrafish fate map established the spatial origins of the germ layers and the general organization of derivative tissues including the epidermis, brain, spinal cord, and somitic mesoderm (Kimmel, Warga, and Schilling 1990). Subsequent fate mapping focused on the anterior to posterior organization of central nervous system progenitors within the dorsal gastrula and cranial placode progenitors from the ventral ectodermal domain (Kozlowski et al. 1997; K. Woo and Fraser 1995). Additional fate maps identified marginal domains

that produced mesodermally and endodermally derived tissues, revealing early patterns that correlate with later position (Dougan et al. 2003; Melby, Warga, and Kimmel 1996; Ward, Warga, and Prince 2007; Warga, Kane, and Ho 2009; Warga and Nüsslein-Volhard 1999). While these fate maps were generated using a range of strategies to label single cells, small clones, or regions within the embryo, they can be compared to one another because the positions of the labeled cells were recorded relative to the dorsal organizer at shield stage. Insights from these fate maps have been invaluable for establishing the zebrafish as a powerful developmental model.

While previous zebrafish fate maps clarified the overall organization of the dorsal, animal, and marginal gastrula domains in detail, they provided less information about progenitor domains within the ventral ectoderm (Dougan et al. 2003; Kimmel, Warga, and Schilling 1990; Kozlowski et al. 1997; Melby, Warga, and Kimmel 1996; Ward, Warga, and Prince 2007; Warga, Kane, and Ho 2009; Warga and Nüsslein-Volhard 1999; K. Woo and Fraser 1995). Limited data suggested ventral contributions to a wide array of tissues, including the epidermis, spinal cord, somitic mesoderm, cranial placodes, and neural crest. However, the details of the arrangement of progenitor domains for these tissues and their contributions to different axial levels remained unresolved. Some ventral derivatives are restricted to the cranium, while others are present at all axial levels throughout the embryonic body, raising the question of how regionalized cell fates arise from this domain. Additional information about the precise organization of the ventral domain is required to investigate the diverse array of cell types and structures that it generates during embryogenesis.

Previously published fate maps also leave a major gap in our knowledge about the origin of the neural crest in zebrafish. The neural crest is a transient vertebrate cell type that migrates extensively throughout the developing body and differentiates into numerous derivatives along the AP axis. Neural crest gives rise to cartilage, bone and connective tissue in the cranial region, as well as neurons and glia of the entire peripheral nervous system,

cardiomyocytes, and pigment cells (D. W. Raible, Wood, et al. 1992; D. W. Raible and Eisen 1994; Rocha, Singh, et al. 2020; Schilling and Kimmel 1994). As a result, specification of the neural crest during early embryogenesis is important for development of craniofacial structures, sensory systems, and the peripheral nervous system. This cell type plays a key role in vertebrate development as well as the evolution of vertebrates in general. In accord with the importance of the neural crest, it has received intensive study over many years and across multiple vertebrate models, including zebrafish (Rocha, Beiriger, et al. 2020).

Despite ongoing interest in neural crest development, previous fate maps provide little insight into the position of neural crest progenitors in the zebrafish gastrula. The original zebrafish fate map identified three ventral clones that gave rise to neural crest, neural tube, and somitic mesoderm (Kimmel, Warga, and Schilling 1990). Woo and Fraser identified ventral neural crest progenitors, but their organization and abundance were obscured during analysis by grouping together with otic placode and epidermis progenitors (K. Woo and Fraser 1995). Schematized fate maps have nevertheless suggested a wide variety of ventro-lateral positions from which the neural crest may arise (Fuentes et al. 2020; Kane and Warga 1994; Kimmel, Ballard, et al. 1995; Smith and Kimelman 2020; Tuazon and Mullins 2015). These proposed positions seem to be extrapolated from the limited fate mapping data or inferred from later neural crest specification and neural plate border (Rocha, Singh, et al. 2020). Additional fate mapping is required to situate the neural crest appropriately within the zebrafish gastrula.

In this study, we have generated a fate map that defines the organization of the ventral gastrula in the zebrafish. This ventral fate map encompasses the prospective placodal ectoderm and extends into the previously described neurectoderm and mesoderm domains. We provide detailed information about the spatial origin of the zebrafish neural crest and other significant tissues and structures throughout the embryo. Analysis of the fate map reveals contributions of progenitor regions to multiple cell types and uncovers differential spread of

these progenitor regions along the primary body axis.

2.4 Results

2.4.1 A region-based strategy for fate mapping the zebrafish ventral gastrula

We generated a detailed fate map of cell types from 86 labeled regions that were primarily located within the understudied ventrolateral gastrula (Figure 2.1 C). Note that this and subsequent fate map panels represent the center of each labeled region for clarity, rather than the total labeled area. We focused on ventral regions animal to the germ ring because the most marginal domain has already been thoroughly mapped (Dougan et al. 2003; Melby, Warga, and Kimmel 1996; Ward, Warga, and Prince 2007; Warga, Kane, and Ho 2009; Warga and Nüsslein-Volhard 1999). Our region-based fate mapping approach allowed us to identify the full range of cell fates that arise from small regions of the gastrula and document their contribution to the 30 hpf body plan (outlined in Figure 2.2). We provide examples of images collected during the fate mapping process in Figure 2.3. Photoconverted regions are shown in two 6 hpf (shield stage) specimens, together with low magnification images of the same specimens at 30 hpf, after Sox10 immunolabeling (Figure 2.3 A-D). The region shown in Figure 2.3 C is located 4-5 cell diameters above the margin, representative of the marginal limit of photoconverted regions in this study.

Cell type identification was aided by our use of membrane-localized Kaede (Ando et al. 2002), as membrane morphology is apparent in both photoconverted (magenta) and adjacent unconverted cells (cyan). We also took advantage of immunolabeling to identify neural crest cells that express Sox10 protein at 30 hpf. However, the ectomesenchymal neural crest cells of the pharyngeal arches no longer express Sox10 protein at this stage. Our analysis of *Tg(sox10:mRFP)* specimens immunolabeled for Sox10 protein confirmed that long-lasting mRFP protein is present in all neural crest cells at 30 hpf while Sox10 protein expression

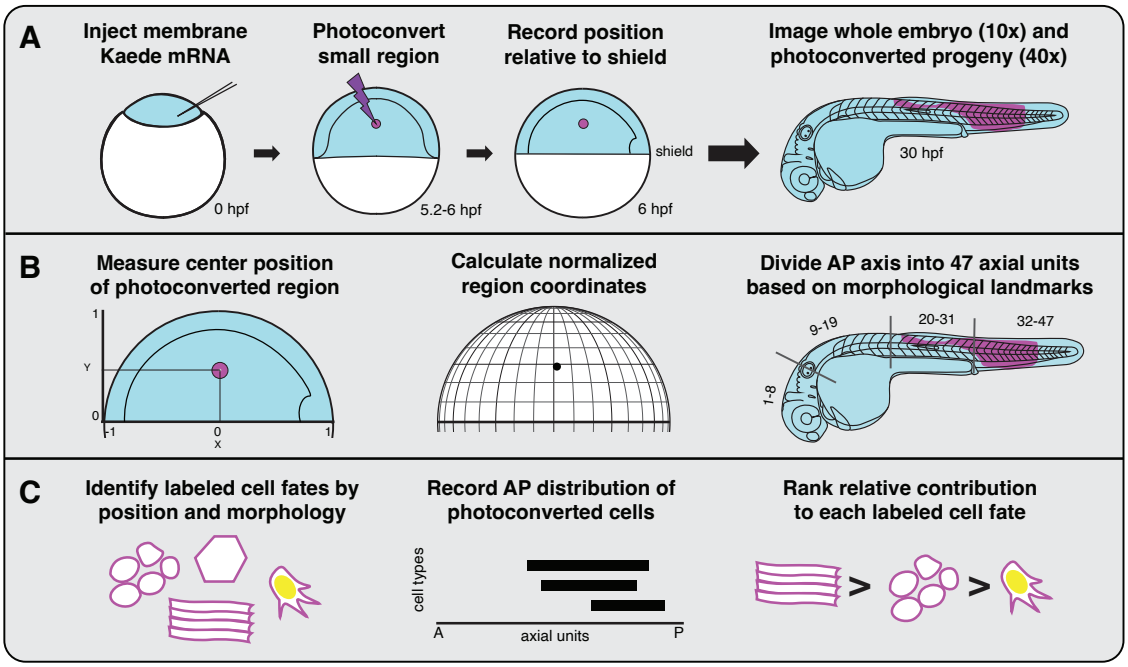

Figure 2.2: **Strategy to generate a new ventral gastrula fate map.** (A) Summary of experimental approach. Membrane Kaede mRNA (cyan) was microinjected at the one-cell stage, a small region in the 5.2-6 hpf gastrula was photoconverted (magenta) and the position of the photoconverted region was recorded relative to the shield at 6 hpf. Specimens were raised to 30 hpf and immunolabeled for Sox10 protein expression. Low (10x) and high (40x) magnification confocal z-stacks were collected for each specimen, allowing for careful determination of labeled cell fates. (B) Summary of embryo normalization approach. The center position of the photoconverted region was measured relative to the dorsal shield at 6 hpf and normalized coordinates were calculated, allowing for comparison between specimens. The anteroposterior (AP) position was assigned along 47 normalized axial units of approximately equivalent length, based on embryo morphology and anatomical landmarks, allowing us to record the location of labeled cells along the body axis at 30 hpf. (C) Summary of data collection. Cell fates were identified based on position, morphology, and Sox10 expression status. The AP distribution of photoconverted cells was recorded, and the relative contribution to each cell fate was ranked for each specimen.

is absent specifically in pharyngeal arch neural crest cells (Figure 2.3 E). The pharyngeal arch neural crest was identified by characteristic cuboidal cell membrane morphology and position within the cranium. The Sox10+ neural crest was identified by nuclear localization of Sox10 protein and membrane morphology. Consequently, we were able to reliably identify both sub-populations of neural crest cells present at 30 hpf.

Neural crest cells take on a variety of morphologies depending on their position at 30 hpf (Figure 2.3 F-K). In the cranium, we observed cuboidal pharyngeal arch neural crest cells (Figure 2.3 F; arrowheads), migratory Sox10+ neural crest cells (Figure 2.3 G; yellow nuclei), and Sox10+ neural crest contributions to the anterior lateral line ganglion (Figure 2.3 H, arrowheads; placode-derived cells, which are not Sox10+, are indicated by asterisks). In the trunk, we observed neural crest cells localized dorsal to the neural tube (Figure 2.3 I), migrating ventrally to contribute to the dorsal root ganglion (DRG; Figure 2.3 J), and clustered in the developing posterior tail (Figure 2.3 K).

We also provide examples of other labeled cell types, including retinal epithelium (Figure 2.3 L), epithelial cells of the otic vesicle (Figure 2.3 M), somitic mesoderm cells with characteristic elongated morphology (Figure 2.3 N), neural tube epithelium (Figure 2.3 O), including neural tube cells in the roof plate (Figure 2.3 P), and large, flat epidermis cells and neural tube cells in the tail (Figure 2.3 Q). The criteria used to identify 20 distinct cell types in this study are provided in Figure 2.4. We excluded poorly represented mesodermal cell types, germ cells, and the periderm, resulting in 15 unique cell types that were considered in subsequent analysis. As expected, we did not observe any endoderm derivatives, consistent with our exclusion of the most marginal domain of the gastrula.

2.4.2 Overall organization of fates within the ventral gastrula

Our dataset includes all major embryonic components of the central nervous system, cranial placodes, neural crest cells, epidermis, and all but the most anterior somites (Figure 2.5 A-

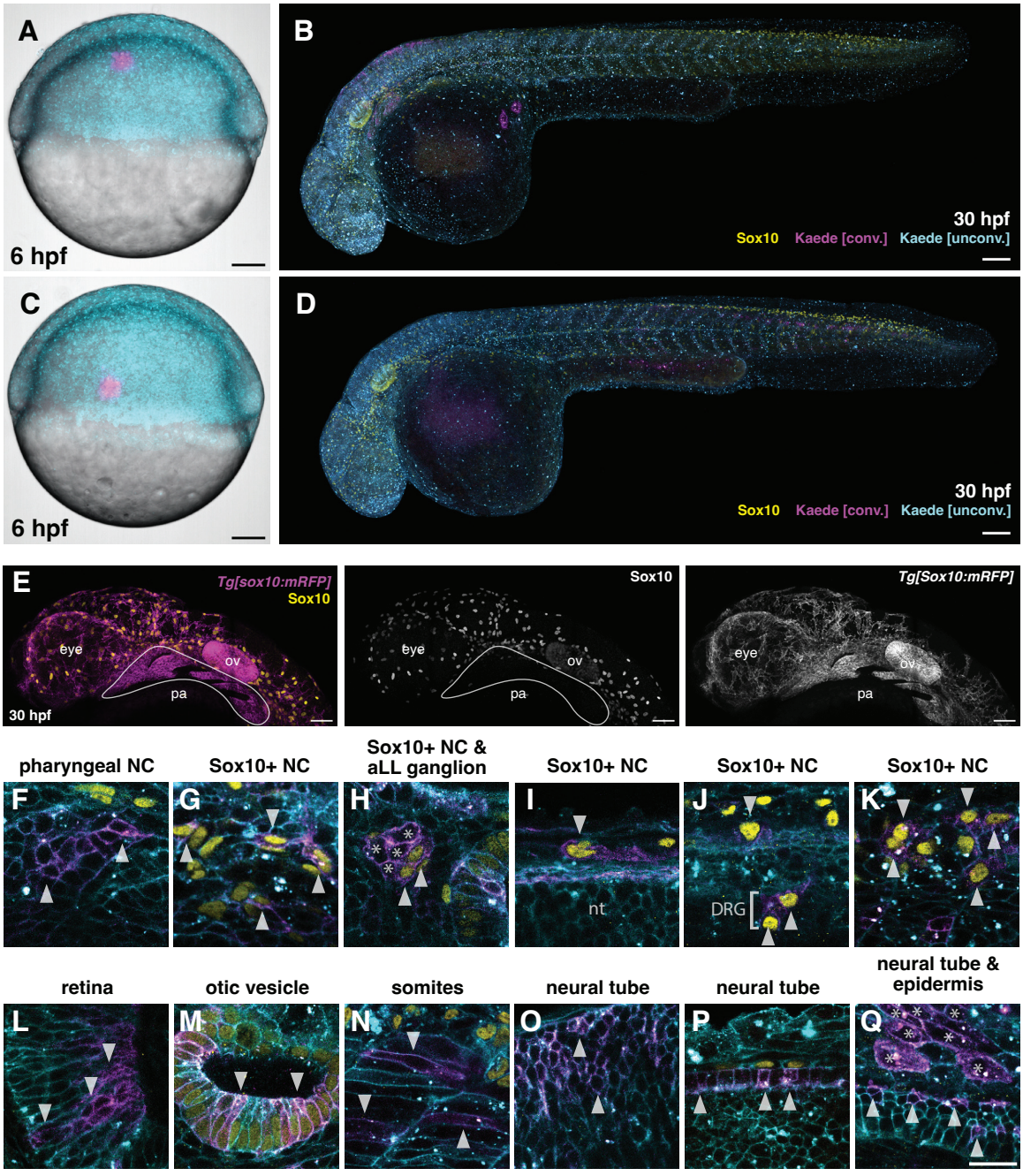

Figure 2.3: **Photoconversions and cell type identification.**

Figure 2.3: Continued. (A) Maximum projection confocal image of a 6 hpf embryo (lateral view, animal pole to top, dorsal to right), microinjected with mRNA encoding mKaede (cyan), showing a 40-50-cell photoconverted region (magenta). Scale bar = 100 µm. (B) Same specimen at 30 hpf, fixed and immunolabeled for Sox10 (yellow) low magnification view (10x objective; lateral view, anterior to left and dorsal to top). Scale bar = 50 µm. (C) Image of a second 6 hpf embryo, showing an example of a photoconversion that lies above the germ ring. (D) Same specimen at 30 hpf. (E) Confocal maximum projection of the cranial region of a 30 hpf *Tg(Sox10:mRFP)* specimen (mRFP shown in magenta and as single channel, right) immunolabeled with anti-Sox10 antibody (nuclei shown in yellow and as single channel, center), in lateral view with dorsal to the top. Pharyngeal arch neural crest cells (outlined region, pa) did not express Sox10 protein at this stage. The otic vesicle (ov) is also labeled by the Sox10 transgene and expresses a low level of Sox10 protein. Scale bar = 50 µm (F-Q) High magnification views (40x objective; lateral view) of single z-slices from representative labeled specimens. Photoconverted cell membranes are magenta; dorsal to the top and anterior to the left in all cases. Representative cells are indicated with arrowheads unless otherwise noted. (F-K) Neural crest cell morphologies. (F) pharyngeal arch neural crest cells (magenta membranes); (G) cranial Sox10+ neural crest cells (yellow nuclei with magenta membranes); (H) cranial Sox10+ neural crest cells (arrowheads) and anterior lateral line (aLL) ganglion cells (asterisks), with anterior edge of otic vesicle visible on right side of panel; (I) trunk Sox10+ neural crest cells located dorsal to the neural tube (nt); (J) trunk Sox10+ neural crest cells migrating ventrally into a dorsal root ganglion (DRG); (K) Sox10+ neural crest cells in the tail. (L-P) Other cell type morphologies along the AP axis. (L) retinal epithelium cells; (M) otic vesicle cells; (N) somitic muscle cells; (O) neural tube epithelial cells; (P) neural tube roof plate cells, located immediately ventral to unlabeled Sox10+ neural crest cells; (Q) epidermal cells (asterisks) and neural tube cells (arrowheads). Scale bar = 20 µm.

Cell type	Morphology and identifying features	# specimens
Neural tube	Tightly packed epithelial cells, organized into a contiguous tube that forms the developing brain (with visible lumen) and spinal cord. The neural tube is located in between the bilateral somites, and dorsal to the rod-like notochord, lying along the entire dorsal midline. The most dorsal neural tube cells of the spinal cord form a cuboidal row of roof plate cells at the midline.	53
Retina	Epithelial cells in a circular organization that surrounds the lens of the eye.	7
Somite	Elongated cells stretching between somite boundaries, located on either side of the trunk. Posterior somitic cells are less differentiated and thus less elongated.	35
Epidermis	Epithelial monolayer located superficially, beneath the periderm.	32
Sox10+ neural crest	All cells with Sox10+ nuclei, with the exception of cells within the otic vesicle. The Sox10+ neural crest includes mesenchymal protrusive cells in the cranium, organized in broad migratory sheets surrounding the eye, between the eye and otic vesicle, dorsal to the pharyngeal arch neural crest and anterior to the fin bud, as well as mesenchymal trunk/tail cells at or adjacent to the dorsal midline, or migrating ventrally in single-cell streams adjacent to the middle of each somite.	25
Pharyngeal arch neural crest	Cells in the pharyngeal region showing the characteristic cuboidal morphology of differentiating cartilage elements. These cells to not express Sox10 protein at 30 hpf.	14
Olfactory epithelium	Tightly packed epithelial rosette at the most anterior aspect of the embryo.	3
Lens	Spherical group of cells localized within the retina.	3
Otic vesicle	Elongate, tightly packed epithelial cells forming the ovoid otic vesicle, located bilaterally, superficial to hindbrain rhombomere 5. Most nuclei are Sox10+.	10
Trigeminal ganglion	An organized, tightly packed, triangular cluster of cells, lying immediately posterior to the eye on both sides of the head.	4
aLL ganglion	An organized, tightly packed, rounded cluster of cells, lying immediately anterior to the otic vesicle on both sides of the head.	4
pLL ganglion	An organized tightly packed, rounded cluster of cells, lying immediately posterior to the otic vesicle on both sides of the head	4
aLL primordium	A group of cells that migrates bilaterally towards the anterior, just under the skin, away from the aLL ganglion. At 30 hpf the primordium is beginning to bifurcate to extend both above and below the eye and has deposited the first two otic neuromasts.	4
pLL primordium	A coherent migratory group of ~100 cells, which begin adjacent to the pLL ganglion and migrates posteriorly along the horizontal myoseptum. The primordium is located just beneath the skin and above the somites. By 30 hpf, the pLL primordium has dropped off 2-3 sensory neuromasts from its lagging edge at regular intervals along the trunk.	4
pLL nerve	Nerve that extends along the trunk from the pLL ganglion to the pLL neuromasts and primordium.	1
Pectoral fin mesenchyme	A lateral plate mesoderm derivative located within the fin bud, which lies adjacent to somite 4.	1
Germ cells	Large round cells located bilaterally above the anterior hindyolk extension.	4
Vasculature	Diffuse squamous endothelial cells located in the intersomitic vessels.	2
Pronephros	Small cuboidal cells derived from the intermediate mesoderm, located in the pronephric ducts which are located bilaterally immediately above the hindyolk extension.	1
Periderm	Very thin cells that each cover a large area, arranged in a superficial monolayer. Usually adjacent to one another and separate from other labeled cell types due to lack of participation in gastrulation movements.	85

Figure 2.4: **Cell type identification criteria.**

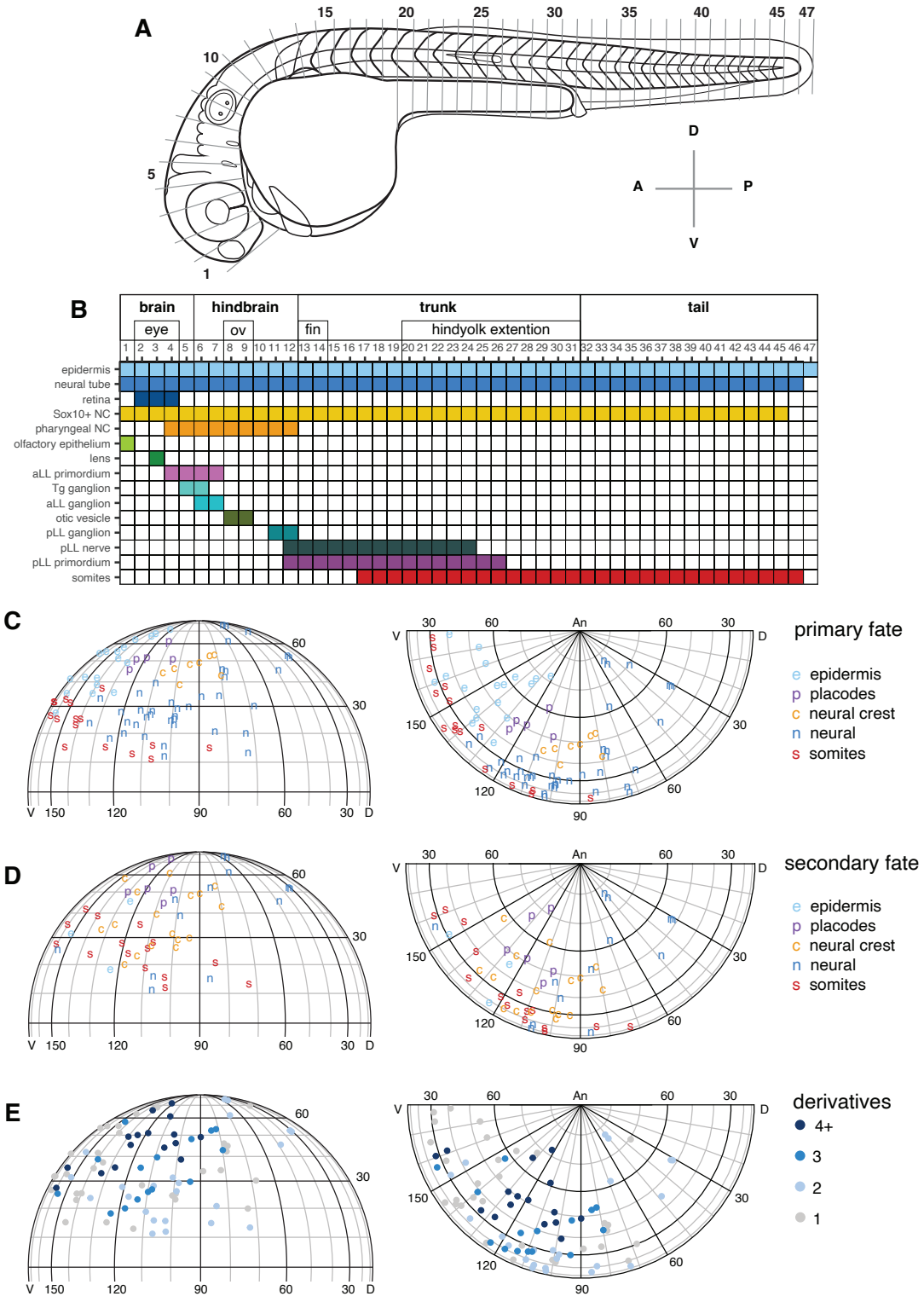

Figure 2.5: **Axial coverage and overview of the ventral fate map.**

Figure 2.5: Continued. (A) Schematic of axial subdivisions of the 30 hpf embryo. All specimens were subdivided into the 47 axial regions based on morphology and anatomical landmarks, allowing normalization between individuals. (B) Summary spreadplot showing the aggregate axial contributions of cell types derived from all 86 regions across the 47 axial units, with broad anatomical regions and landmarks indicated. ov = otic vesicle, NC = neural crest, aLL = anterior lateral line, pLL = posterior lateral line, Tg = trigeminal. Note that the cell type-specific color coding used here is also used in Figures 2.6, 2.8, 2.9 and Supplemental Figure 2.12. (C) Summary fate map showing the primary (top ranked) fate produced by each region: e = epidermis; p = placode derivatives (lens, olfactory bulb, otic vesicle, trigeminal ganglion, and lateral line ganglia/primordia/nerve); c = Sox10+ and pharyngeal arch neural crest; n = neural tube and retina; s = somitic mesoderm. (D) Summary fate map showing the secondary (second ranked) fate produced by each region. (E) Fate map indicating the number of different cell fate derivatives produced by each region, ranging from one cell type (grey) to four or more cell types (darkest blue).

B). We analyzed the overall organization of primary and secondary fate contributions from each region (Figure 2.5 C-D). For simplicity, we grouped all placodal cell types (p), Sox10+ and pharyngeal arch neural crest cells (c), and retina cell fates with the neural tube (n). Primary fate data, based on top ranked cell fates, align well with the organization described in previous fate maps (compare Figure 2.5 C with Figure 2.1 B), and provide further detail about ventral gastrula contributions to somitic mesoderm, epidermis, and neural tube (spinal cord) fates. Importantly, we identified domains that primarily contributed to neural crest and cranial placodes. Their positions fit into the previous gap in the ventrolateral gastrula fate map, between neural tube and epidermis-producing domains. However, mapping secondary fates (second ranked cell fates) reveals additional complexity within the ventral gastrula fate map, especially for neural crest, cranial placode, and somite fates (Figure 2.6 D).

To investigate how cell fate potential is distributed across the embryo, we analyzed the number of derivative cell fates that originated from each labeled region (Figure 2.5 E). This analysis distinguishes between domains of the embryo that are capable of producing single versus multiple cell fates. It is important to note that because each labeled region included multiple cells this is not an analysis of individual cell potency. Some regions made only a single cell type at 30 hpf, indicating that the labeled progenitors within these regions

were not multipotent. By contrast, the cranial ectodermal domain within the ventrolateral gastrula frequently contributed to four or more cell types. A small domain on the far ventral side also produced multiple posterior derivatives. These results demonstrate that specific domains within the embryo are capable of producing multiple cell types, highlighting the possibility of multipotency within these domains.

2.4.3 The ventral gastrula fate map

We present a comprehensive fate map for the origins of 15 cell types in the zebrafish gastrula (Figure 2.6). The locations for the progenitors of primary ectodermal derivatives, the epidermis, retina, and neural tube are in agreement with previously published fate maps (Figure 2.6 A-C) (Kimmel, Warga, and Schilling 1990; K. Woo and Fraser 1995). We build upon the work of Woo and Fraser by documenting the origin of neural tube at all axial levels, extending the progenitor domain for this fate into the far ventral gastrula. An extensive domain of the ventral fate map produces somitic mesoderm, expanding the domain described in previous studies towards the animal pole (Figure 2.6 D) (Dougan et al. 2003; Kimmel, Warga, and Schilling 1990; Warga and Nüsslein-Volhard 1999).

The neural crest is divided into two sub-populations; the expansive Sox10+ neural crest population and cranially-localized pharyngeal arch neural crest. Sox10+ neural crest cells arise from a broad domain that extends from the lateral to the ventral side of the gastrula (Figure 2.6 E). Importantly, this progenitor domain contributes to neural crest along the entire AP extent of the embryo. In addition, pharyngeal arch neural crest progenitors overlap with the most animal and lateral progenitors of Sox10+ neural crest, while also extending further towards the animal pole (Figure 2.6 F). The neural crest has now been situated within the overall zebrafish fate map, allowing for further investigation of neural crest development.

The fate map also shows the origins of multiple placodal cell types: olfactory epithelium, lens, otic vesicle, trigeminal ganglion (Tg), anterior lateral line (aLL) and posterior lateral

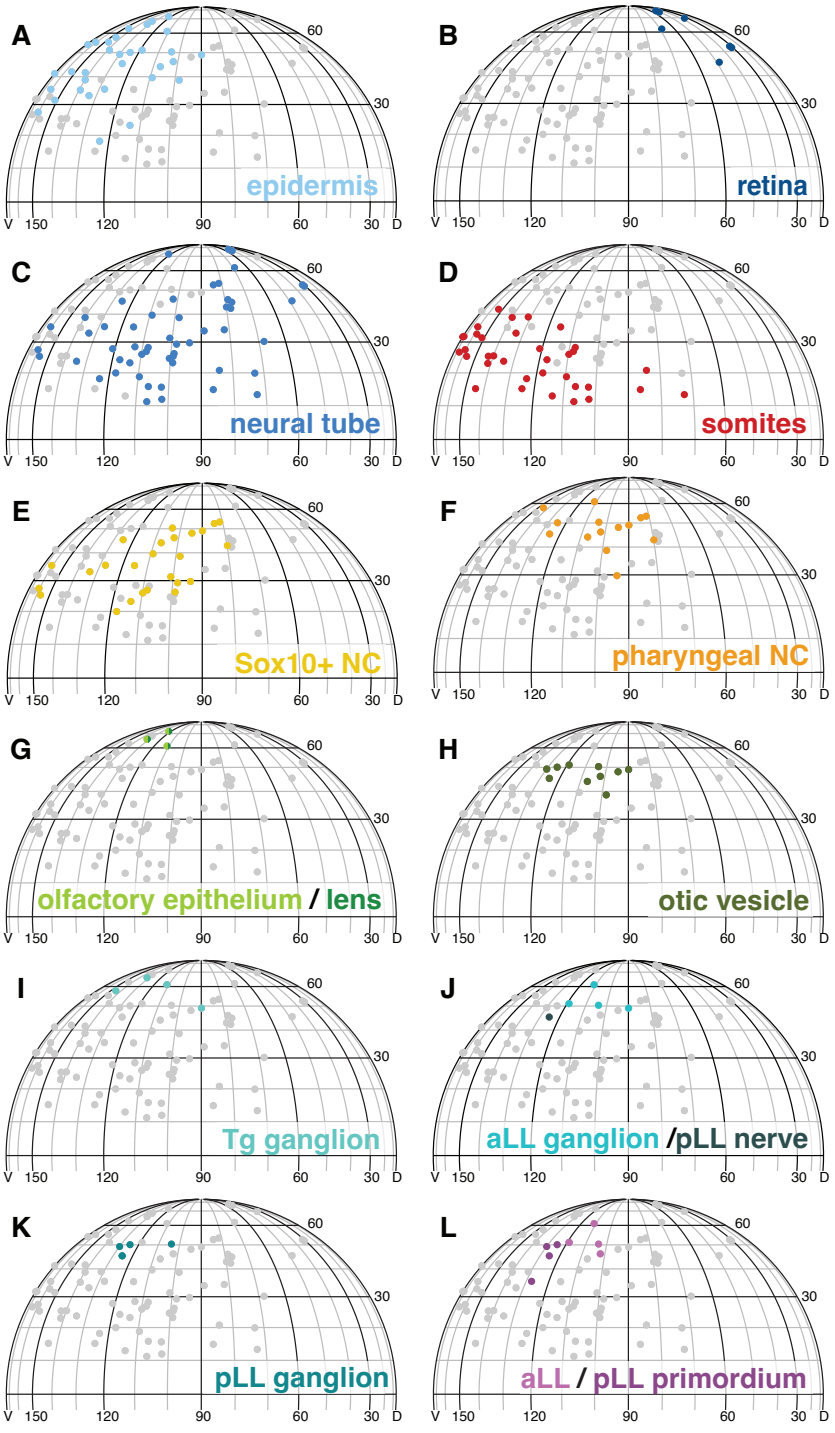

Figure 2.6: **Cell type-specific ventral gastrula fate maps.**

Figure 2.6: Continued. Fate map data organized by cell type, with all 86 regions indicated (gray). Individual maps show regions that contributed to (A) epidermis; (B) retina; (C) neural tube; (D) somites; (E) Sox10+ neural crest; (F) pharyngeal arch neural crest; (G) olfactory epithelium and lens–all three regions produce both cell types; (H) otic vesicle; (I) trigeminal (Tg) ganglion; (J) aLL ganglion and pLL nerve; (K) pLL ganglion; (L) aLL primordium and pLL primordium. Cell type-specific regions are color-coded as in Figure 2.5B.

line (pLL) ganglia and primordia. (Figure 2.6 G-L). The overall animal to marginal distribution of placode progenitors largely correlates with the later distribution of their derivatives from anterior to posterior. Our map reveals close association between lens and olfactory epithelium progenitors (Figure 2.6 G), and an extended domain that contributes to the otic vesicle, the cranial ganglia, and the lateral line system (Figure 2.6 H-L). Overall, the cranial placode domain is highly heterogeneous, in agreement with the previous region-based placode fate map that broadly identified overlapping placode progenitor domains (Kozlowski et al. 1997). As individual regions frequently contributed to multiple placodes, adding additional resolution to the placode fate map would require mapping smaller regions or single cells within this domain.

Our fate mapping strategy provides detailed information about the full complement of cell fates that co-occur within each labeled region. By comparison of the panels in Figure 2.6, it can be appreciated that in many cases a single region produced multiple cell fates (see also Figure 2.5E). Data presented here are complemented by comprehensive spreadplots for each specimen, which depict the axial extent of all cell types in rank order (Supplemental Figure 2.12). We also provide fate maps for a subset of cell types showing the relative abundance of the cell type across all regions (Supplemental Figure 2.13). While a variety of questions could be addressed with this comprehensive dataset, we primarily focused our analysis on the newly defined neural crest progenitor domain.

2.4.4 Organization within the neural crest progenitor domain

Considering neural crest progenitor regions in aggregate, we investigated their contribution to neural crest cells along the AP axis at 30 hpf (Figure 2.7 A). Anterior cranial neural crest cells arise from gastrula regions that lie closest to the animal pole, 40-60 degrees above the margin. This sub-domain spans the lateral to ventral gastrula, from 80 to 150 degrees from the dorsal shield. The posterior cranial neural crest cells arise from gastrula regions that lie further from the animal pole, 25-50 degrees above the margin, and between 90 and 125 degrees from the dorsal shield. The trunk neural crest cell progenitors lie both more ventral and more marginal within the gastrula, approximately 20-35 degrees above the margin and 110-135 degrees from the dorsal shield. Finally, the most posterior neural crest in the tail, lies in a separate, even more ventral domain, >150 degrees from the shield. In summary, the zebrafish neural crest progenitor domain extends over a broad area of the ventrolateral gastrula and contributes to neural crest at all axial levels.

Within the cranial neural crest sub-domain, we examined the relative contribution to Sox10+ and pharyngeal arch neural crest sub-populations. We found three regions that produced pharyngeal arch but not Sox10+ neural crest and eleven regions that produced both (Figure 2.7 B). Within the domain producing both types of cranial neural crest cells, regions producing more pharyngeal arch neural crest tend to lie within a tight lateral domain, while regions that give rise to more Sox10+ neural crest occupy the dorsal and marginal edges. Regions that produce Sox10+ neural crest are distributed more ventrally and marginally, consistent with their contribution to Sox10+ neural crest along much of the AP axis.

We analyzed pharyngeal arch neural crest progenitors in more detail by separating out the first and second (mandibular and hyoid) arches from the more posterior branchial arches (Figure 2.7 C). Our data indicate that these tissues are already regionalized in the 6 hpf fate map, such that the more posterior branchial arch neural crest generally derives from a more ventral and marginal sub-domain than the mandibular and hyoid arch neural crest. Taken

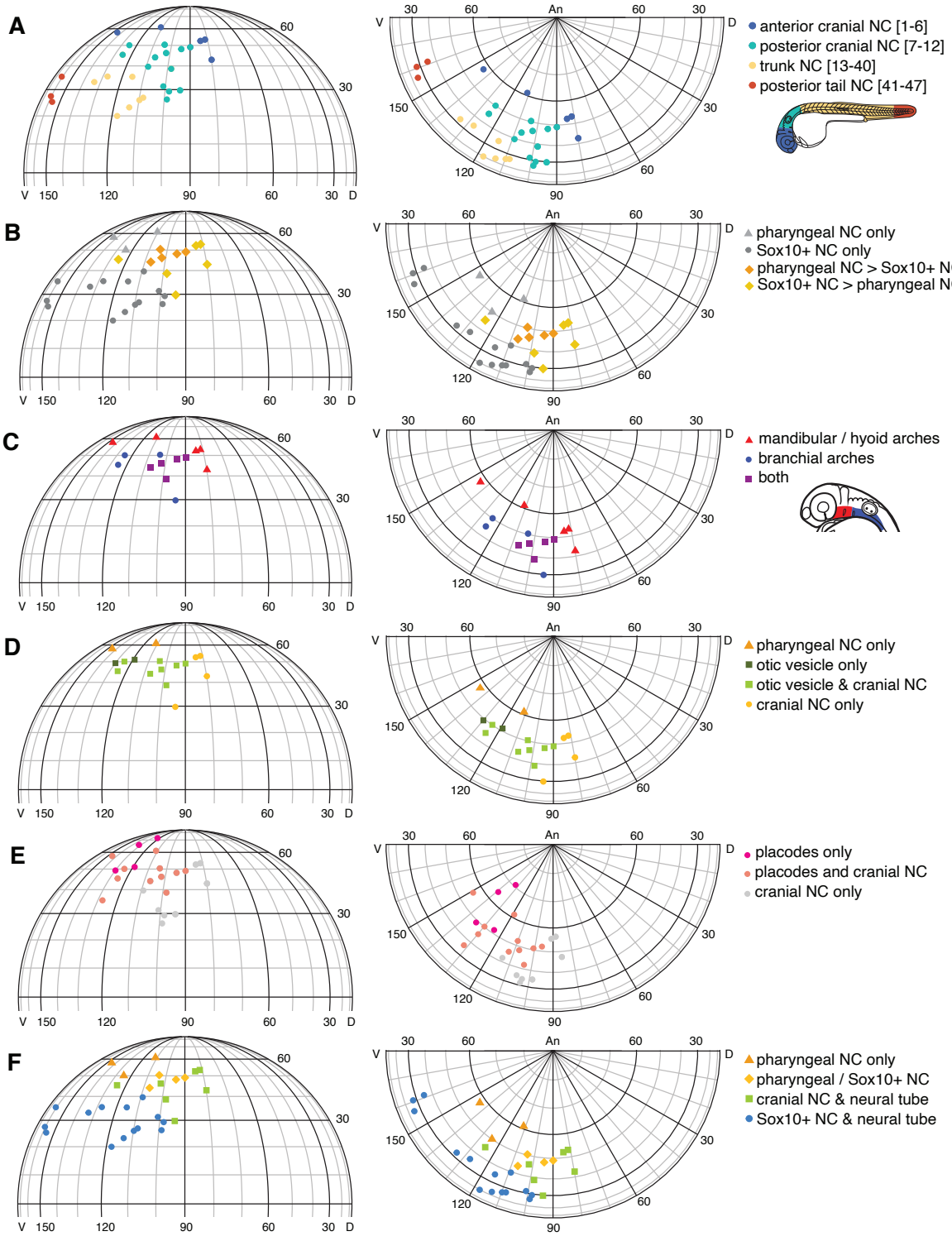

Figure 2.7: **Neural crest progenitor domain relationships.**

Figure 2.7: Continued. (A-F) Fate maps shown in lateral view (left) and animal pole view (right); data points from both left and right sides are consolidated onto the left side. (A) Gastrula-stage neural crest progenitor sub-domains for neural crest cells at different axial levels (as schematized on right): anterior cranium (neural crest cells centered in axial regions 1-6; dark blue); posterior cranium (neural crest cells centered in axial regions 7-12; teal); trunk (neural crest cells centered in axial regions 13-40; orange); posterior tail (neural crest cells centered in axial regions 40-47; red). (B) Comparison of neural crest progenitor sub-domains for: pharyngeal arch neural crest (grey triangles); Sox10+ neural crest (grey circles); both with pharyngeal arch neural crest as the top-ranked derivative (orange diamonds); and both with Sox10+ neural crest as the top-ranked derivative (yellow diamonds). (C) Sub-fates of pharyngeal arch neural crest cells, comprising mandibular and hyoid (first and second anterior pharyngeal arches only; red triangles); branchial arches only (posterior arches 3-7; blue circles); both anterior and posterior pharyngeal arches (purple squares). The schematic indicates the locations of the different arches. (D) Relationship of neural crest progenitors to otic vesicle progenitors; pharyngeal neural crest only (orange triangles); otic vesicle only (dark green squares); otic vesicle and pharyngeal and Sox10+ neural crest progenitors (light green squares); Sox10+ and pharyngeal NC progenitors (yellow circles). (E) Relationship of cranial neural crest progenitors to placode progenitors: placode progenitors only (magenta); cranial neural crest and placode progenitors (peach); cranial neural crest progenitors only (grey circles). (F) Relationship of neural crest progenitors to neural tube progenitors: pharyngeal arch neural crest progenitors (orange triangles); pharyngeal arch and Sox10+ neural crest progenitors (yellow diamonds); pharyngeal arch and Sox10+ neural crest plus neural progenitors (green squares); Sox10+ neural crest plus neural progenitors (blue circles).

together, our results reveal an orderly arrangement of neural crest progenitors within the gastrula that corresponds with the later position of neural crest derivatives along the AP axis.

2.4.5 Cranial neural crest and cranial placodes arise from a shared progenitor domain

We further explored the broad mixed cranial domain revealed by our fate map. There was striking overlap between pharyngeal arch neural crest and otic vesicle progenitors, indicating that these tissues may be very closely associated in development (Figure 2.7 D). In general, there is a high degree of overlap between most placodal derivatives and both cranial neural crest populations (Figure 2.7 E). Within this shared cranial progenitor domain, regions produced the cell fate diversity that is required to build the cranial and sensory structures of the vertebrate head. Placode producing regions that did not contribute to neural crest are located more animal and ventral than the shared domain. These regions primarily produced epidermis and made smaller contributions to the anterior placodal derivatives, including the lens, olfactory epithelium, trigeminal ganglion, and anterior lateral line, indicating that we have mapped the ventral limits of the cranial placode domain in the gastrula. The dorsal limit of the placode and neural crest progenitor domain is located around 90-100 degrees, such that this shared progenitor domain does not extend into the dorsal blastoderm.

This analysis demonstrates that the prospective non-neural ectoderm arises from a set of overlapping yet ordered progenitor domains within the ventral gastrula, complementing the order and coherence found for dorsal neural progenitors (K. Woo and Fraser 1995). Starting from the far ventral gastrula, furthest from the shield, the blastoderm produces epidermis, mixed cranial placodes, pharyngeal arch neural crest, and Sox10+ neural crest. The cranial placode and neural crest domains border the cranial neural tube progenitor domain. Our data reveal a close relationship between progenitors for cranial neural crest and cranial

placodes, but a more complex relationship with the neural tube.

2.4.6 Cranial neural crest and neural tube arise from partially overlapping progenitor domains

To understand the degree to which neural crest sub-populations and neural tube share origins within the gastrula, we explored the degree to which they co-occur within our dataset (Figure 2.7). We found a substantial sub-domain of cranial neural crest progenitors that is spatially segregated from the neural tube progenitor domain, represented by seven regions within the neural crest domain (triangles and diamonds). This sub-domain is located on the ventral side of the gastrula, 45 degrees or more above the margin, and contributes to both anterior and posterior pharyngeal arch neural crest, as well as Sox10+ neural crest. Specifically, three regions that contributed to pharyngeal arch neural crest (triangles), and four regions that produced a combination of pharyngeal arch and Sox10+ neural crest (diamonds) did not contribute any cells to the neuroepithelium of the developing brain. Seven regions produced Sox10+ and pharyngeal arch neural crest as well as cranial neuroepithelium (squares). These regions lie more dorsally within the cranial neural crest sub-domain. All regions that produced post-cranial neural crest contributed to the spinal cord (circles). Our findings suggest that cranial and trunk neural crest may have different lineage relationships with the neural tube, a finding we discuss further below.

2.4.7 Multiple cell types arise with neural crest at all axial levels

To resolve patterns that emerge within the neural crest progenitor domain, we analyzed all specimens that generated any neural crest at 30 hpf. We provide spreadplots showing the AP position and ranking of all cell types present at 30 hpf for the 28 specimens that contributed to the neural crest. Figure 2.8 focuses on cranial neural crest and Figure 2.9 focuses on trunk neural crest. These data were grouped by the presence of neural crest

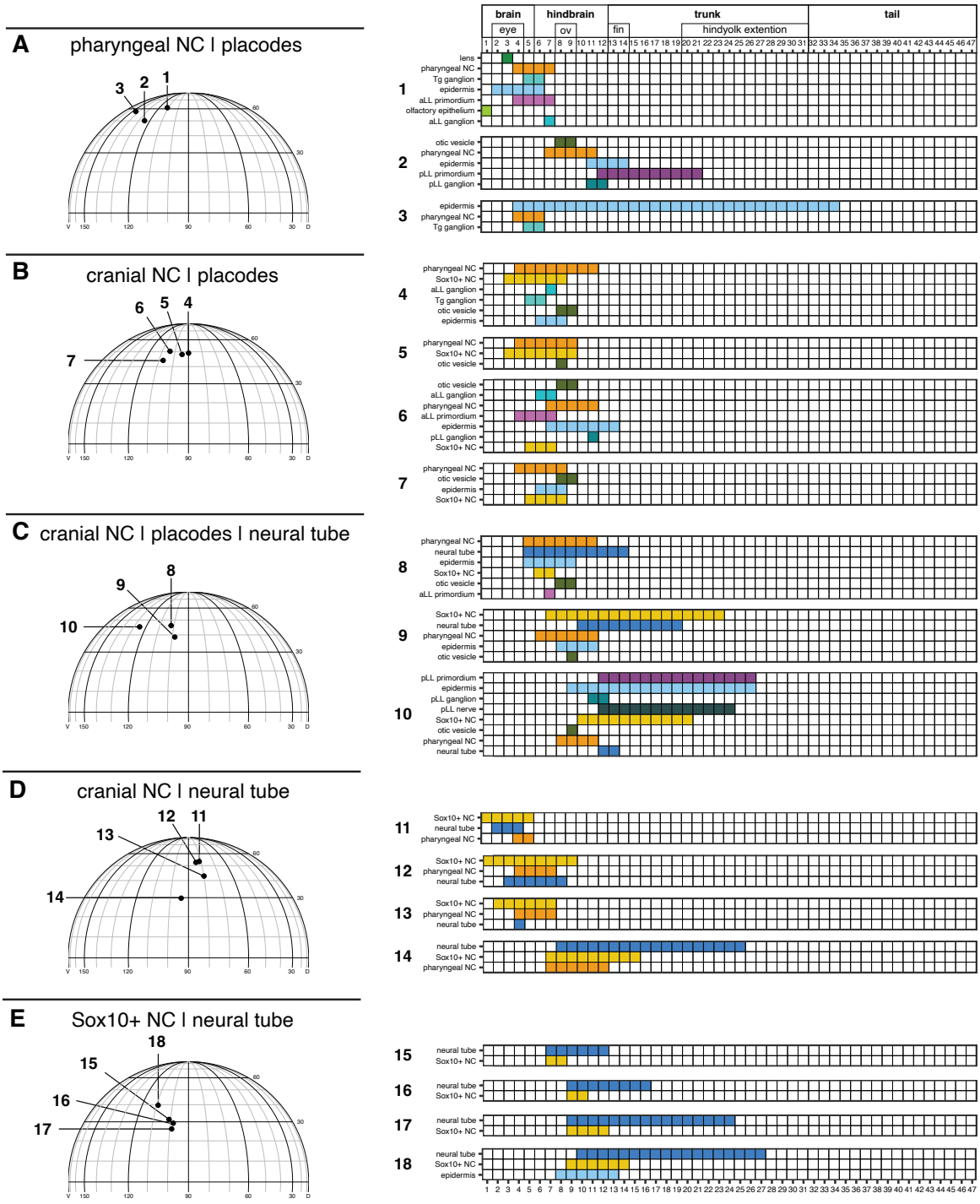

Figure 2.8: **Cell fate data from all regions that produced cranial neural crest.**

Figure 2.8: Continued. (A-E) Spreadplots showing all cell types produced by the 18 gastrula regions that contributed to cranial neural crest. (A) Regions that contributed to pharyngeal arch but not Sox10+ neural crest (orange triangles in Fig. 2.7F), and cranial placodes. (B) Regions that contributed to pharyngeal arch and Sox10+ neural crest (yellow diamonds in Fig. 2.7F), and cranial placodes. (C) Regions that contributed to pharyngeal arch and Sox10+ neural crest plus neural tube, as well as cranial placodes (dorsal subset of green squares in Fig. 2.7F). (D) Regions that contributed to pharyngeal arch and Sox10+ neural crest plus neural tube, but not cranial placodes (ventral subset of green squares in Fig. 2.7F). (E) Regions that contributed to Sox10+ neural crest and neural tube (subset of blue circles in Fig. 2.7F).

sub-populations, contribution to the neural tube, and axial position. This analysis further details axial organization of the embryo and explores potential relationships between the neural crest and other cell types.

Within the neural crest domain that does not overlap with the neural tube, three regions contributed to pharyngeal neural crest and one or more placodes (Figure 2.8 A). Region 1 generated mandibular/hyoid pharyngeal arch neural crest and a variety of placodal derivatives anterior to the otic vesicle. In contrast, Region 2 contributed to posterior cranial structures, including the otic vesicle, branchial pharyngeal arches, and posterior lateral line components. Region 3 primarily produced epidermis around the yolk and hindyolk extension, revealing that this region extended dramatically along the AP axis. The pharyngeal arch neural crest is not the highest ranked cell type in any instance, suggesting that this group defines the animal and ventral limits of the cranial neural crest domain. Four regions contributed to both pharyngeal arch and Sox10+ neural crest (Figure 2.8 B). Regions 4 and 5 contributed highly to both populations of neural crest, representing the center of the cranial neural crest domain. Regions 6 and 7 generated more pharyngeal arch neural crest and less Sox10+ neural crest, expanding the primary pharyngeal arch domain laterally.

In specimens that produced both sub-populations of cranial neural crest and neural tube, the neural crest contribution was frequently ranked higher than the neural tube contribution (Figure 2.8 C-D). Three regions contributed to cranial neural crest together with neural

tube, epidermis, and placodes (Figure 2.8 C). While both regions 8 and 9 contributed a wide range of derivatives, including both neural crest and neural cells, it is noteworthy that nearby regions 4-7 did not contribute neural tube. Region 10, the most ventral region in this group, made a minor contribution to the neural tube and primarily contributed to posterior lateral line components and epidermis. The Sox10+ neural crest from regions 9 and 10 localized to the lateral line nerve at the horizontal myoseptum, suggesting that these cells migrated posteriorly behind the lateral line primordium (Lyons et al. 2005). Four regions contributed to cranial neural crest together with neural tube and did not contribute to the placodes or epidermis (Figure 2.8 D). These regions lie more dorsal than those shown in Figure 2.8 A-C. Regions 11-13 produced large numbers of neural crest cells, similar to nearby regions 4 and 5, further defining the center of the cranial neural crest domain. Region 14, which is located further from the animal pole, produced more neural tube cells. Finally, posterior cranial Sox10+ neural crest cells arose with neural tube that extended into the trunk (Figure 2.8 E). Regions 15-18 produced neural crest cells at the level of the posterior hindbrain and contributed to progressively more posterior neural tube. In aggregate, the data in Figure 2.8 define the extent of the cranial neural crest and the edge of the neural ectoderm progenitors within the gastrula.

In the trunk and tail, Sox10+ neural crest and neural tube always arose together (Figure 2.9). In this group, labeled neural crest cells were observed adjacent to labeled cells in the dorsal neural tube or along characteristic ventral migration pathways. Figure 2.9 A shows data from regions that produced neural tube along a significant proportion of the trunk and tail. Regions 19 and 20 labeled Sox10+ neural crest in the anterior trunk, and neural tube throughout the trunk and tail, similar to regions 15-18. However, these regions also produced somitic mesoderm in the posterior tail. By contrast, regions 21 and 22 showed extensive Sox10+ neural crest, neural tube, and epidermis contributions throughout the trunk and tail. Regions 23-25 contributed to progressively more posterior neural tube, neural crest,

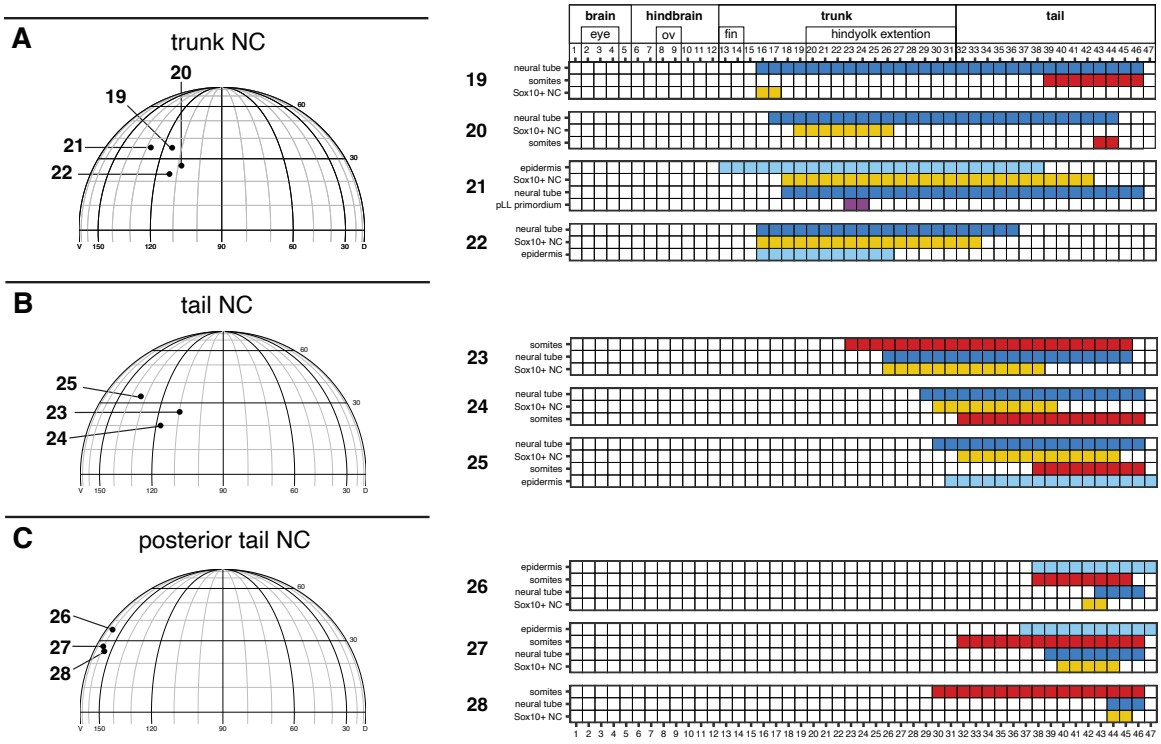

Figure 2.9: **Cell fate data from all regions that produced post-cranial neural crest.** Spreadplots showing all cell types produces by the 10 regions that contributed to post-cranial neural crest. (A) Regions that contributed to trunk neural crest (subset of yellow circles in Fig. 2.7 A). (B) Regions that contributed to tail Sox10+ neural crest (subset of yellow circles in Fig. 2.7 A). (C) Regions that contributed to posterior tail neural crest tail neural crest (red circles in Fig. 2.7 A).

and somites at similar axial levels (Figure 2.9 B). Together, regions 21-25 gave rise to neural crest over a large proportion of the trunk and tail. Finally, the most ventral regions within the neural crest domain produced the most posteriorly localized neural crest cells (Figure 2.9 C). This ventral domain primarily produced epidermis and somitic mesoderm and gave rise to a small number of neural tube and Sox10+ neural crest cells at the tip of the tail. Regions 26-28 were separated from the domain that produced the rest of the trunk neural tube, suggesting that there is an independent domain of mixed progenitors which facilitates development of the most posterior part of the embryo.

2.4.8 Differential AP distribution of major cell fates

To investigate how the gastrula contributes to development of the AP axis of the later embryo, we mapped the position and spread of labeled cells at 30 hpf back to their initial positions in the gastrula, independent of cell fates (Figure 2.10A). The most anterior parts of the 30 hpf embryo derive from the most animal/dorsal regions of the gastrula, with progressively more posterior fates along the trunk deriving from ventrolateral locations further from the animal pole. The most posterior tissues derive from the far ventral side of the gastrula, 30-40 degrees above the margin. We also analyzed the extent to which the progeny of labeled regions spread out along the AP axis during morphogenesis (Figure 2.10 B). The broad animal domain of the gastrula that gives rise to the most anterior structures of the 30 hpf embryo exhibits little spread along the primary body axis. By contrast, ventrolateral regions that give rise to trunk structures exhibit extensive spread over many axial units (up to 34 units or 72% of body length). The most ventral regions of the gastrula that give rise to the most posterior structures spread out less than regions contributing to the trunk. Taken together, the aggregated AP center and axial spread data highlight how the blastoderm contributes to the overall body plan.

We also analyzed AP position and axial spread data for individual cell types: epidermis,

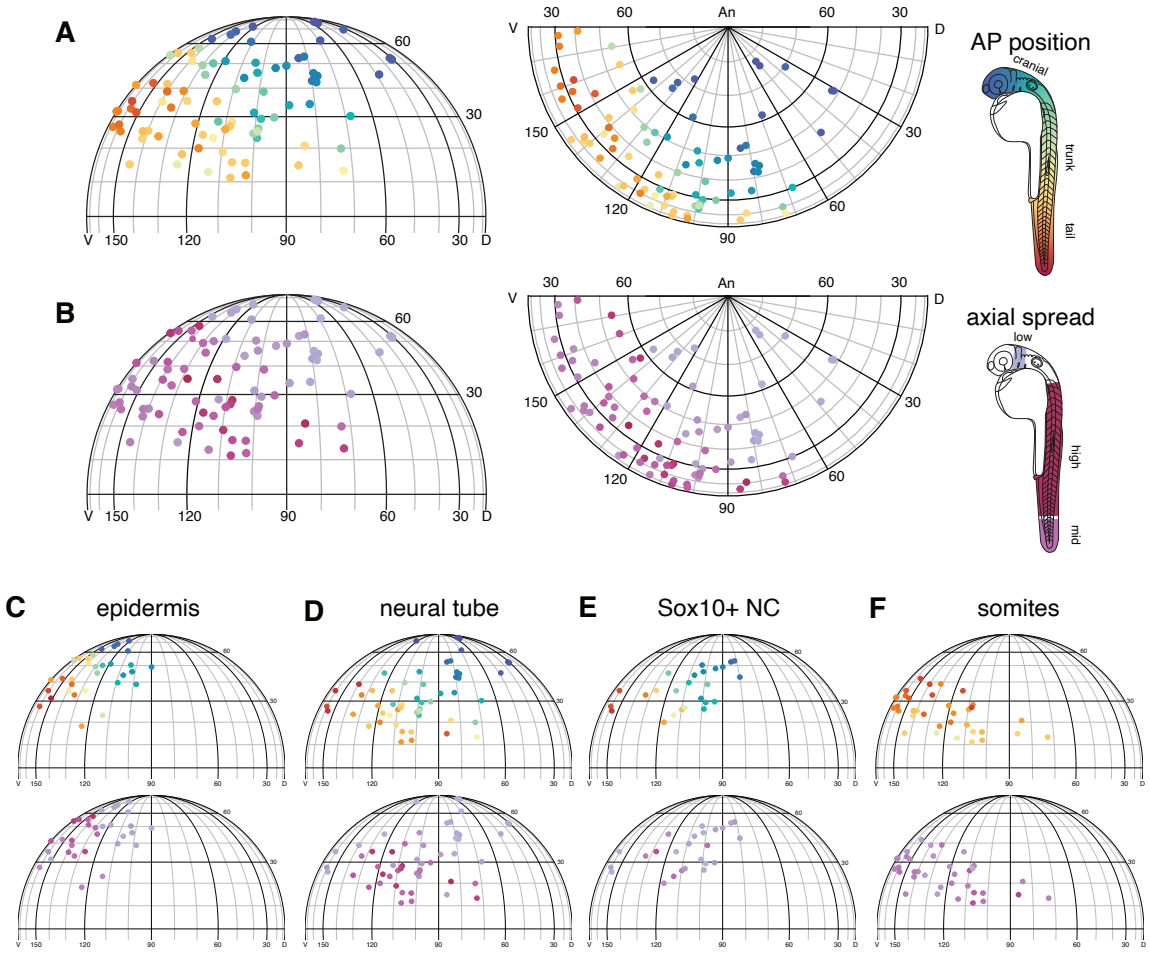

Figure 2.10: **AP position and axial spread of cell fates.** (A) Relationship of gastrula progenitor positions to later AP position in the 30 hpf embryo. AP position shows the center axial position of all progeny identified in each 30 hpf specimen, color-coded from anterior (violet) to posterior (red). (B) Axial spread shows the extent of AP spread of all progeny in each 30 hpf specimen, of up to 34 axial units, indicated by a color gradient from pale lavender (minimal spread) to deep magenta (maximal spread). (C-F). Axial distribution summary fate maps for single cell types: (C) epidermis (D) neural tube, (E) Sox10+ neural crest, and (F) somitic mesoderm. The upper plots show AP position while lower plots show axial spread, with the same color schemes as above.

neural tube, Sox10+ neural crest, and somites (Figure 2.10 C-F). High spread within the epidermis correlates with the position where the evacuation zone will form a few hours later (Kimmel, Warga, and Schilling 1990; Kimmel, Ballard, et al. 1995). The neural tube spread data reveal regions that contributed to a large proportion of the body axis, consistent with previous analysis of neural clones (Kimmel, Warga, and Kane 1994). Sox10+ neural crest typically populated a smaller proportion of the axis relative to the neural tube, as also shown in Figure 2.9. Ectodermal derivatives show similar patterns of axial contribution across the gastrula, consistent with their related morphogenetic movements during gastrulation. The most posterior ectoderm arises from a restricted ventral domain, while the most posterior somitic mesoderm comes from a broad domain well above the margin that extends more than 40 degrees towards the animal pole.

Consideration of axial contributions and abundance of cell types produced by each region highlights differences along the dorsoventral axis (see also Supplemental Figures 2.12 and 2.13). Lateral somitic mesoderm-producing regions that were furthest from the margin produced fewer somite cells than regions closer to the margin (Supplemental Figure 2.12). The regions that made minor contributions to somites made major contributions to the neural tube. These findings from the lateral gastrula are consistent with the previously mapped transition between ectoderm and mesoderm (Kimmel, Warga, and Schilling 1990). By contrast, those regions that lie ventral (beyond 120 degrees from the shield), even when far above the margin, produce large numbers of somitic mesoderm cells. Our fate map also reveals that the far ventral side of the gastrula makes only a minor contribution to the most posterior neural fates. Together, these data indicate that the mesoderm/ectoderm transition is not uniform across the dorsoventral extent of the gastrula: the far ventral gastrula predominantly produces mesodermal and non-neural ectoderm fates (Figure 2.10 C-F).

2.5 Discussion

2.5.1 The ventral fate map reveals progenitor domain organization

In this study we have generated a new fate map of the zebrafish ventral gastrula. Our 6 hpf fate map provides insight into the broad relationships between ventral progenitor domains and resolves their overall organization. For the first time, we have identified the origins of neural crest at all axial levels in the zebrafish. We find significant overlap in the progenitors of cranial neural crest and cranial placodes, two cell types that are key to vertebrate development and evolution. We have also demonstrated that a subset of cranial neural crest arises from a progenitor pool that is spatially segregated from neural tube progenitors. The locations of early progenitor domains for the full axial extent of ectodermal derivatives, including the neural crest, cranial placodes, central nervous system, and epidermis have now been mapped in detail. In Figure 2.11, we provide schematics synthesizing the primary features of this fate map. On a practical level, the information we have provided about early embryonic organization may guide transplantation experiments into the ventral gastrula and, of particular interest, into cranial or trunk neural crest domains.

Where there is overlap with cell types characterized in other zebrafish fate maps, our findings corroborate and often extend those previous reports (Kimmel, Warga, and Schilling 1990; Kozlowski et al. 1997; K. Woo and Fraser 1995). We add resolution to the germ layer fate map by clarifying the ventral embryonic domains that contribute to neural and non-neural ectoderm, as well as the somitic mesoderm (Kimmel, Warga, and Schilling 1990). While Woo and Fraser's neural fate map did not discriminate between neural crest, placode, and epidermal progenitors, the aggregate domain they reported for these three cell types fits with our findings (K. Woo and Fraser 1995). We expand upon the previous neural fate map, which did not attempt to map the posterior spinal cord, by identifying a broad domain that contributes to the spinal cord throughout the trunk and into the most posterior regions of the

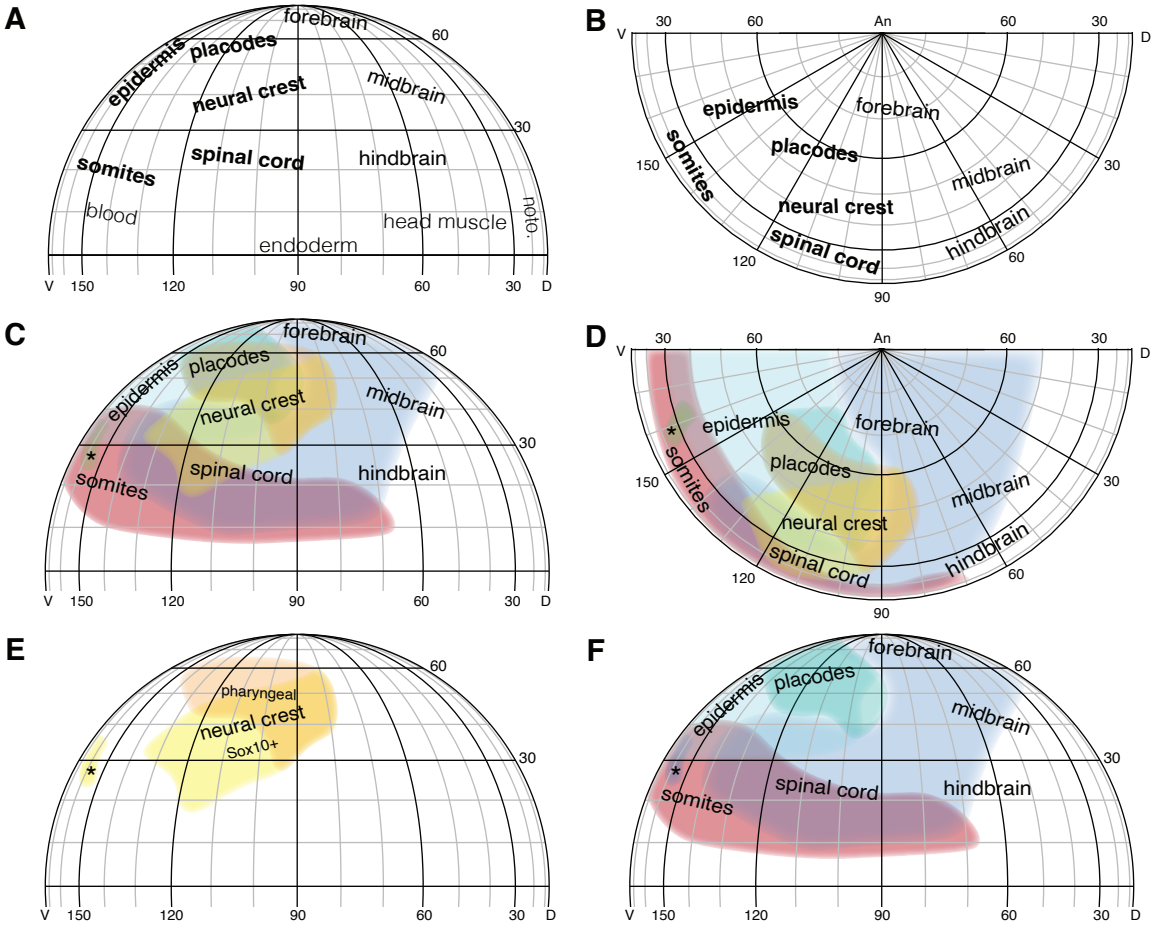

Figure 2.11: **Summary of the ventral fate map.** (A-B) Summary of updated fate map showing the general organization of the blastoderm in (A) lateral and (B) animal pole views. (C-D) Overlay of cell type domains mapped in this study in (C) lateral and (D) animal pole views. The extent of each domain is indicated by colored shading: yellow = Sox10+ neural crest; orange = pharyngeal neural crest; teal = placodes; blue = neural tube (labeled as forebrain, midbrain, hindbrain, spinal cord); pale blue = epidermis; and red = somitic mesoderm. Asterisk indicates the position of the far ventral mixed fate domain. (D) Sox10+ and pharyngeal neural crest domains together. (E) Epidermis, placodes, neural tube, and somite domains together.

tail (K. Woo and Fraser 1995). Our results highlight significant overlap between ectodermal and mesodermal tissues, with many regions contributing to both germ layers in trunk and tail. Our fate map additionally reveals a multi-fated ventral domain that will go on to form the most posterior part of the body.

2.5.2 Orderly arrangement within the neural crest progenitor domain

Our study provides a comprehensive description of the neural crest progenitor domain in the zebrafish gastrula. Importantly, we have identified sub-domains within the gastrula that contribute to cranial, trunk, and tail neural crest cells, and demonstrated that these have an orderly arrangement that predicts their later AP locations. Much of the cranial neural crest arises from a lateral domain of the gastrula, which explains why blastula cells transplanted into this sub-domain form cranial neural crest derivatives (Lister et al. 2006; H.-H. Yu and Moens 2005). The trunk neural crest arises from a relatively more marginal and ventral domain within the gastrula, with the most posterior neural crest population originating from a separate sub-domain on the far ventral side (Figure 2.11 E). While we cannot draw conclusions about vagal and cardiac neural crest derivatives, which are not identifiable at the stage of our analysis, we have situated the entire AP extent of the neural crest within the zebrafish fate map.

We can now consider how the newly-mapped neural crest progenitor domain fits into overall ectoderm progenitor organization. Zebrafish cranial ectodermal progenitors produce, from ventral to dorsal, epidermis, placodes, cranial neural crest, and neural tube cells. In general, the zebrafish fate map fits with accepted understanding of how ectodermal progenitors become organized at later stages to establish the cranial neural plate border (Thawani and Groves 2020). There is extensive overlap between the zebrafish cranial placode and neural crest progenitor domains at 6 hpf, revealing that the close relationship between these cell types is established early in zebrafish development (Figure 2.11 C and D). Placodes and

neural crest cooperate extensively to build the sensory organs and thus play critical roles in both development and evolution of vertebrate crania (Edens and Bronner 2024).

2.5.3 Developmental relationships between neural crest and neural tube

The neural crest is commonly described as a secondary cell fate that derives from the dorsal aspect of the developing neural tube (Baggiolini et al. 2015; Bronner-Fraser and Fraser 1988; D. W. Raible, Wood, et al. 1992; Rocha, Singh, et al. 2020). This model suggests that both neural crest cells and neuroepithelial cells arise from the same lineage. If this model is true at all axial levels, then every neural crest producing region in our fate map should also contribute to the neural tube. In the trunk and tail, our fate mapping data support the classical model, as Sox10+ neural crest always arose together with the neural tube at these levels. However, as several regions contributed to pharyngeal arch and cranial Sox10+ neural crest, but not to the neuroepithelium of the developing brain, the model is not sufficient to explain the origin of all cranial neural crest. While our region-based approach cannot directly uncover specific lineage relationships or address the potential of individual cells, analysis of cell fate contributions from small regions does provide insight into the range of cell fates that arise from small areas of the gastrula. If two cell types do not arise from the same region at 6 hpf, they cannot be related by lineage. Therefore, we can conclude that a substantial population of cranial neural crest must arise from an independent progenitor pool that is present within the 6 hpf gastrula.

Where our data show that cranial neural crest and neural tube arise from the same regions, there are a range of possible lineage relationships that may generate these tissues. It is possible that some sub-populations of cranial neural crest cells are more closely related to the neuroepithelium, while others arise from a separate progenitor pool. One hypothesis about the origin of cranial neural crest sub-populations, based on evidence from mice and other species, suggests that "authentic" neurogenic and pigment neural crest derivatives are

neuroectodermally-derived, while ectomesenchymal pharyngeal arch derivatives arise in a spatially-segregated "metablast" domain (Weston, Yoshida, et al. 2004; Weston and J. P. Thiery 2015). While there is some separation between pharyngeal and Sox10+ neural crest in the fate map, this model is not sufficient to explain our findings. Rather, both pharyngeal (primarily chondrogenic) and Sox10+ (neurogenic and pigment-producing) zebrafish neural crest progenitors can arise together from gastrula regions that do not produce neural cells.

A previous study has addressed the relationship between pharyngeal and neurogenic neural crest at a later stage. Single-cell lineage tracing experiments at 12 hpf, shortly after gastrulation concludes, have shown that pharyngeal and neurogenic (Sox10+) neural crest progenitor pools are spatially separated along the dorsoventral axis of the cranium (Schilling and Kimmel 1994). At this stage, the more dorsally localized neural crest cells are destined to produce cartilage and connective tissue of the pharyngeal arches, while the more ventrally localized neural crest cells produce neurogenic derivatives. We found a distinction between zebrafish Sox10+ and pharyngeal arch neural crest progenitors, which suggests that these fates are already becoming segregated at the onset of gastrulation. It will be interesting to investigate how the progenitor sub-domains of the 6 hpf embryo form the organized cranium of the 12 hpf neurula, and to understand the cell movements that connect these stages.

The fact that cranial neural crest can arise without neural tube, while trunk neural crest invariably arises with the neural tube, suggests regionalized differences in neural crest cell lineage. We hypothesize that there is a transition point along the AP axis, likely within the posterior hindbrain, where the canonical neural tube/neural crest relationship begins and extends into the posterior body. Anterior to this transition, the developmental relationships between neural crest sub-populations and the neural tube remain less clear. Our fate map has shown a ventral to lateral arrangement of placodes, pharyngeal arches, Sox10+ neural crest, and neural tube progenitors at the onset of gastrulation, which warrants further investigation in the context of later neural plate border formation and neurogenesis. Ultimately, single

cell labeling and lineage analysis at 6 hpf will be needed to definitively resolve relationships between the neural crest and related cell fates at all axial levels.

2.5.4 Cranial cell fate relationships across vertebrates

The organization of cranial placode, neural crest, and neural tube progenitors that we have documented in the zebrafish gastrula raises questions about how these cell types are related to one another in other vertebrate embryos. Previous fate maps for chick and Xenopus illustrate a broadly conserved spatial relationship between the developing neural tube and neural crest territories (Ezin, Fraser, and Bronner-Fraser 2009; Hatada and Stern 1994; Dale and Slack 1987). In the trunk, it has been established that individual cells in the chick and mouse dorsal neuroepithelium produce both dorsal neural tube and neural crest cells (Bronner-Fraser and Fraser 1988; Baggiolini et al. 2015). However, in the cranium, these relationships have not been rigorously evaluated across species. A comprehensive fate map of the anterior neural crest and dorsal neural tube has been generated for the chick gastrula (Ezin, Fraser, and Bronner-Fraser 2009), but without tracking the derivatives of individual cells, their precise lineage relationships remain unclear.

Following gastrulation, all cranial ectodermal cell types derive from the neural plate border. The molecular and morphological identity of the neural plate border has attracted significant attention (Schlosser 2010; Groves and LaBonne 2014; Streit 2025). Recent single cell sequencing analyses have suggested that the chick neural plate border is a highly heterogeneous cell population at gastrulation stages (A. P. Thiery et al. 2023; R. M. Williams et al. 2022). Detailed lineage tracing experiments and spatial analysis of gene expression, at gastrulation and neurulation stages, in a variety of vertebrates, would provide insight into lineage relationships and restriction of cell fate potential across species. Careful consideration of species-specific developmental trajectories, especially differences in developmental timing and axial regionalization, is required to explore homology of cell fate acquisition.

2.5.5 Signatures of morphogenesis within the fate map

Collecting detailed information about the final positions of labeled cells allows us to explore signatures of morphogenesis within the fate map. During gastrulation, convergence and epiboly movements generate flow within the embryo that establishes and elongates the primary body axis (Bhattacharya et al. 2021; Shah et al. 2019; M. L. K. Williams and Lilianna Solnica-Krezel 2020). Our fate map shows that progenitors of the most anterior and posterior structures are positioned close to each other in the ventral gastrula at 6 hpf. Around 8 hpf, these domains will rapidly separate from one another as the evacuation zone forms (Kimmel, Warga, and Schilling 1990; Kimmel, Ballard, et al. 1995). Recent imaging studies and tissue flow studies showing pan-embryo dynamics provide insight into the overall shape changes that occur during morphogenesis (Bhattacharya et al. 2021; Shah et al. 2019). During gastrulation, cranial progenitors swirl towards the animal pole, forming the complex structures of the head. The most posterior progenitors, which are located just marginal to where the evacuation zone will form, swirl vegetally during tailbud formation (Shah et al. 2019). In the future, it would be useful to study how anterior and posterior cell fates become distinguished during morphogenesis, in the context of the early embryonic organization we have described in this study.

The morphogenetic movements of gastrulation differ along the dorsoventral axis. These differing movements have been studied extensively in the mesoderm, which exhibits convergence movements on the dorsal and lateral sides and vegetally directed migration on the ventral side of the gastrula (M. L. K. Williams and Lilianna Solnica-Krezel 2020). The extensive axial spread that we have mapped from the lateral gastrula reflects convergence and extension movements of both mesoderm and ectoderm derivatives that form the trunk (Concha 2025). Our findings for the neural ectoderm are consistent with the previously described broad distribution of labeled neural clones along the AP axis (Kimmel, Warga, and Kane 1994). More posterior structures of the embryo are formed by morphogenetic movements

that differ from those that produce the trunk (Attardi et al. 2019; Kanki and Ho 1997; D. C. Myers, Sepich, and Lilianna Solnica-Krezel 2002). In addition to the most ventral cells moving vegetally into the tailbud during gastrulation, they also undergo complex movements during posterior extension (Kanki and Ho 1997; D. C. Myers, Sepich, and Lilianna Solnica-Krezel 2002; Ben Steventon, Duarte, et al. 2016; Stooke-Vaughan et al. 2025; Neaverson and Benjamin Steventon 2025).

Differences between ectodermal and mesodermal contributions along the body axis at 30 hpf reflect the fact that these germ layers follow different trajectories. During gastrulation, mesodermal progenitors internalize to form an inner layer that lies under the ectodermal progenitors. This process initiates as the shield and germ ring are forming, between 5 and 6 hpf, and continues as gastrulation progresses. Whole embryo time lapse imaging analyses have shown that the ventral mesoderm internalizes slightly later than the dorsal mesoderm (Keller et al. 2008). Our fate mapping strategy identified several ventral regions that produced somitic mesoderm exclusively, independent of any ectodermal fates. As our labeling strategy captured cells throughout the full thickness of the blastoderm, we can conclude that these labeled mesoderm cells were not yet positioned under the ectoderm. While our fate mapping study has focused largely on ectodermal derivatives, it also raises new questions about the details of ectoderm versus mesoderm germ layer specification along the dorsoventral axis.

Finally, our fate map has identified a small ventral domain, separate from the main neural tube and Sox10+ progenitor domains, that goes on to produce multiple tissue types within the most posterior part of the tail. This suggests that ectodermal and mesodermal cell types in the most posterior part of the tail develop from a multipotent progenitor population that is present at 6 hpf. We hypothesize that this distinct ventral domain is likely to contain neuromesodermal progenitors (NMPs) (Martin and Benjamin Steventon 2022). Further study of the far ventral gastrula will provide additional insight into the processes that drive formation

of the posterior body. The timing of germ layer specification and mesoderm internalization, cell fate specification within the small mixed posterior fate domain, and the morphogenetic trajectories of posterior progenitors, are of particular interest based on our findings.

2.5.6 Implications of the ventral gastrula fate map

Classical embryology approaches provide important information about early embryonic organization that can be integrated with modern imaging and molecular approaches. For example, our fate map data could be integrated with transcriptomics data to give insights into signaling and gene regulatory networks (Farrell et al. 2018; Xia et al. 2019; Wan et al. 2026). Lineage tracing would clarify the range of fates that arise from single progenitors, particularly within the heterogenous cranial and posterior ventral progenitor domains defined in this study. As each cell must undergo specific movements and pass through particular signaling environments, which are largely dictated by point of origin in the gastrula, considering the fate map together with data on morphogenesis and signaling would be especially informative. Integrating these different levels of information will generate a more complete understanding of the developmental mechanisms that produce complex body plans.

2.6 Supplemental Figures

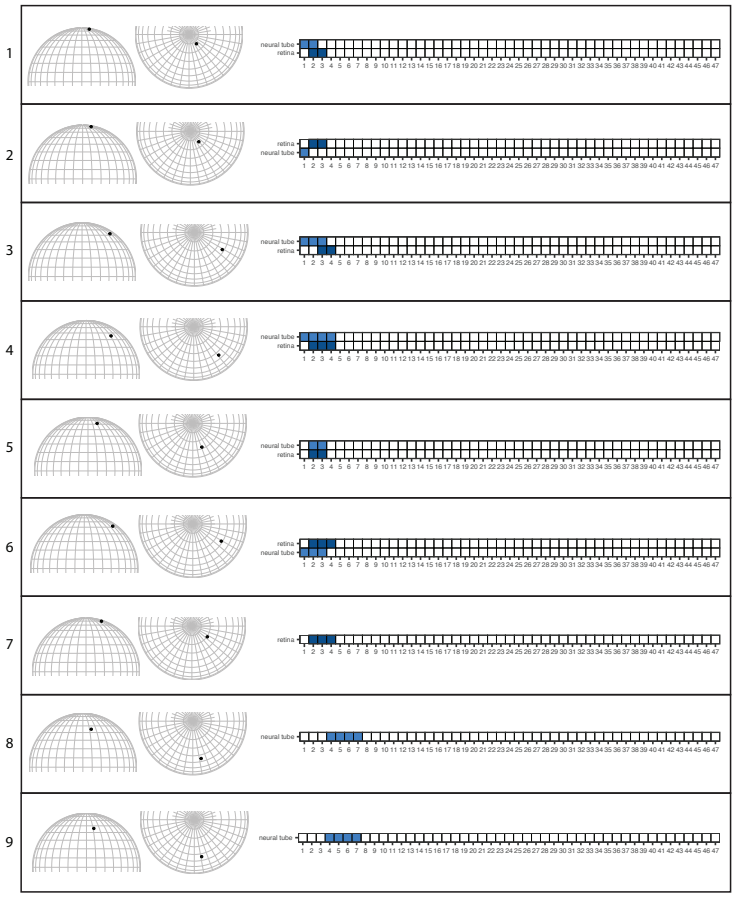

Figure 2.12: **Spreadplots for all 86 specimens.** The location of the labeled region in the 6 hpf gastrula indicated in lateral and animal pole views. Each spreadplot shows the axial extent of all cells documented for each cell type, with cell types shown in rank order (top ranked cell type shown first). Specimens are grouped by first ranked cell type and ordered by AP position: neural tube (and retina) only (1-18), neural tube(19-38), neural crest (39-46), cranial placodes (47-51), epidermis (62-69), somites (70-86).

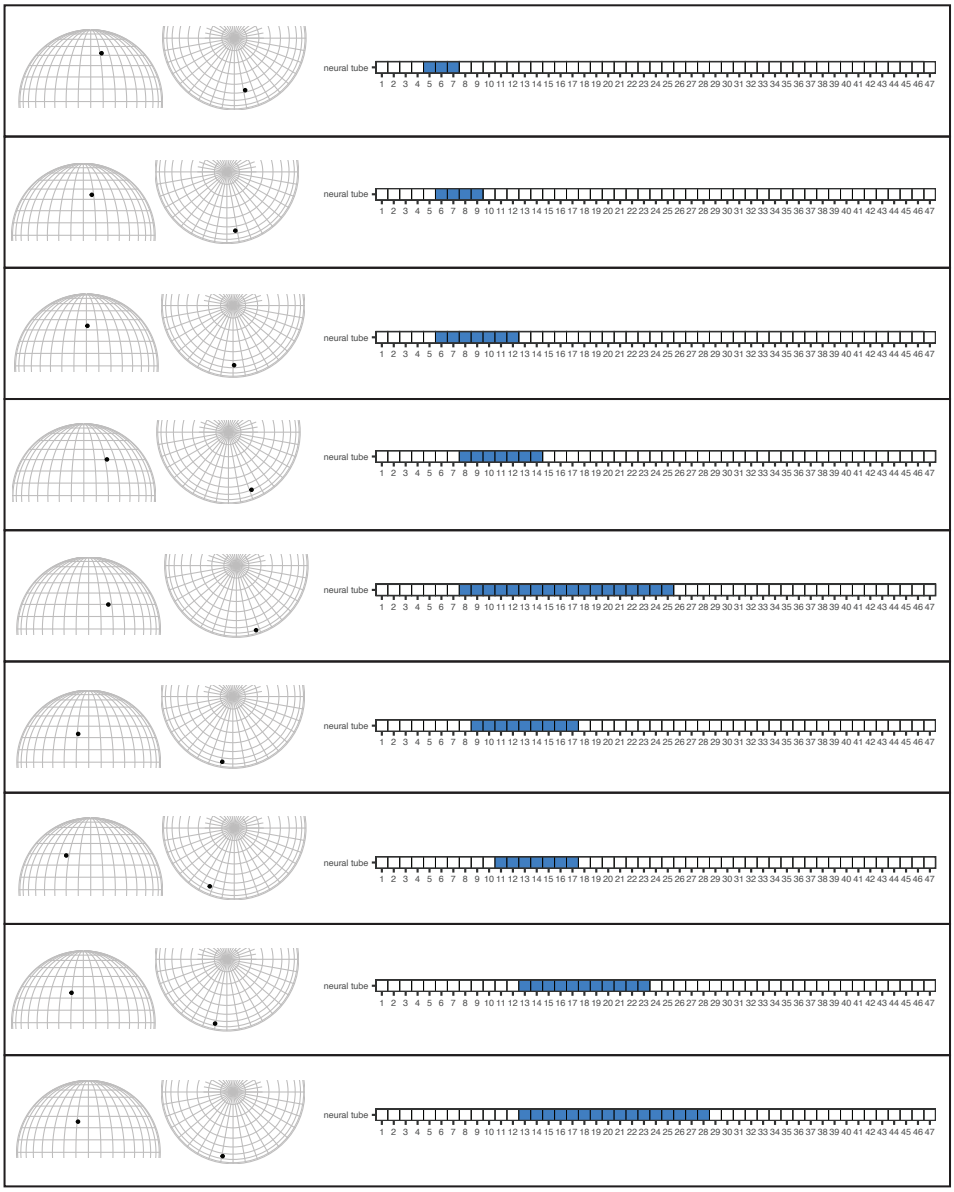

Figure 2.12: Continued.

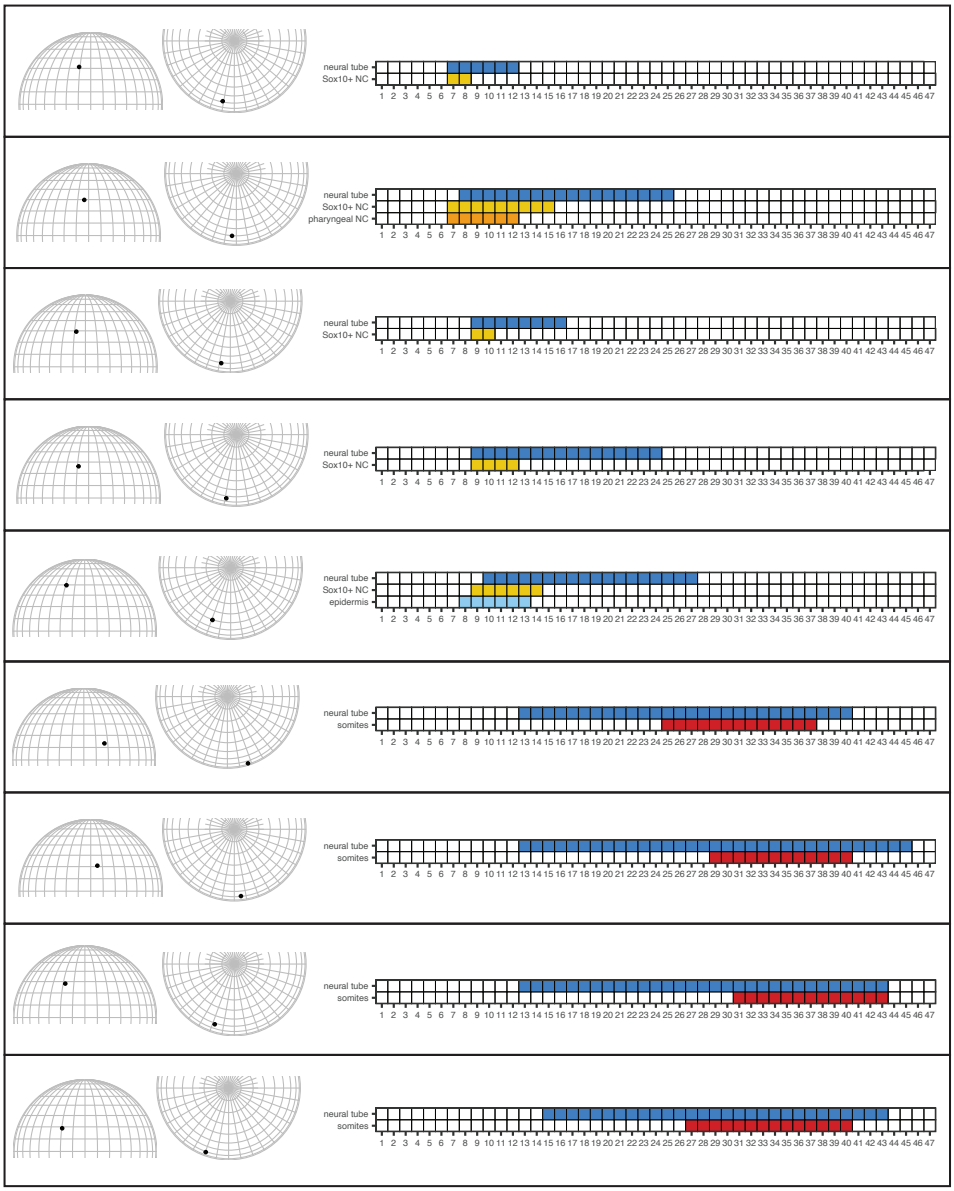

Figure 2.12: Continued.

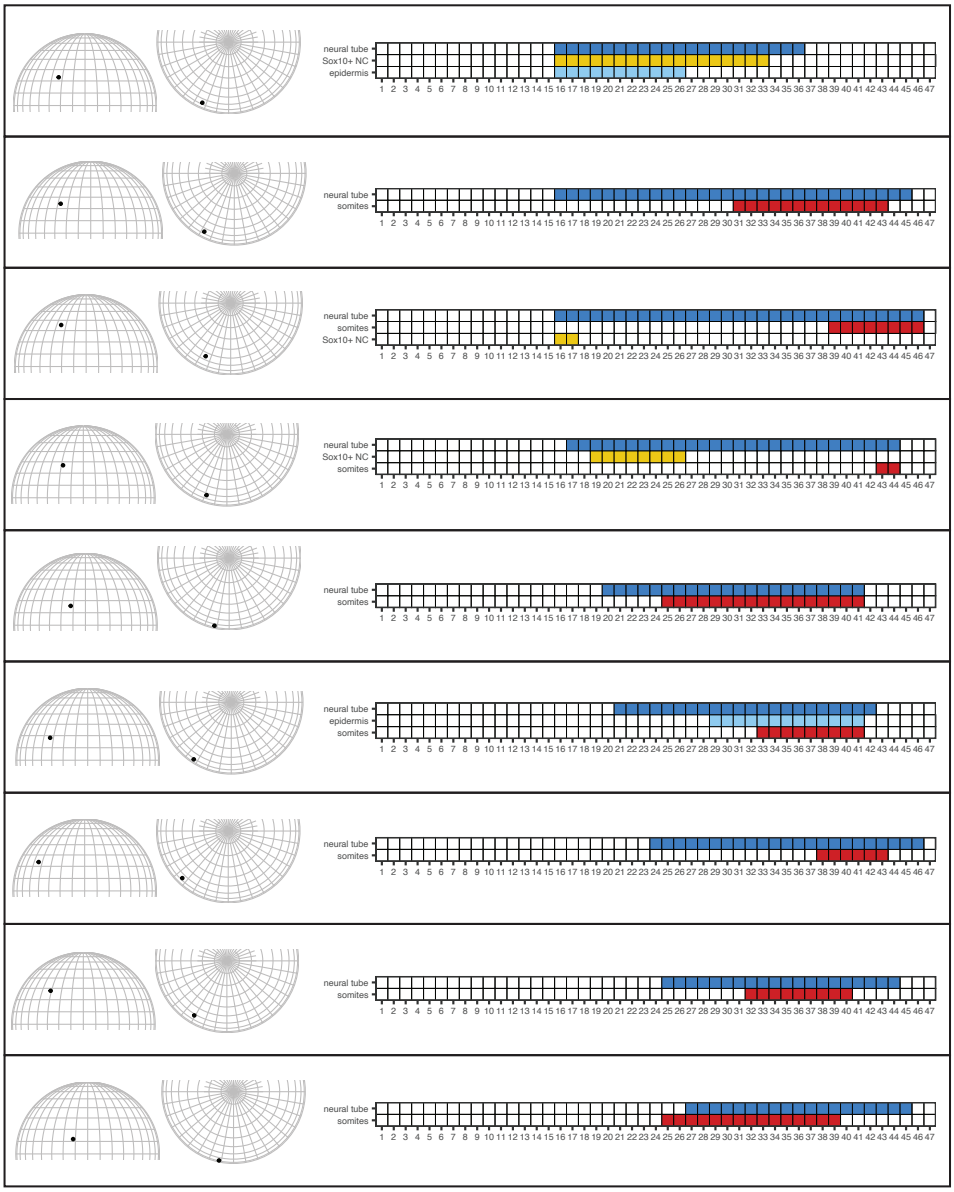

Figure 2.12: Continued.

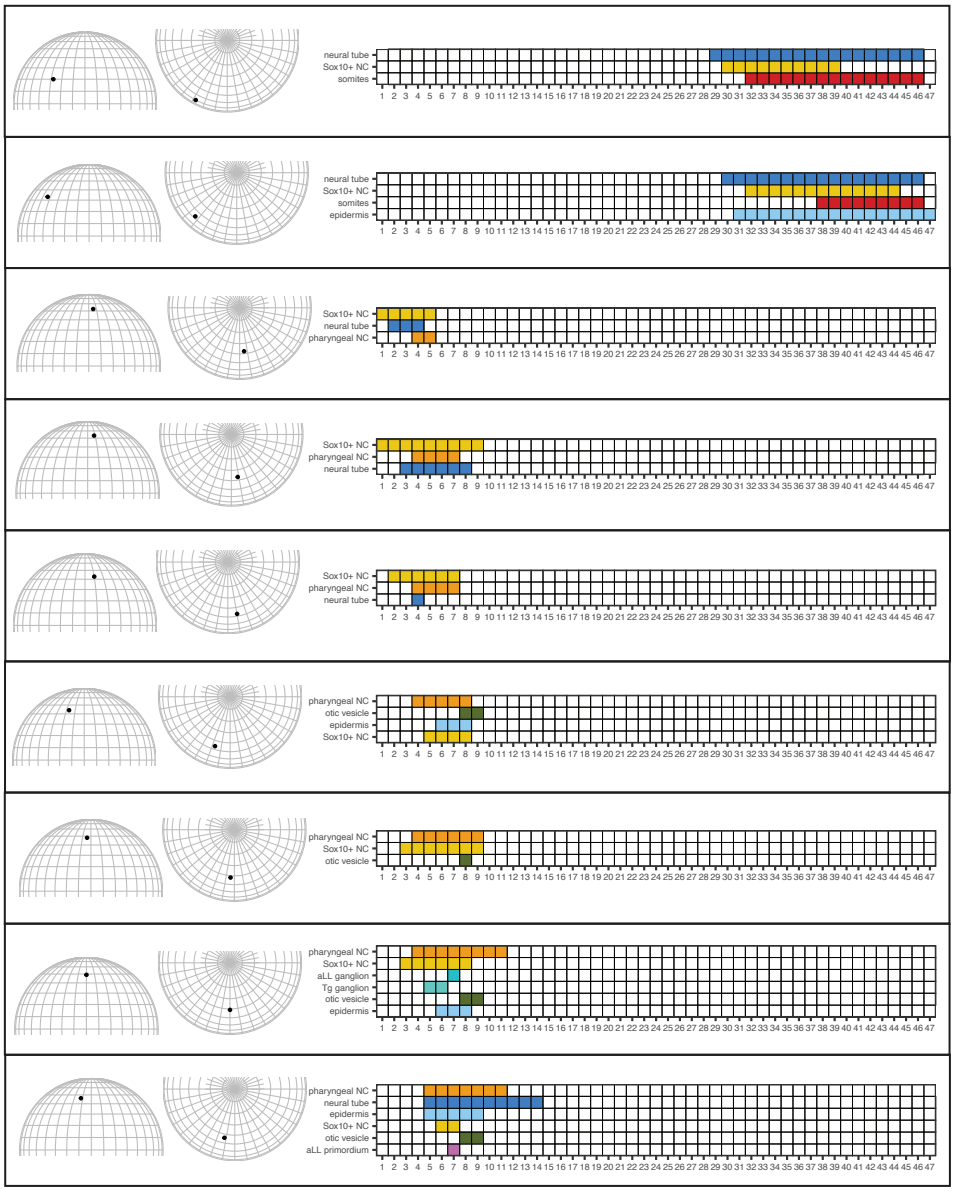

Figure 2.12: Continued.

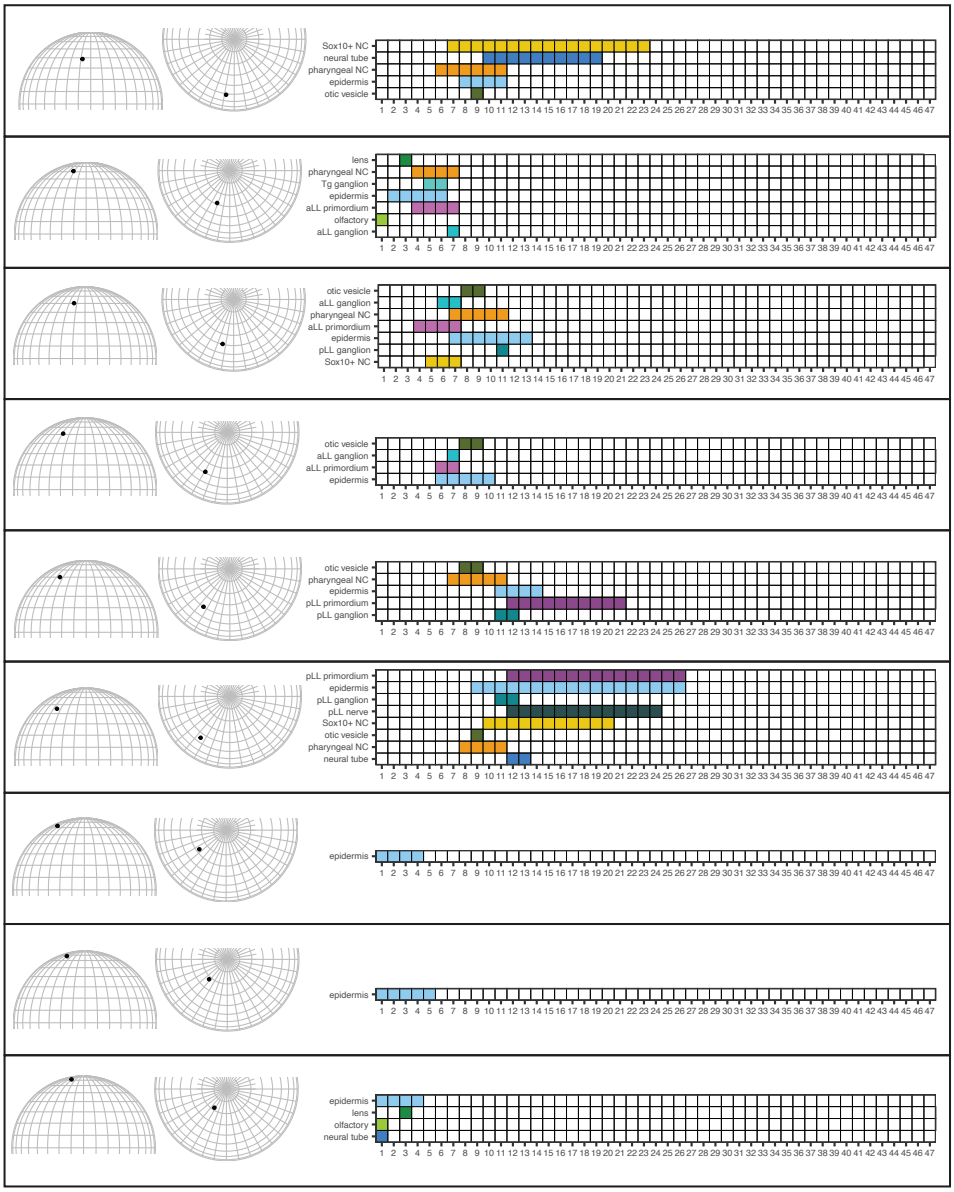

Figure 2.12: Continued.

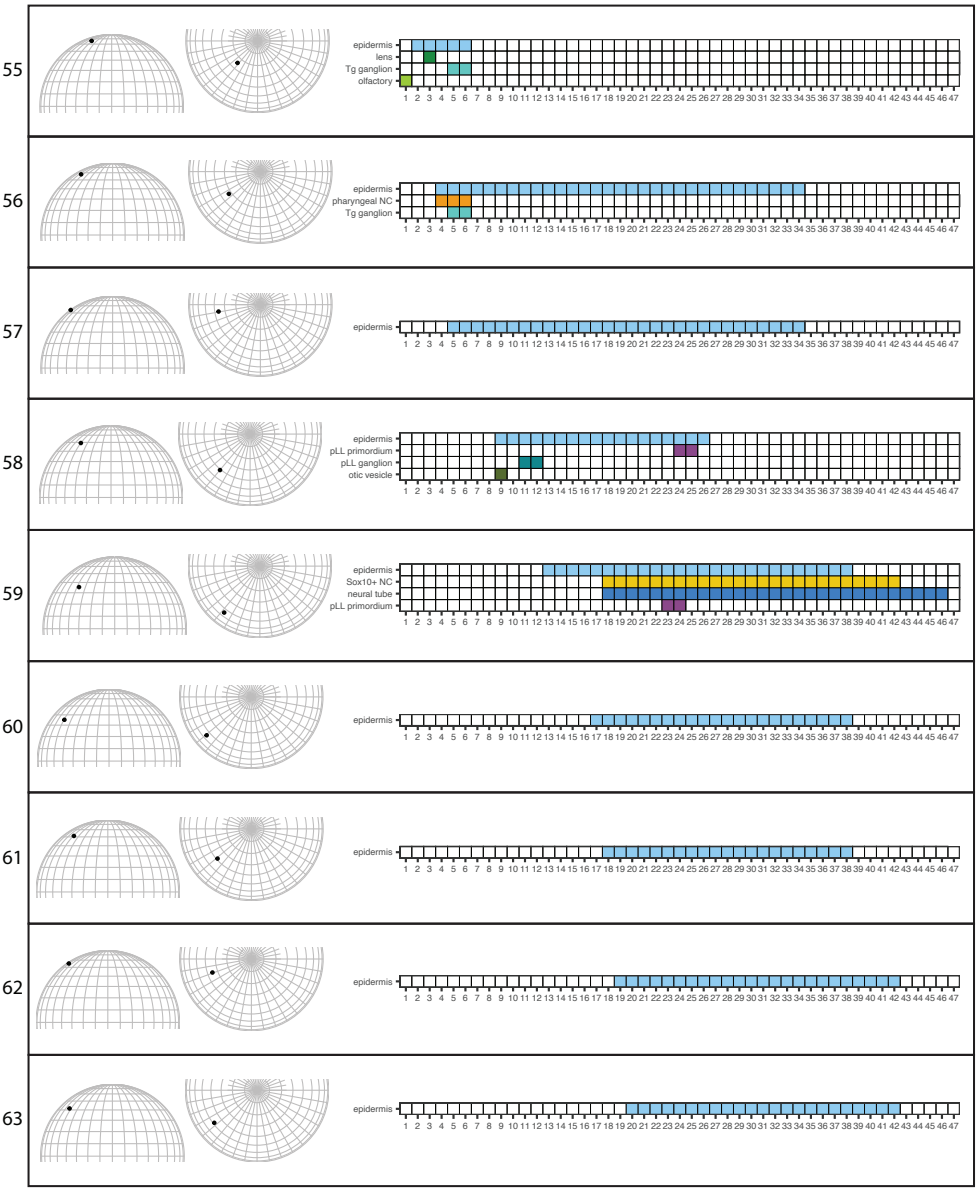

Figure 2.12: Continued.

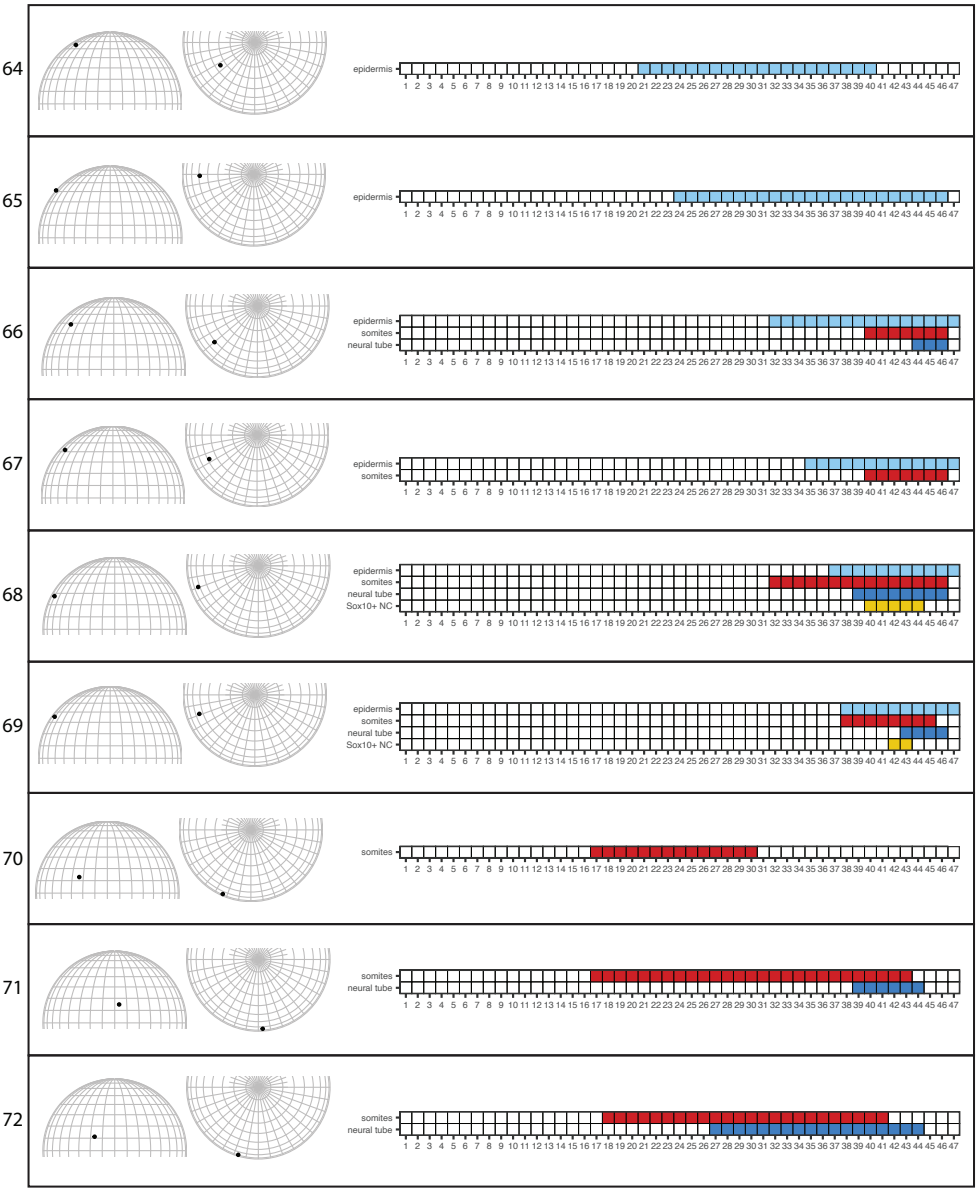

Figure 2.12: Continued.

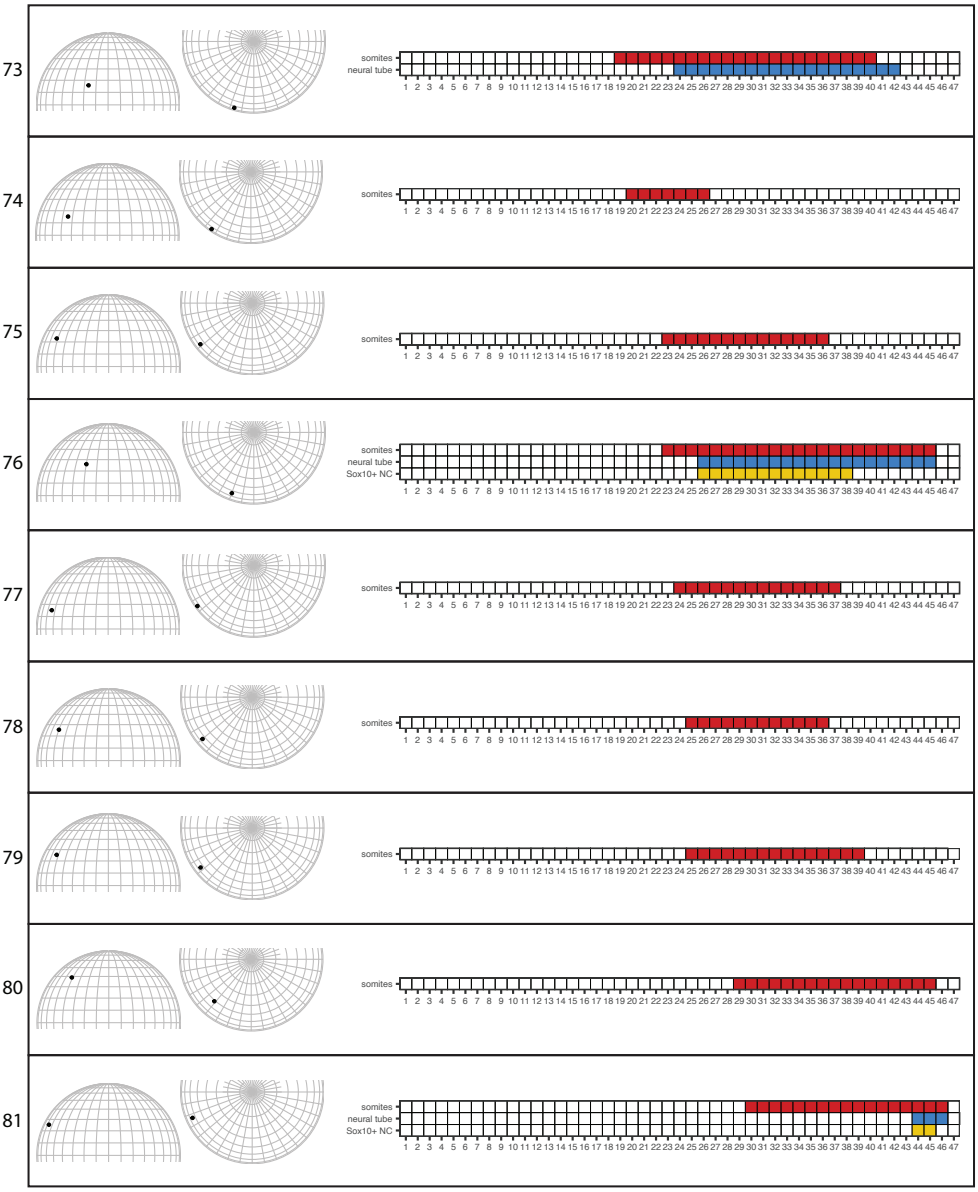

Figure 2.12: Continued.

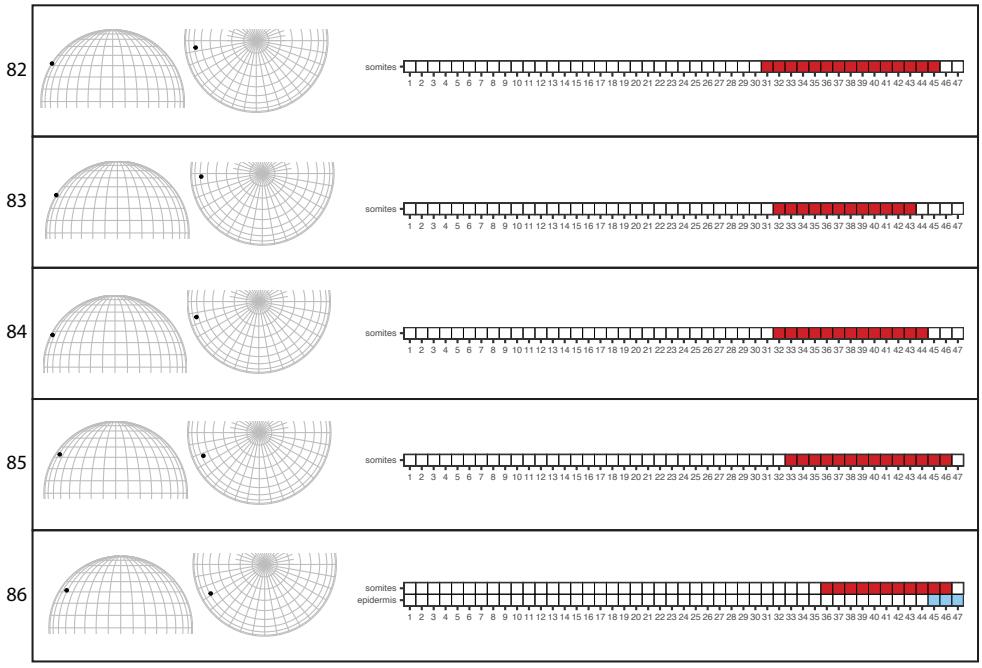

Figure 2.12: Continued.

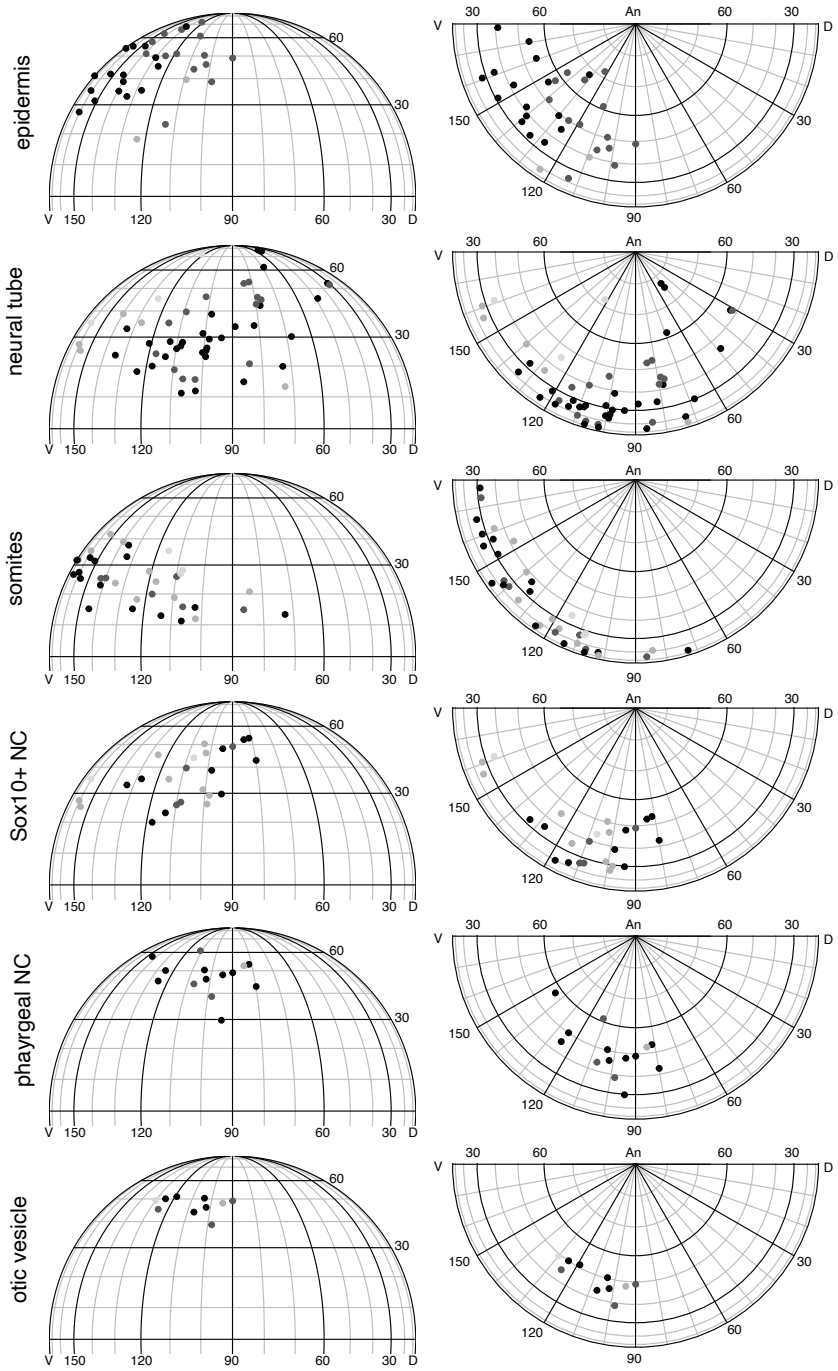

Figure 2.13: **Abundance of major cell types.** Fate maps for individual cell types indicating abundance of cells produced by each region, denoted as high (black), medium (dark gray), low (intermediate gray), and sparse (light gray). Both lateral and animal pole view fate maps are provided for each cell type shown.

CHAPTER 3

SIGNALING AND MORPHOGENESIS DURING GASTRULATION

3.1 Abstract

At the onset of gastrulation, cells integrate information from signaling activity and physical forces to determine their position within the embryo. Positional cues direct gene expression and morphogenetic movement responses across the blastoderm. Complex interactions between major signaling pathways, including BMP, Nodal, FGF and Wnt, pattern the developing embryo during gastrulation. While previous studies demonstrate that FGF signaling is involved in mesoderm induction and later posterior development, the role of FGF in patterning these structures during gastrulation had not been elucidated. I investigated the role of FGF signaling on cell type specification and morphogenesis at the onset of gastrulation. I perturbed FGF signaling at the onset of gastrulation using SU5402, an FGF receptor inhibitor, and characterized the broad scale morphological and gene expression pattern changes that resulted. My analysis focused on fates that derive from the ventral gastrula, including cranial neural crest and placodes, and posterior neural and mesodermal cell fates. When FGF signaling levels are reduced at the onset of gastrulation, embryos exhibit both a loss of tail and trunk structures and reduction of the cranial placodes and pharyngeal arch neural crest. Loss of FGF at the onset of gastrulation results in dysregulation of gastrulation movements and shifted expression of neural plate border and axial patterning genes. These findings suggest that FGF signaling plays a major role in regulating gastrulation movements in the ventral gastrula to ensure robust pre-patterning of the embryonic body plan.

3.2 Contributions

I would like to thank Patrick Byrne and Adam Kuuspalu for their collaboration on parts of this project. During his rotation in the Prince lab, Patrick assisted with performing HCRs for axial markers and neural plate border genes and imaging the resulting specimens. He also helped with live imaging experiments and phenotype identification. Adam assisted with early HCR experiments and contributed to image processing of the *Tg(His:GFP)* time series data. While I developed the experimental and analytical approaches for this research and performed a bulk of the experimental work in this chapter, this work was much improved by their contributions.

3.3 Introduction

Coordination of signaling and cell movements at the onset of gastrulation is essential for cell fate specification later in development. Gastrulation stage patterning is highly controlled in both development and evolution. While modes of gastrulation differ across species, core signaling pathways and gene regulatory networks are highly conserved (Nájera and Weijer 2023). Complex regulatory interactions between major signaling pathways and their effectors direct the formation of distinct embryonic domains, through differential control of gene expression and morphogenetic movements (Langdon and Mullins 2011). Gastrula stage fate maps clarify the relationship between positions in the early embryo and later developmental outcomes, as shown in Chapter 2 (E. E. Kushkowski and Prince 2026). However, fate maps do not provide direct information about the signaling pathways and morphogenetic processes that control embryogenesis.

At the onset of gastrulation, BMP, Nodal, Wnt, and FGF signaling provide positional information throughout the blastoderm (Agathon, C. Thisse, and B. Thisse 2003). A ventrolateral BMP gradient generated by antagonists from the dorsal organizer patterns the

dorsoventral axis. Short-range Nodal and long-range Wnt and FGF from the margin pattern the marginal-animal axis in the gastrula. The ratio of Nodal and BMP confers axial identity across the dorsoventral axis (Fauny, B. Thisse, and C. Thisse 2009). Working in combination, these overlapping signals produce highly stereotyped patterns of positional information at the onset of gastrulation (Agathon, C. Thisse, and B. Thisse 2003; Londin, Niemiec, and Sirotkin 2005; Garnett, Square, and Medeiros 2012). Cellular responses to positional cues drive changes in cell behavior, gene expression, and ultimately influence axial identity and cell fate later in development (E. J. Cooper and Scholpp 2024; Concha 2025).

At early stages, FGF is involved in formation of the dorsal organizer, germ layer specification, animal-marginal and dorsoventral patterning, as well as convergence-extension movements (Fürthauer et al. 2004). Wnt, BMP, and FGF signaling inputs are integrated across the ectoderm to establish the neural plate border (Garnett, Square, and Medeiros 2012; Esmaeli et al. 2024). The neural plate border forms at the interface between neural and non-neural ectoderm, and subsequently gives rise to both the neural crest and cranial placodes. Gastrulation-stage FGF signaling has also been shown to influence later pharyngeal arch development (Lin et al. 2013). BMP, Nodal, and FGF signaling at the onset of gastrulation modulate posterior development of mesodermal and ectodermal tissues (K. J. P. Griffin and Kimelman 2003; Kudoh, Concha, et al. 2004). Treatment with SU5402, an FGF receptor inhibitor, results in axial patterning defects and reduced mesoderm specification (K. J. P. Griffin and Kimelman 2003). Later in development, FGF signaling is important for formation of the midbrain/hindbrain boundary, somitogenesis, otic vesicle patterning, and many other functions (Reifers et al. 1998; Maier and Whitfield 2014).

Appropriate integration of signaling pathway inputs is essential for directing axial identity across the embryo and setting up later structures, including the neural plate border (for examples, see (Ben Steventon, Araya, et al. 2009; Groves and LaBonne 2014; Tuazon and Mullins 2015). Previous studies have shown that FGF has major roles in axial patterning

and mesodermal development by the end of gastrulation, but earlier effects of FGF signaling in modulating embryonic patterning and gastrulation dynamics remain less well understood. As both cranial placodes/neural crest and posterior neural and mesodermal structures arise from the ventral gastrula, I wanted to explore the role of early FGF signaling in setting up axial patterning and neural plate border formation. Building on my findings in Chapter 2, I hypothesized that ventral gastrula progenitor domains would be especially sensitive to FGF signaling perturbation at the onset of gastrulation.

To investigate the role of FGF signaling in morphogenesis and patterning of the embryonic body plan, I pharmacologically inhibited FGF signaling with the receptor antagonist SU5402, a reversible inhibitor that has been used to study FGF signaling in a variety of developmental contexts (Mohammadi et al. 1997). I assessed later phenotypes in live and fixed specimens to gain a better understanding of the morphological consequences of early FGF inhibition. I then characterized the specific effects of FGF signaling on morphogenesis and gene expression in the gastrula and neurula. I show that FGF signaling at the onset of gastrulation is important for regulating gastrulation movements and ventral gastrula fates. This work provides insight into one of the major signaling pathways that directs morphogenesis and cell type specification in the embryo.

3.4 Results

3.4.1 Methodological considerations for interpreting the effects of SU5402 treatment

From an experimental design perspective, the timing and concentration of SU5402 treatment have important consequences for interpretation of developmental outcomes. When studying signaling in the gastrula, precise timing of experimental manipulations is required because of rapid change during development. Collecting embryos within a 10-15 minute window

minimizes differences in stage between embryos of the same clutch. The timing of SU5402 treatment is also critical, as small changes in the developmental stage of FGF signaling inhibition have significant consequences. In the literature, a wide array of SU5042 concentrations and treatment regimens (e.g. (Kudoh, Concha, et al. 2004; Shimizu, Bae, and Hibi 2006; Ota et al. 2010) have been used to study the effect of FGF signaling, confounding the comparison of results across studies. Given the wide range of reported treatment concentrations, it is possible that different lots of SU5402 have dissimilar efficacy. In my experience, SU5402 loses activity over time, even when stored in appropriate conditions, and it is known to be light sensitive, making it a challenging reagent to use consistently across experiments and groups. Establishment of a dose response curve for each batch of SU5402 and checking for similar activity after storage periods are important steps for generating consistent and reproducible data with this pharmacological inhibitor.

3.4.2 Defining experimental conditions for FGF signaling inhibition in the gastrula

As my interest was in the effect of FGF on gastrulation, I tested a range of SU5402 concentrations and treatment timings to identify an experimental approach that would reliably inhibit FGF signaling at the onset of gastrulation (data not shown). I defined the following experimental approach based on these pilot experiments. SU5402 treatments were performed on embryos from the same clutch to minimize genetic and environmental variability. Embryos in their chorions were divided into groups in 12 or 24 well plates, then immersed in 1 mL of DMSO carrier control or SU5402 in E3 medium. Treatments started at 5.2 hpf and lasted for 45 minutes to provide a short pulse of FGF signaling inhibition. At 6 hpf, embryos were washed >3 times in excess E3 and transferred to a new well to prevent residual SU5402 from influencing development at later developmental timepoints. Embryos were incubated at 28.5°C until fixation at the desired stage(s). Embryos were fixed in 4% PFA overnight at

4°C and transferred to PBS for further processing. Immunohistochemistry and HCR were used to visualize specific cell types and gene expression patterns. I also performed time lapse imaging of *Tg(His:GFP)* embryos, in which all nuclei are labeled, to study the morphogenetic movements during early development.

The exact timescale over which FGF signaling was inhibited in these experiments is not clear. The SU5402 inhibitor binds non covalently to FGF receptors, and the interaction is thus expected to be reversible (Mohammadi et al. 1997). Previous washout experiments have shown that FGF inhibition is indeed transient, with signaling reactivated in the order of hours in the case of posterior lateral line primordium migration (Lecaudey et al. 2008).While the exact timing of FGF inhibition and reactivation has not been clearly defined in this system, I think that the capacity for FGF signaling activity is likely to return by 7 hpf in my pulse-treatment set up. However, it is unknown if the timing of signaling reestablishment may be influenced by the concentration of SU5402 used. Nevertheless, in my experiments signaling activity was restored to varying degrees at all SU5402 treatment concentrations used, suggesting that the phenotypes I have described are not the result of ongoing inhibition of FGF signaling after washout.

I documented slight variations across SU5402 treatments of the same concentration between experiments. These variations were expected, as application over a wide range of concentrations in other studies similarly gave variable results. It is likely that phenotype strength at a given concentration is influenced by the production lot, age and storage conditions of the reagent among other variables. The effects of these variations were minimized, when possible, by using multiple concentrations of SU5402 in each experiment and using embryos from the same clutch when making comparisons between treatments.

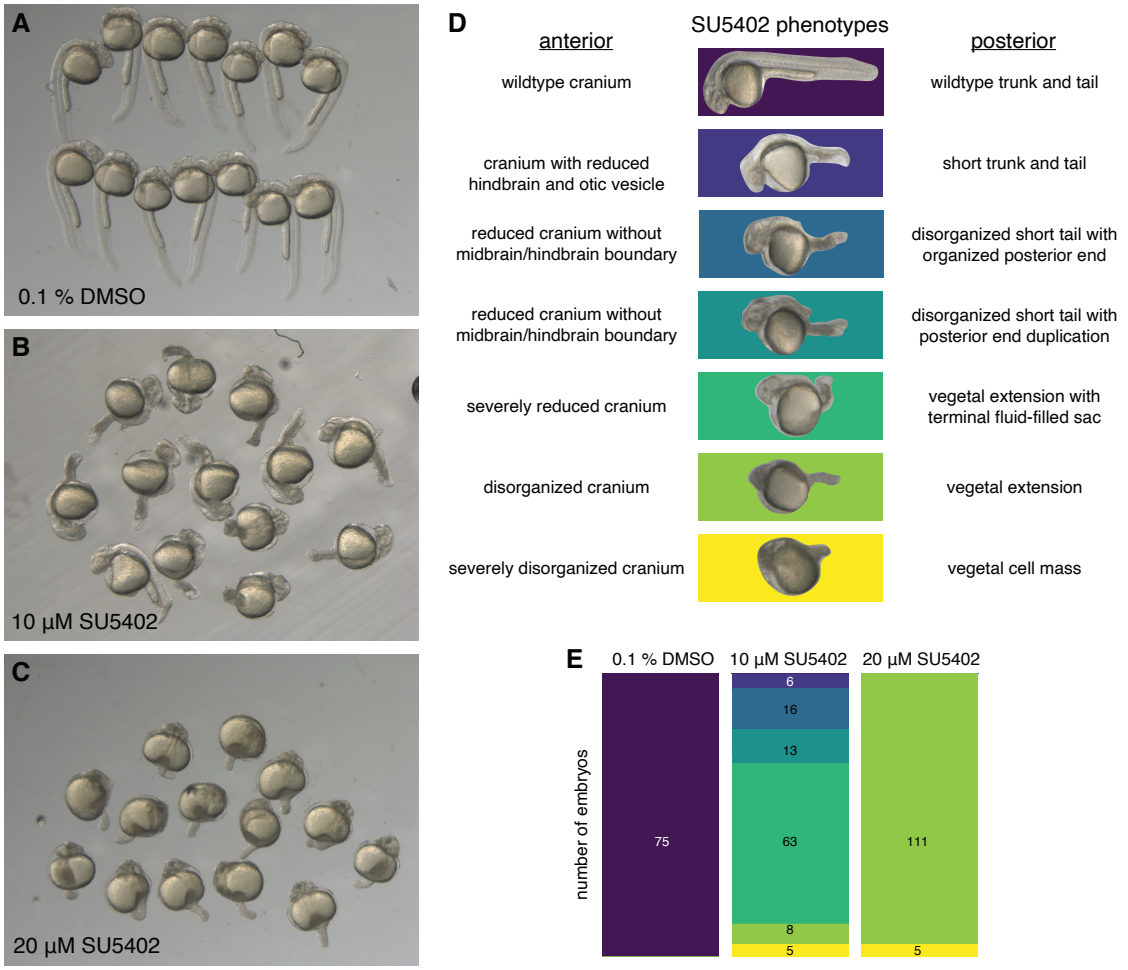

Figure 3.1: **Gross morphological consequences of inhibiting FGF signaling at gastrulation onset.** FGF signaling was transiently inhibited at the onset of gastrulation by treatment with SU5402 inhibitor between 5.2 and 6 hpf. Specimens were imaged under a dissecting microscope and evaluated for gross morphological defects at 30 hpf. (A-C) Low-magnification images of embryo clutches at 30 hpf. (A) 0.1% DMSO carrier treated control specimens show normal morphology, including an elongated trunk and tail, an elongated hindyolk extending from the spherical yolk ball, and a well-developed cranium with visible eye, otic vesicle, and midbrain-hindbrain boundary. (B) 10 µM SU5402 treated specimens were reduced in AP length, frequently lack a hindyolk extension, showed kinking or buckling of the trunk posterior to the yolk, disorganized tails, heart edema, and a disorganized cranium that lacked a clear midbrain-hindbrain boundary. (C) 20 µM SU5402 treated specimens were dramatically reduced in AP length, highly dysmorphic, lacked a normal tail and instead had a vegetal extension or cell mass, as well as dramatically reduced cranial structures. (D) Representative examples of 30 hpf phenotypes, with phenotypic classes color coded. (E) Quantification of the proportion of embryos in each phenotypic class by treatment condition; the number of embryos in each class is indicated.

3.4.3 FGF signaling inhibition at the onset of gastrulation causes abnormal morphology at 30 hpf

My initial experiments used the pulse-inhibition approach described above to study how inhibition of FGF signaling at the onset of gastrulation altered embryo morphology at 30 hpf. I identified a concentration-dependent range of phenotypes in embryos treated with SU5402 between 5.2 and 6 hpf (Figure 3.1). Treatment with 0.1% DMSO carrier control did not alter embryo morphology at 30 hpf, while treatment with 10 µM and 20 µM SU5402 resulted in dysmorphic morphology along the entire body axis (Figure 3.1 B-C). Specimens treated with a pulse of 10 µM SU5402 exhibited cranial phenotypes including reduced or disorganized cranial structures and loss of the midbrain-hindbrain boundary. These specimens also exhibited a wide range of posterior phenotypes, ranging from short tails with distinguishable somites to vegetal extensions with no distinguishable features. The most common posterior phenotype at this concentration was an elongated vegetal extension with a fluid-filled cavity at the terminal end. At 20 µM SU5402, specimens exhibited reduced and disorganized cranial structures and, in the posterior, vegetal extensions or cell masses.

The range of phenotypes that resulted from SU5402 treatments indicates that the reduction or absence of FGF signaling at the onset of gastrulation has somewhat variable, yet severe, consequences for overall body patterning and morphogenesis. As FGF signaling was inhibited early in gastrulation, these phenotypes are the culmination of altered axial patterning and cell movements during gastrulation. The range of phenotypes in the 10 µM SU5402 treatment group suggests that FGF signaling may be reduced but not completely blocked at this concentration. In these specimens, I observed that embryos with larger yolks tended to develop less severe phenotypes that retained some posterior organization, such as short tails or disorganized short tails. By contrast, embryos with smaller yolks tended to exhibit more severe phenotypes that impacted the full AP extent of the body. The phenotypes I observed are similar to those described in a similar experiment in *Xenopus* (Delaune, Lemaire,

and Kodjabachian 2005). In the future, it would be useful to quantify these differences and investigate the underlying mechanisms. At 10 and 20 µM SU5402, the vegetal extension phenotype is particularly interesting, because these structures lack any resemblance to normal tail morphology. This observation raised the question of whether these structures form by a similar mechanism to normal tailbud extension, a topic I return to below.

3.4.4 Loss of FGF signaling causes defects in neurulation and somitogenesis at 24 hpf

To characterize the effect of early FGF signaling on later embryo morphology in more detail, I treated embryos with a range of SU5402 concentrations (5, 10, 15, 20, 25 µM SU5402) and fixed specimens at 24 hpf. Specimens were stained with the nuclear label DAPI to reveal overall morphology and immunolabeled for Sox10 and Myosin heavy chain (Myhc) to reveal neural crest and muscle specification, respectively. Figure 3.2 shows multichannel images of two representative specimens from each treatment group in lateral and dorsal views, while Figures 3.3, 3.4, and 3.5 provide additional detail with single channel images of the same embryos. Overall, embryo morphology mirrored the phenotypes seen in Figure 3.1, with increased loss of cranial and posterior structures at higher concentrations of SU5402 (see Figure 3.2 legend for detailed description of phenotypes). In specimens treated with 5 to 15 µM SU5402, DAPI staining revealed progressive shortening of the neural tube. In specimens treated with lower concentrations (5-10 µM SU5402), the neural tube typically terminated adjacent to the posterior limit of the yolk, and occasionally neural tube organization briefly resumed further posterior (Figure 3.3 F). I observed that neural structures were similarly truncated in 15 to 25 µM SU5402 specimens, and there was also progressive loss of other cranial organization, including pharyngeal arches and cranial placode-derived sensory structures (Figure 3.3 G-L).

Immunolabeling for Sox10 revealed that Sox10+ neural crest cells were present in all treat-

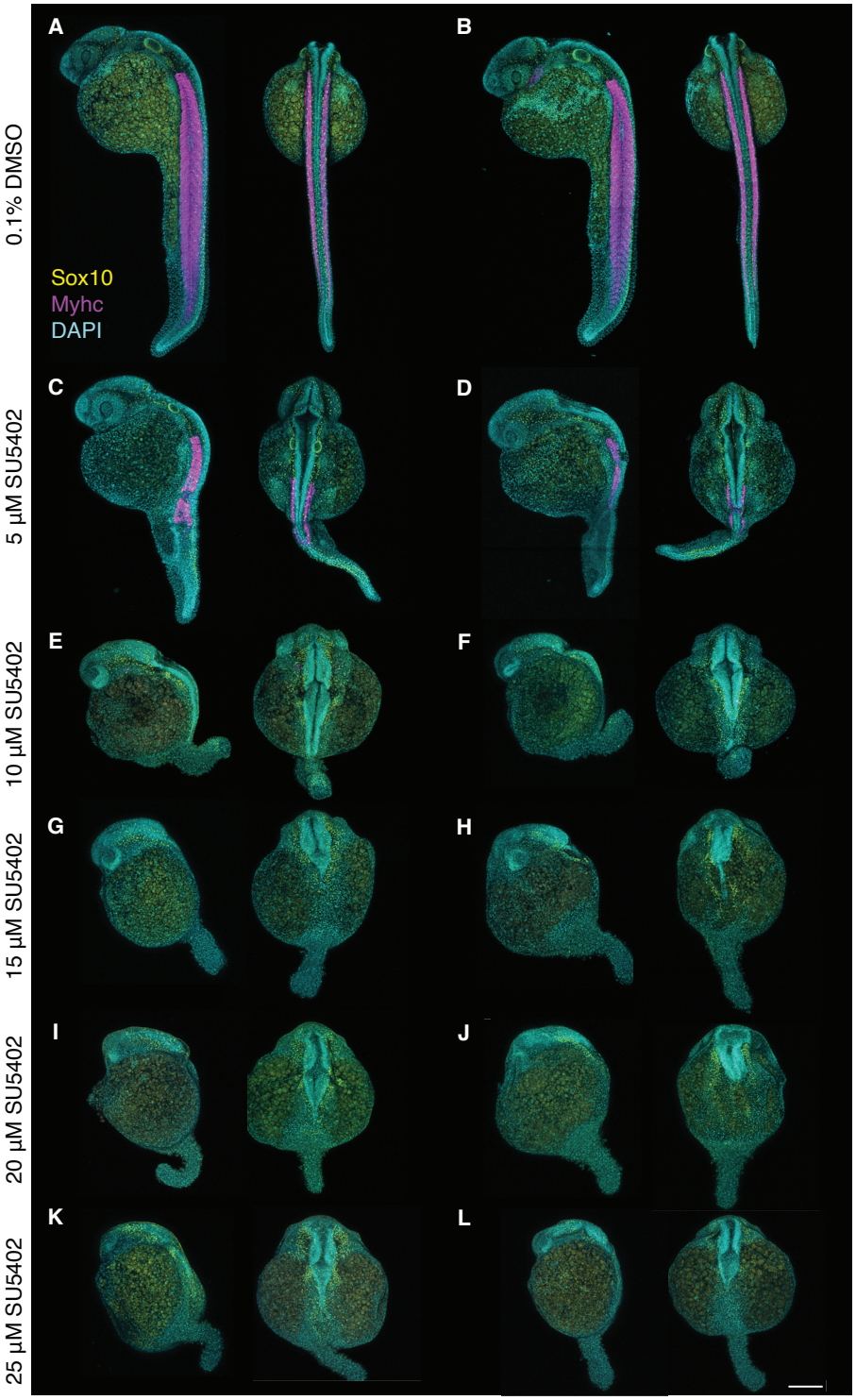

Figure 3.2: See next page for caption.

Figure 3.2: **Loss of FGF signaling at the onset of gastrulation affects axial patterning and cell type specification.** FGF signaling was transiently inhibited at 5.2-6 hpf using SU5402 inhibitor, specimens were incubated to 24 hpf and processed for immunolabeling. Muscle cells were labeled with anti-Myosin heavy chain (Myhc) antibody (magenta); nuclei of neural crest cells were labeled with anti-Sox10 antibody (yellow; with exception of pharyngeal arch neural crest, which does not express Sox10 at this stage); specimens were counterstained with DAPI to show all nuclei (cyan). Two representative examples of whole embryos (confocal maximum projections, imaged using a 10x objective) are shown for each treatment condition, scale bar= 200 µm. (A, B) 0.1% DMSO carrier treated control specimens showing segmentally organized elongate muscle cells in the somites (magenta), and neural crest cells (yellow nuclei) along the AP extent of the embryo, including dorsally localized pre-migratory neural crest and migrating cells that lie more ventrally. (C, D) 5 µM SU5402 treated specimens showing characteristic shortening of the posterior of the embryo, muscle cells are retained in the anterior trunk but show disruptions along the AP axis and are absent in the posterior, neural crest cells are present along the entire AP extent of the embryo. (E, F) 10 µM SU5402 treated specimens, showing more drastic morphological disruptions, including lack of a normal tail and a reduced cranium. Muscle cells are largely absent, but neural crest cells are present along the trunk and in the cranium. The cranial neural crest cell population is at increased density relative to untreated specimens. (G, H) 15 µM SU5402 treated specimens. (I, J) 20 µM SU5402 treated specimens. (K, L) 25 µM SU5402 treated specimens. As the SU5402 treatment concentration was increased, the embryos were progressively more truncated in the posterior and became increasingly dysmorphic. Neural crest cells were retained in all specimens but became increasingly limited to the cranial region. For additional details, see single channel images in Figs. 3.3, 3.4, and 3.5.

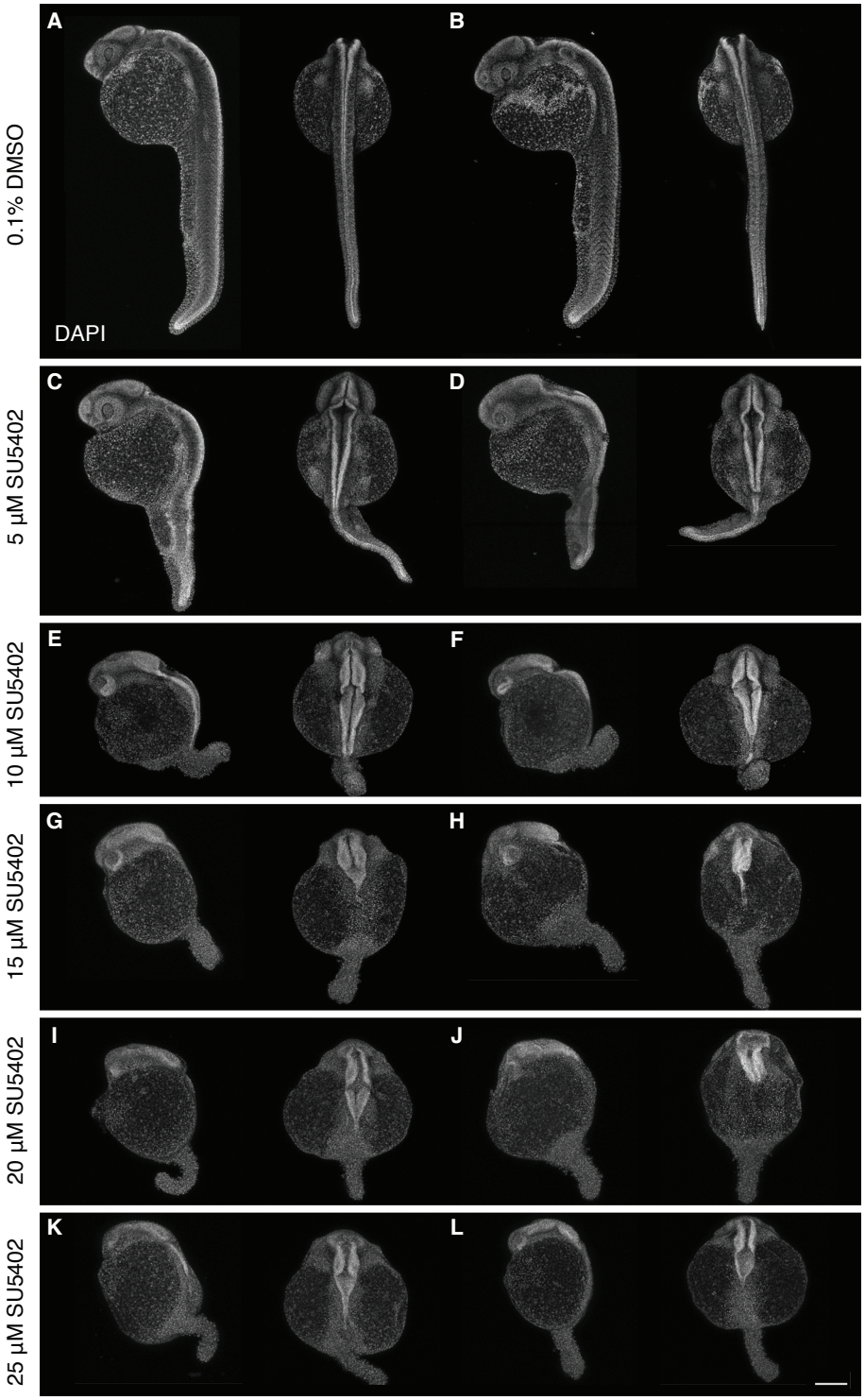

Figure 3.3: **DAPI single channel images from Fig. 3.2.**

ment conditions (Figure 3.4 A-L). At 5 µM SU5402, a migratory Sox10+ neural crest population in the cranial region invaded the zone where the Sox10-negative pharyngeal arch neural crest normally resides (Figure 3.4 C, D). The pharyngeal arch neural crest sub-population and otic vesicle were both reduced in these specimens, consistent with their similar spatial origins in the fate map (Chapter 2). In the anterior trunk, ectopic neural crest cells were visible laterally, likely because of migration out of the reduced trunk and out over the yolk ball. In untreated specimens, there was a pre-migratory neural crest population that extended into the tail in conjunction with the neural structures. More migratory neural crest was visible in the trunk and tail in the specimen shown in Figure 3.4C, while the neural crest appeared to be specified but not migratory in the specimen shown in Figure 3.3D. At 10 µM SU5402, the Sox10+ neural crest population expanded laterally in the cranium and was present adjacent to the neural tube in the anterior trunk (Figure 3.4 E, F). The Sox10+ neural crest population extended past the truncated neural tube into the posterior in these specimens. Some organization was retained within the vegetal extension at this concentration, and the presence of Sox10+ cells suggests that dorsal vegetal extension cells can be biased toward neural crest fate. At 15 µM SU5402 and above, the cranial Sox10+ neural crest population exhibited migration defects, and Sox10+ cells in the hindbrain/trunk showed further limitation to a smaller proportion of the body axis, and were not present in posterior structures (Figure 3.4 G-L). These data support a model in which FGF signaling at the onset of gastrulation plays a role in appropriate allocation of cells into Sox10+ and pharyngeal arch neural crest sub-populations.

In accord with previous studies, I observed that inhibition of FGF signaling led to major disruptions in mesoderm development (Figure 3.5 A-F) (K. J. P. Griffin and Kimelman 2003). Immunolabeling for the muscle cell marker Myhc showed that 5 µM SU5402 treatment caused asymmetric somite defects, including occasional gaps in the AP organization of the somites, and consistent loss of posterior somitic muscle cells (Figure 3.5 C-D), while nearly all muscle

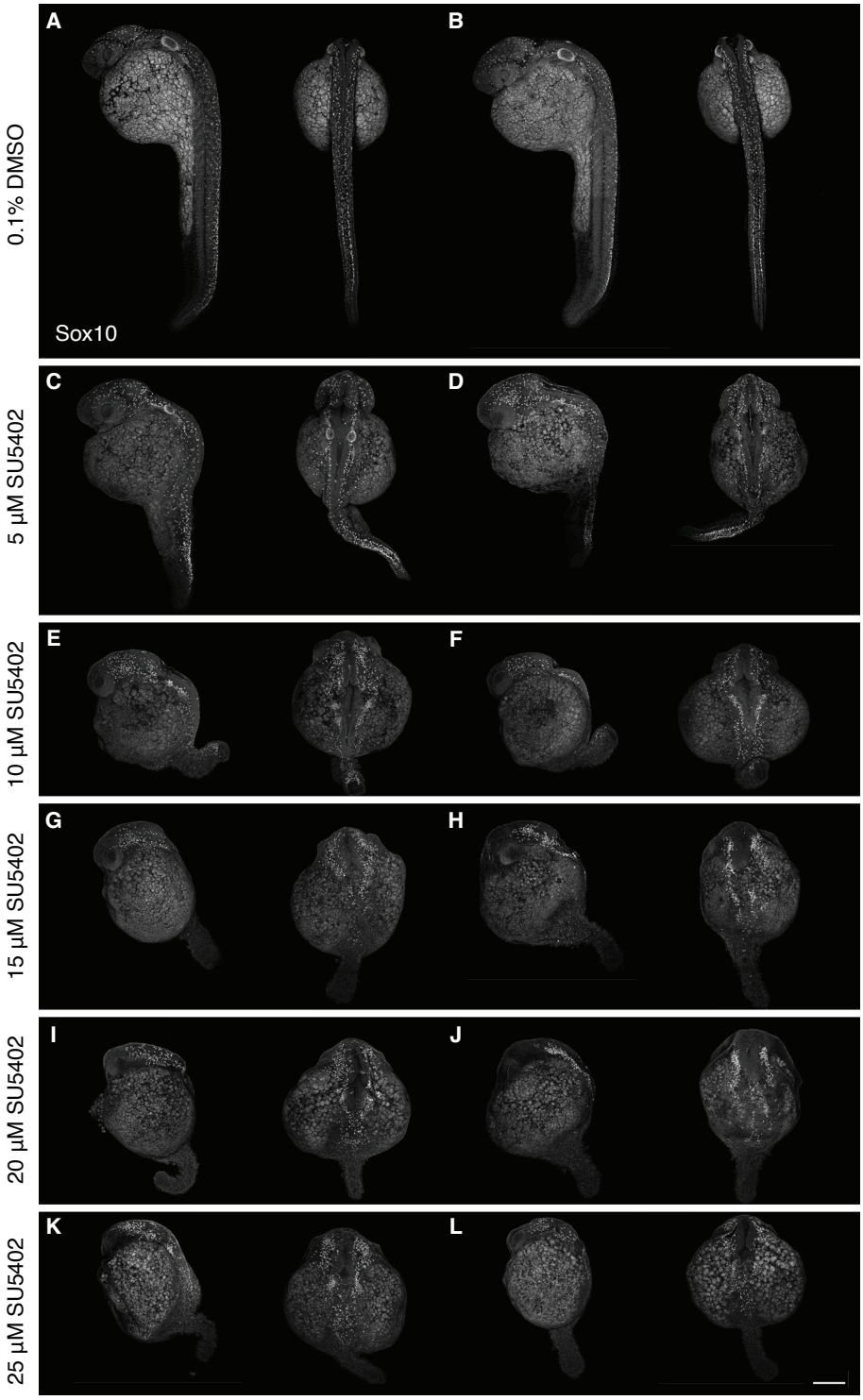

Figure 3.4: **Sox10 single channel images from Fig. 3.2.**

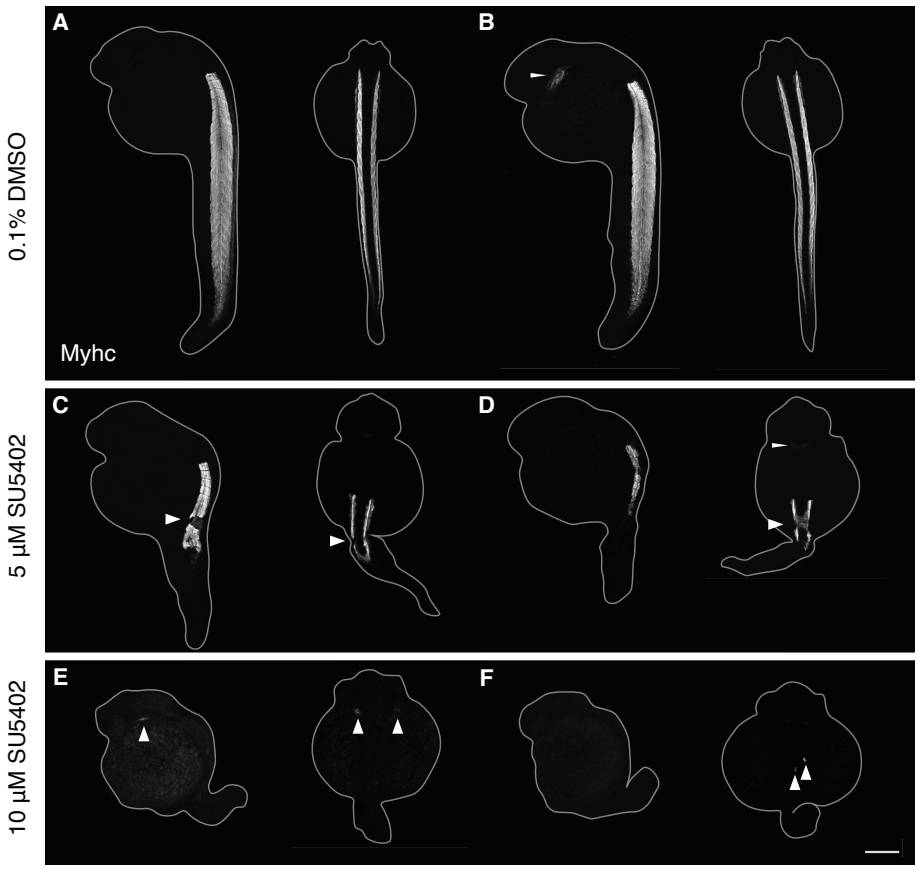

Figure 3.5: **Myosin heavy chain single channel images from Fig. 3.2.** Data for 15-25 µM SU5402 treatments omitted because there was no Myhc expression at these concentrations.

was lost at 10 µM SU5402 (Figure 3.5 E-F). In response to treatment with 15 µM SU5402 and above, there was a complete loss of muscle cells. While not revealed directly by this expression analysis, the changes in morphology suggest that both mesoderm and endoderm failed to develop in these specimens. Taken together, these results demonstrate that reduction or loss of FGF signaling at the onset of gastrulation causes significant loss of major germ layer derivatives and overall axial patterning by 24 hpf. To investigate when during development these defects begin to appear, I next focused on characterizing the developmental processes that are affected by FGF inhibition at the onset of gastrulation.

3.4.5 Wildtype ventral gastrula morphogenesis and formation of posterior structures

Morphogenetic movements have been generally well documented in the zebrafish gastrula, however, there has been less of a focus on ventral gastrula morphogenesis than on the dorsal side. I therefore performed live imaging in *Tg(His:GFP)* specimens, in which all cell nuclei are fluorescently labeled, to observe the broad morphogenetic movements that occur between shield and segmentation stages (Figure 3.6 A, B). Starting with lateral and animal pole views between 6 hpf and 11 hpf, I observed complex swirling movements within the gastrula that drive separation of cranial and posterior progenitors (Shah et al. 2019). By 8 hpf, the evacuation zone has begun to become morphologically apparent on the ventral side of the gastrula, as cranial and posterior progenitors have begun to follow different morphogenetic trajectories. By 9 hpf the dorsal half of the embryo was characterized by increased nuclear density and there was reduction in nuclear density within the ventral-animal quadrant. Between 9 and 11 hpf, rotational tissue flow brought cells from the ventral cranial progenitor domain into apposition with dorsally derived neural progenitors as they shift ventrally past the animal pole. By 11 hpf, the anterior is characterized by a thickened neural plate border, forming in a horseshoe shape at the edge of the neural plate. In the vegetal third of the embryo, posterior progenitor cells are less condensed and occupy a broad domain lateral to the dorsal midline.

Looking from the vegetal pole, starting at 8 hpf, I observed that yolk syncytial layer (YSL) nuclei were present in advance of the entire margin (Figure 3.6 E), with an increased density of forerunner cell nuclei indicating the location of the dorsal midline (D'Amico and M. S. Cooper 2001; Moreno-Ayala et al. 2021). The margin uniformly progresses towards the vegetal pole, forming a yolk plug by 9 hpf and leaving just a slight opening by 9.5 hpf. Prior to yolk plug closure, the opening shifts ventrally because of the swirling movements that initiate tailbud formation and posterior extension. By 10.5 hpf, organization at the

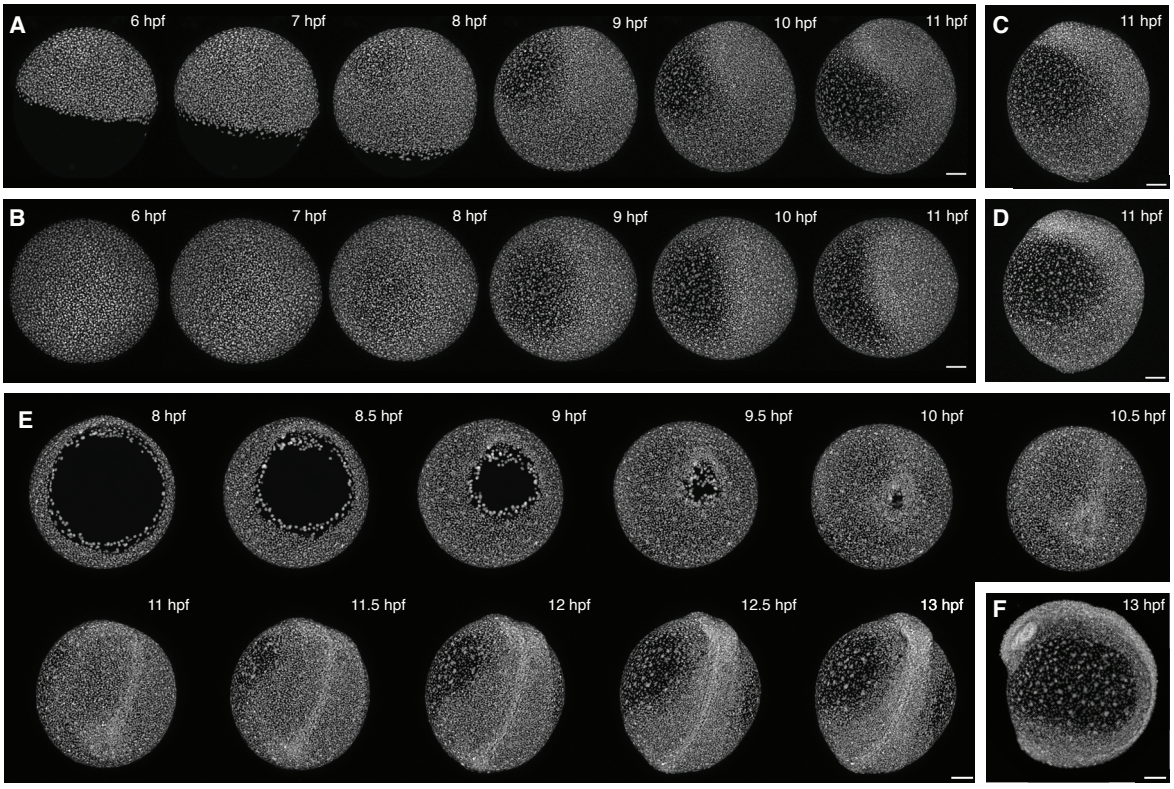

Figure 3.6: **Gastrulation and tailbud formation in untreated embryos.** Still images are shown from timelapse confocal z-stacks of untreated *Tg(His:GFP)* specimens during gastrulation and tailbud formation. Specimens were dechorionated and positioned in an agarose embryo mold during imaging. Images were captured using a 10x dipping objective. Scale bar = 100 µm. (A) Lateral view of gastrulation from 6-11 hpf with animal pole to top and dorsal to the right, and (B) same specimen, repositioned into lateral view at 11 hpf. (C) Animal pole view of gastrulation from 6-11 hpf with dorsal to the right and (D) same specimen, repositioned into lateral view at 11 hpf. (E) Vegetal pole view illustrating yolk plug closure (8-9.5 hpf), tailbud formation (9.5-10.5 hpf), and the beginning of segmentation (10.5-13 hpf), with (F) same specimen, repositioned into lateral view at 13 hpf.

dorsal midline is visible, extending posteriorly into the ventral vegetal domain, and the yolk plug has fully closed. Over the next few hours, convergence movements continue to direct cells toward the midline, further refining the broad domain of vegetal tissue. At the same time, neurulation and somitogenesis proceed in an anterior to posterior direction, causing extension of the body around the yolk. By 13 hpf, the anterior and posterior termini are near one another on the ventral side of the embryo (Figure 3.6 F).

Appropriate axial patterning requires tightly orchestrated coordination between the dramatic swirling, convergence, and extension movements that define morphogenesis during gastrulation. Together, my timelapse images of normal development provide additional insight into morphogenesis of the ventral gastrula and rearrangement of the spherical embryonic axes into the bilateral adult body plan. Note that this description of overall morphogenetic movements is primarily focused on epiblast/ectoderm movements because my approach does not distinguish between epiblast and hypoblast movements. The movements of mesodermal cells after internalization have previously been well described using genetic markers of mesodermal identity (M. L. K. Williams and Lilianna Solnica-Krezel 2020). In the future, it would be possible to characterize the range and complexity of movements within ventral epiblast further by tracking individual cell movements over time.

3.4.6 Loss of FGF signaling accelerates formation of the evacuation zone and disrupts posterior development

To understand the effect of FGF signaling on overall morphogenesis during and after gastrulation, I first generated a fixed time series of control and treated *Tg(His:GFP)* specimens. I performed SU5402 treatments at 10 and 20 µM, collected fixed specimens between 8 and 26 hpf, and acquired high resolution images to reveal detailed embryo morphology. In control embryos, morphological changes observed during gastrulation were similar to the timelapse images provided in Figure 3.6 (Figure 3.7 A).

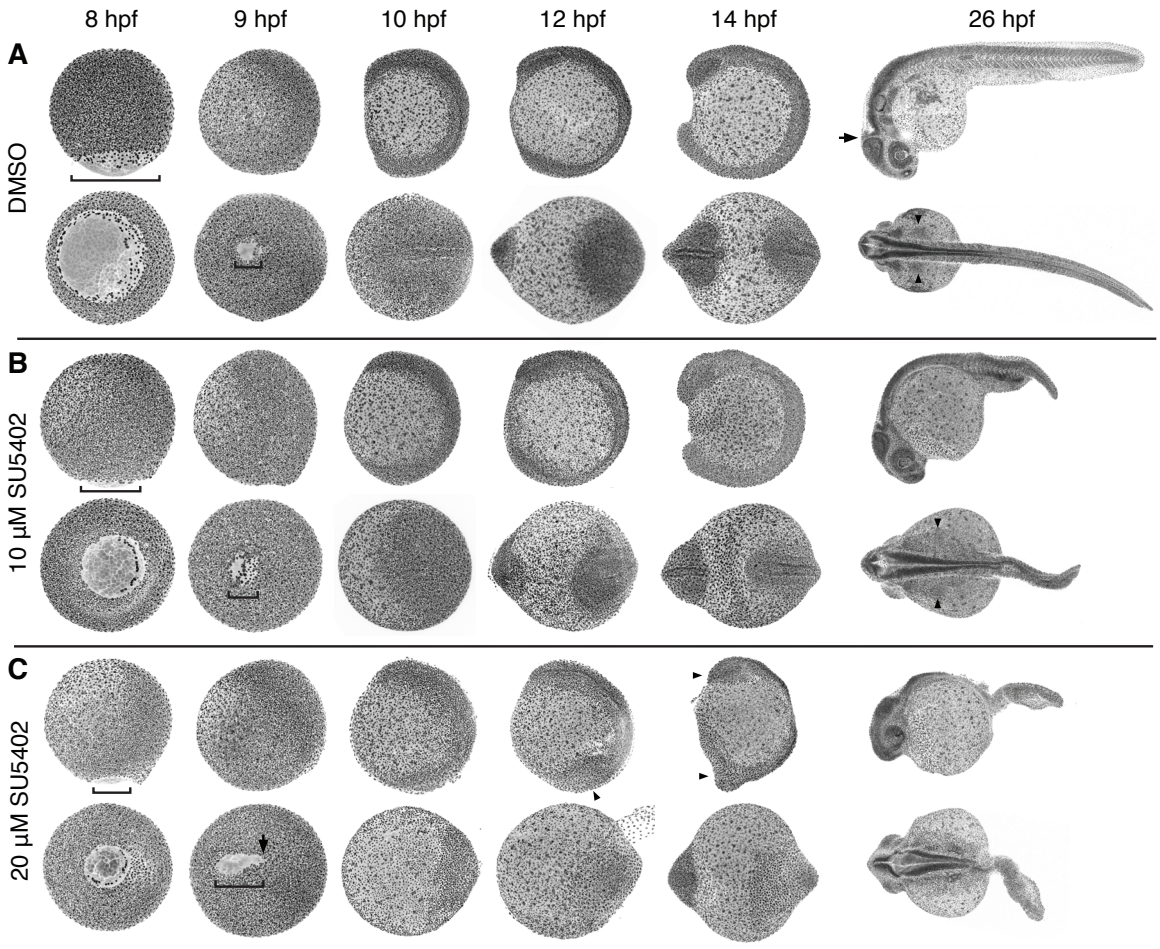

Figure 3.7: **Disruptions in development caused by inhibition of FGF signaling at gastrulation onset.**

Figure 3.7: Continued. *Tg(His:GFP)* specimens, in which all cell nuclei are labeled, were transiently treated with DMSO carrier or SU5402 from 5.2-6 hpf to inhibit FGF signaling. Specimens were fixed at carefully timed stages from 8 to 26 hpf for confocal imaging. (A-C) Confocal z-stack maximum projection images of representative specimens at 6 hpf, 9 hpf, 10 hpf, 12 hpf and 26 hpf. Specimens are shown in lateral view with dorsal to the right (top row) and vegetal view with dorsal/posterior to the right (bottom row). 26 hpf specimens are shown in lateral (top) and dorsal (bottom) views with anterior to the left. (A) DMSO carrier treated control specimens, which are indistinguishable from untreated specimens (data not shown). At 8 hpf, nuclei of the forerunner cells are present vegetal to the blastoderm margin, which has reached 80% epiboly. By 9 hpf, the yolk plug has almost closed and is spherical in shape (bracket), and the evacuation zone, characterized by sparser nuclei, is beginning to form on the ventrolateral sides of the specimen. At 10 hpf, the AP axis of the developing embryo is forming on the dorsal side, with the forming neural tissue apparent at the midline in vegetal view. The developing head and tail appear progressively closer together at 12 and 14 hpf, with the eye and otic vesicle becoming apparent. At 26 hpf, the midbrain-hindbrain boundary has been established (arrow), the ventricles of the developing brain are visible, and the eye, olfactory epithelium, otic vesicle, and developing pharyngeal arches are all easily discerned. The segmentally organized chevron-shaped somites lie bilaterally, adjacent to the developing spinal cord, along the fully extended trunk and tail. The bilateral fin buds have begun to form (arrowheads). (B) 10 mM SU5402 treated specimens. At 8 hpf, epiboly has progressed further than in untreated controls, but by 9 hpf the yolk plug is of normal size though slightly disorganized (brackets). By 12 hpf, the posterior region is reduced relative to untreated controls, with the cell mass not extending as far lateral in vegetal views at 12 hpf and 14 hpf. The individual somites are greatly reduced in AP length and are not chevron-shaped at 26 hpf. The hindbrain and anterior spinal cord appear relatively normal, but the entire cranium is reduced in size. The otic vesicles and fin buds are either very small or missing (arrowheads). (C) 20 mM SU5402 treated specimens. At 8 hpf, epiboly has progressed even further than for the 10 mM SU5402 treated specimens (bracket). By 9 hpf, the yolk plug is elongated along the dorsoventral axis (bracket), rather than circular, due to arrest of the dorsal margin (arrow). At 10 hpf, the developing anterior and posterior limits of the embryo are further apart than in other conditions. At 12 hpf, the lateral view reveals that the most posterior cells are developing at the bottom (vegetal pole) of the embryo (arrowhead). Reciprocally, at 14 hpf, the lateral view shows that the cranium is developing at the animal pole (arrowhead). Mislocalized posterior cells have begun to form an ectopic extension from the vegetal pole (arrowhead). At 26 hpf, AP length is dramatically reduced. The hindbrain and anterior spinal cord retain some organization, but cranium size, and structural formation are more dramatically disrupted than in the 10 mM SU5402 treated specimens. The elongated vegetal extension lacks organization, as spinal cord or somites cannot be distinguished.

In 10 µM SU5402 treated specimens, I found that epiboly appeared to progress more quickly, resulting in a larger evacuation zone and smaller yolk plug at 8 hpf (Figure 3.7 B, 8 hpf). By 9 hpf, the yolk plug appeared largely similar in 10 µM treated versus control specimens, though there was some disorganization in the forerunner cells. In 10 hpf treated specimens, the developing tailbud was broader and the dorsal midline was not visibly organized at this stage. Nevertheless, a reduced dorsal midline was apparent by 12 hpf, and neurulation and segmentation continued to pattern neural and mesodermal posterior tissues (Figure 3.7 B, 12 hpf and 14 hpf). By 26 hpf, midline defects were present at the posterior limit of the yolk and tail structures were shortened and dysmorphic (like data shown in Figure 3.2 C,D).

Specimens treated with 20 µM SU5402 displayed an even larger evacuation zone at 8 hpf and yolk plug area like the controls at 9 hpf (Fig. 7C, 8 hpf). However, by 9 hpf the yolk plug was dorsoventrally elongated and there was an absence of YSL nuclei or forerunner cells over the exposed yolk. The yolk plug did eventually close, resulting in a mass of cells at the vegetal pole that enlarged over time (Figure 3.7 C, 10 and 12 hpf). The anterior and posterior limits of the body axis remained at the animal and vegetal poles, respectively, and did not extend towards one another over the ventral side of the yolk. At 14 hpf, the hindbrain and anterior trunk were greatly reduced and somite formation was lost. Some of the vegetal cell mass extended out from the yolk, though no midline structures were present. By 26 hpf, the cranial placodes were largely absent, neurulation terminated at the base of the yolk, and the vegetal cell mass continued to extend to form an elongated vegetal extension (similar to Figure 3.2 E,F).

The fixed time series data highlight a possible increase in the rate of epiboly and changes in the direction of cell movements as a result of early FGF signaling disruption. As gastrulation progresses, early dosage-dependent effects are magnified by subsequent defects in axial patterning and overall shortening of the body axis. At high concentrations of SU5402,

there is a marked defect in yolk plug closure and loss of organized neural and mesodermal structures in the posterior, suggesting that the vegetal extension may form by different mechanisms to normal tailbud extension. Additional analysis would be required to quantify the apparent differences in the rate of epiboly in SU5402-treated embryos, as my data indicate that there may be a dosage-dependent rate difference that is further exacerbated by inherent variation in the yolk size across embryos.

3.4.7 FGF signaling controls ventral/posterior morphogenesis and tail formation

To investigate the observations from the fixed morphology time series in more detail, I performed live imaging of *Tg(His:GFP)* embryos treated with DMSO carrier, 5 µM, or 10 µM SU5402. I predicted that FGF signaling would be reduced but not fully lost due to treatment with these concentrations, allowing me to identify subtle dosage-dependent effects on tailbud formation, neurulation, and segmentation. In control embryos, morphological changes during gastrulation were similar to the untreated time-lapse images shown in Figure 3.6 (Figure 3.8 A). In 5 µM SU5402 treated specimens I observed precocious yolk plug formation (as shown in Figure 3.7), slight disorganization of neural structures along the midline, and a reduction in paraxial mesoderm (Figure 3.8 C, image 1 and 2). Somitogenesis proceeded more quickly than in control embryos, and the resultant somites appear smaller and less uniformly shaped (Figure 3.8 C, image 3 and 4). By 16 hpf, the somites began to take on a characteristic chevron shape and defects appeared less severe in the posterior, similar to the phenotype seen in MZ*oep* mutants (Fig 3.8 D) (Londin, Niemiec, and Sirotkin 2005). This suggests that reduction of FGF signaling at the onset of gastrulation affects the timing of the molecular clock that drives somitogenesis later in development. In 10 µM SU5402 treated specimens, the yolk plug was asymmetrical, and the dorsal midline was less apparent at 9 hpf (Figure 3.8 E, image 1). Neurulation appeared to be restricted at the

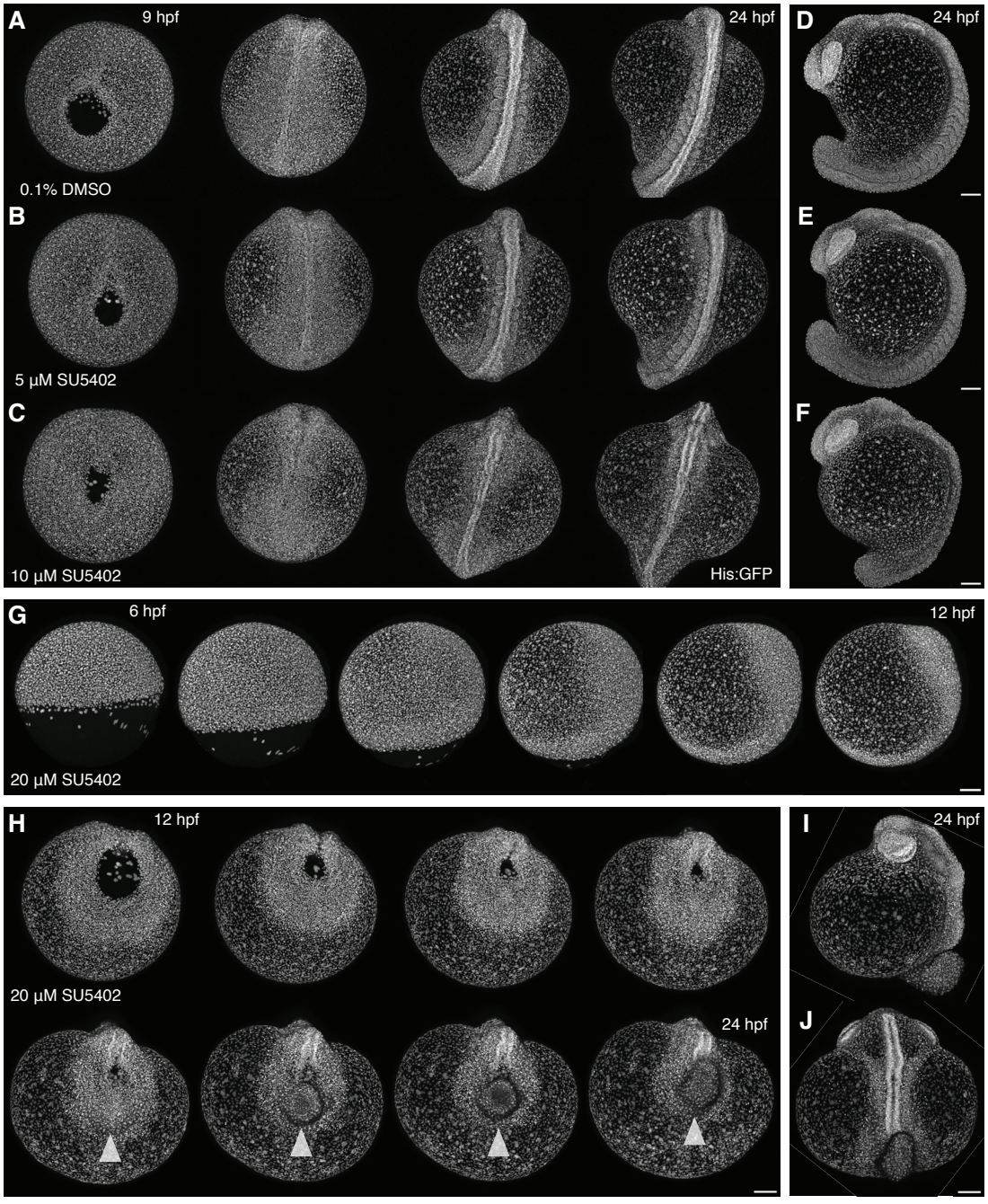

Figure 3.8: **Timelapse analysis of gastrulation and posterior morphogenesis in SU5402-treated embryos.**

Figure 3.8: Continued. Still images are shown from timelapse confocal z-stacks (captured using a 10 x dipping objective) of *Tg(His:GFP)* specimens were treated with DMSO or SU5402 from 5.2-6 hpf. Images were captured in vegetal/dorsal view, with anterior towards top right. Scale bar = 100 µm. Images were captured at stages between 9 and 24 hpf for a (A) DMSO treated control specimen, (B) 5 mM SU5402 specimen, (C) 10 mM SU5402 specimen from the same clutch. (D-F) Lateral views of these same three specimens were captured at completion of the timelapse analysis. As FGF signaling levels were reduced, AP extension of the embryo was progressively disrupted, with concomitant disruptions to somitogenesis. (G-J) Timelapse images of a single specimen treated with 20 mM SU5402 from 5.2-6 hpf (G) 6 hpf to 12 hpf in lateral view, dorsal to the right. At 12 hpf developing anterior and posterior termini of the embryo remain 180 degrees apart, rather than extending towards one another on the ventral side as in untreated embryos. (H) Same specimen, repositioned to be viewed from the vegetal pole, with dorsal side to the top, imaged from 12 hpf to 24 hpf (top row shows 12- 16.5 hpf and bottom row shows 18-24 hpf). Arrowheads indicate the vegetal extension developing on the ventral side. Same specimen repositioned into (I) lateral view, and (J) dorsal view. Together, these timelapse images reveal that as FGF signaling levels were reduced, AP extension of the embryo was progressively disrupted, with the most severe disruptions in FGF signaling causing formation of an ectopic vegetal extension of cells.

point of yolk plug closure but eventually persisted into the tailbud (Figure 3.8 E, image 2-4). By 16 hpf, the cranium was largely normal, the trunk was reduced, and neural organization appeared to be restored in the tailbud (Figure 3.8 F). The SU5402 treatment conditions caused a lack of the constriction of the yolk that normally leads to formation of the hindyolk extension.

I also performed a timelapse analysis of a 20 µM SU5402 treated specimen to characterize gastrula morphology (Figure 3.8 G). I observed that YSL nuclei advanced rapidly over the yolk at 6 hpf. A broad evacuation zone appeared within the ventral gastrula, and the margin appeared to thicken dramatically by 80% epiboly. At 12 hpf, the anterior remained dorsal to the animal pole due to a lack of swirling movements and extension earlier in gastrulation. A mass of marginal cells was visible at the vegetal pole. I repositioned the embryo to observe the vegetal pole and found that the yolk plug had failed to close (Figure 3.8 H). Timelapse imaging in this view revealed that a wide marginal/vegetal mass of cells advanced toward the arrested dorsal margin. The open pore persisted as a vegetal extension emerged from the ventral side of the embryo. By 24 hpf, the embryo had developed a retina, anterior

neural structures, and nearly all the vegetal mass cells had contributed to the elongated vegetal extension (Figure 3.8 I-J). It is likely that this specimen represents an extreme case, however additional observations of multiple specimens confirmed that the vegetal extension reproducibly arises from the ventral side of the embryo. This timelapse analysis clarified that the vegetal extension found in specimens lacking FGF signaling does not arise from the normal tailbud formation and neurulation processes that progress from anterior to posterior.

These data clarify the range of gastrulation, neurulation, and segmentation stage defects that arise from FGF inhibition at the onset of gastrulation. Taken together, Figures 3.6-3.8 highlight the complexity of morphogenesis within the ventral gastrula and suggest that early FGF signaling is involved in patterning a cascade of developmental processes, including epiboly, mesoderm specification, neurulation, and tailbud formation.

3.4.8 FGF inhibition shifts axial marker expression

To understand the effect of FGF signaling on patterning of major regions along the body axis, I used a series of anteroposterior markers. I selected *otx2*, *hoxb1b*, and *eve1* to represent cranial, posterior hindbrain/trunk, and tail domains, as described in previous studies (Kudoh, Concha, et al. 2004; Kudoh, Wilson, and Dawid 2002; Joly et al. 1993; Cruz et al. 2010). I visualized RNA expression of these anterior to posterior markers in control and SU5402-treated embryos using in situ hybridization by chain reaction (HCR; Figure 3.9). In control specimens, expression of posterior marker *eve1* was present near the ventral margin at 6 hpf (Figure 3.9 A). By 8 hpf, cranial marker *otx2* and hindbrain/anterior trunk marker *hoxb1b* were present in complementary dorsal domains, while *eve1* continued to be expressed near the ventral margin. At 10 hpf, this ordered pattern was refined such that a gap formed between the *otx2* and *hoxb1b* expression domains (McClintock et al. 2001), and *eve1* was expressed in the ventral tailbud domain. This pattern persisted at 12 hpf, with high expression of *hoxb1b* in the anterior somites and expanded expression of *eve1* in the

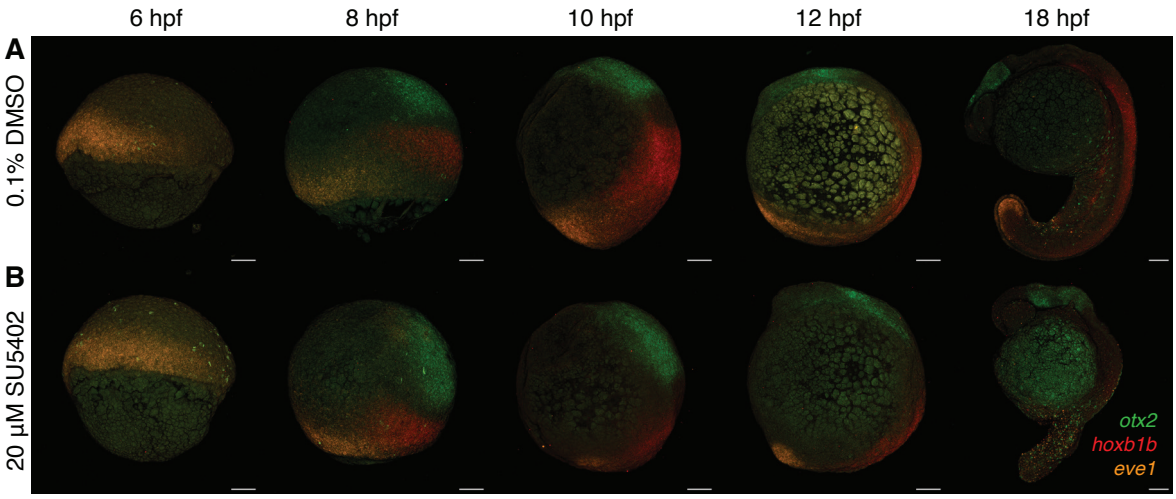

Figure 3.9: **Expression of axial markers *otx2*, *hoxb1b*, and *eve1* in SU5402-treated embryos.** In situ hybridization by chain reaction (HCR) was used to evaluate expression of *otx2*, *hoxb1b*, and *eve1* from 6-18 hpf in embryos treated with 0.1% DMSO carrier control or 20 µM SU5402 treatment at the onset of gastrulation. Embryos are shown in lateral view with animal pole/anterior towards the top and dorsal to the right. Scale bar = 100 µm. (A) In control specimens, the anterior marker *otx2* (green) commences expression in dorsal/animal cells by 8 hpf and becomes localized to the anterior neural tube. The hindbrain/trunk marker *hoxb1b* (red) has an anterior limit of expression close to but not abutting *otx2* at 8 hpf and recedes posteriorly from 10-18 hpf such that the expression-free intermediate domain expands over time. The posterior marker *eve1* (yellow) is expressed in the ventral gastrula at 6 hpf and gradually becomes localized to the posterior of the developing embryo. (B) In SU5402-treated specimens, in which FGF signaling was disrupted at the onset of gastrulation, changes in axial patterning were apparent as early as 6 hpf, with the *eve1* expression domain expanded along the margin towards the dorsal side. By 8 hpf, all three markers were shifted towards the margin, consistent with an increased rate of epiboly. In 10 and 12 hpf specimens, the *otx2*-expressing cranial domain was expanded towards the posterior, *hoxb1b* expression was shifted posteriorly, and the *eve1* posterior domain was reduced in size. By 18 hpf, *hoxb1b* levels were highly reduced and *eve1* expression was undetectable.

elongating tail. At 18 hpf, *otx2* marked the anterior segment of the cranium, while *hoxb1b* was broadly expressed throughout the trunk and tail. In the posterior tail, *eve1* was present at the dorsal midline and in the chordoneural hinge.

Given that FGF signaling is required for posterior development, I expected that posterior marker *eve1* would be diminished while anterior marker *otx2* would expand in SU5402 treated embryos. Inhibition of FGF signaling initially caused a slight expansion of the *eve1* domain at the margin at 6 hpf (Figure 3.9 B). However, at 8 hpf, compared to the untreated controls, *otx2* occupied a marginally expanded dorsal domain, *hoxb1b* was shifted toward the dorsal margin (reducing the size of the dorsal marginal domain that was free of *hoxb1b*), and *eve1* was restricted to a small domain near the margin. At 10 hpf, *otx2* expression expanded dorsally and failed to progress toward the animal pole, while *hoxb1b* was expressed at lower levels in the trunk. *eve1* expression was reduced and restricted to a small domain of vegetal cells. Dorsal/anterior expression of *otx2* continued at 12 hpf, with expansion of the domain toward the posterior. *hoxb1b* remained reduced and localized more posteriorly in the trunk, while *eve1* expression increased slightly within the highly restricted tailbud domain. At 18 hpf, *otx2* was expanded in the cranium, *hoxb1b* was minimally present in the trunk, and *eve1* expression was absent in the posterior.

Based on these expression patterns, my interpretation is that FGF signaling disruption starting at 5.2 hpf has an initial ventralizing effect at 6 hpf, as evidenced by expansion of the *eve1* domain toward the dorsal side. However, persistent expansion of *otx2* by 8 hpf and beyond suggests that there is a long-term dorsalizing effect of FGF inhibition. As development proceeds, *hoxb1b* and *eve1* are lost as the posterior fails to develop normally, indicating that the genetic programs of the developing trunk and tail are initiated during gastrulation but not maintained in the absence of early FGF signaling outputs.

3.4.9 Spatial dynamics of downstream FGF signaling marker etv4 and early neural patterning genes

Given the range of phenotypes in SU5402-treated specimens, I wanted to assess the degree to which later FGF signaling activity was affected by a pulse treatment with SU5042 between 5.2 and 6 hpf. I was also interested in the functional consequences of gastrula stage FGF signaling on the development of the neural plate border and neural crest. I first performed HCR on wildtype embryos to document the normal expression patterns of *etv4*, *foxd3*, and *ap2a* during gastrulation and neurulation (Figure 3.10). The *etv4* transcript is a direct target of FGF signaling, allowing an assessment of how FGF signaling activity changes over time (Roehl and Nüsslein-Volhard 2001; F. Raible and Brand 2001). In the early gastrula (6-7 hpf), FGF signaling activity (*etv4*) is apparent around the margin (Figure 3.10 A). By 9 hpf, FGF signaling activity is broadly present from anterior to posterior and near the ventral margin. After gastrulation, there is high FGF signaling activity in the hindbrain and in a separate, broad posterior domain that extends from the tailbud into the anterior trunk, consistent with the role of FGF signaling in development of both of these tissues (Reifers et al. 1998; B. W. Draper, Stock, and Kimmel 2003).

I also assessed gastrula patterning and formation of the neural plate border using the markers *foxd3* and *ap2a*, as these genes are expressed at gastrula stages and known to be important components in the neural crest gene regulatory network (Rocha, Singh, et al. 2020). At 75% epiboly, transcription factors *foxd3* and *ap2a* are expressed in opposing domains in the embryo (Arduini, Bosse, and Henion 2009; Wang et al. 2011). *ap2a* is expressed in a ventral and animal domain, while *foxd3* is expressed marginally around the shield and mirroring the curve of the region that will give rise to the central nervous system. Just a few hours later, *ap2a* defines the lateral edge of the neural plate border and *foxd3* is expressed in bilateral stripes as neural crest cells are specified. *ap2a* and *foxd3* double mutants show a loss of all NCC derivatives and, consequently, dramatic craniofacial defects

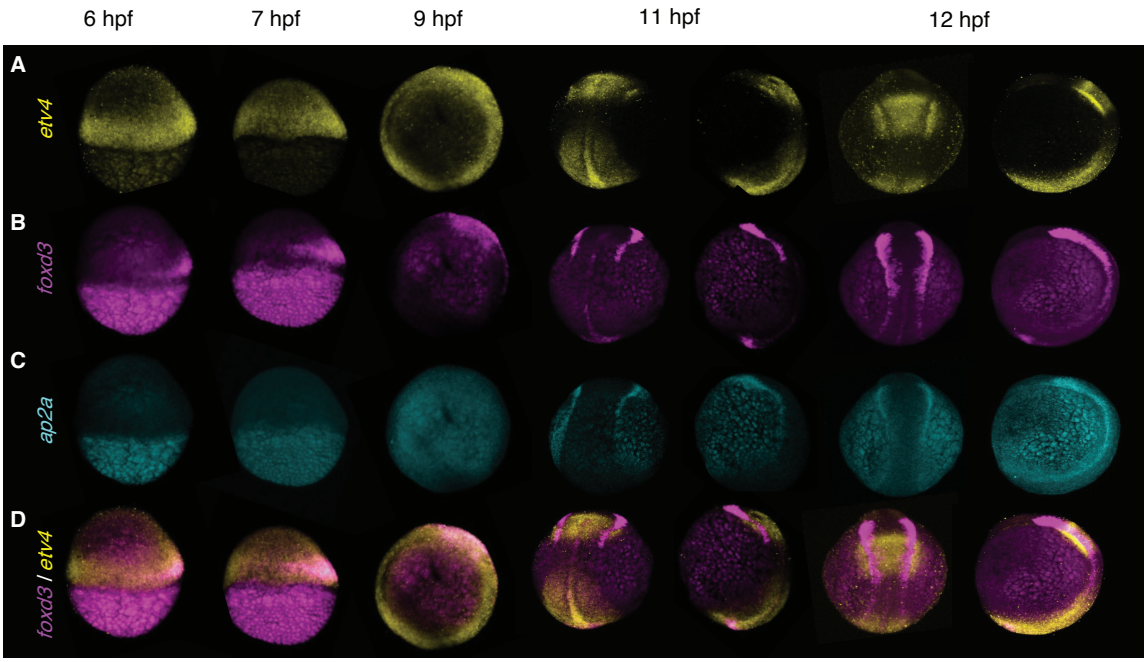

Figure 3.10: **Wildtype expression of FGF signaling activity reporter *etv4* and neural plate border markers *foxd3* and *ap2a*.** In situ hybridization by chain reaction (HCR) was used to evaluate expression of *etv4*, a direct target of FGF signaling activity, and transcription factors *foxd3* and *ap2a*, in wildtype embryos between 6 and 12 hpf. Lateral views, dorsal to right, are shown for all stages, and dorsal views, anterior to the top, are shown at 11 and 12 hpf. Note that at early stages there is non-specific autofluorescence in the yolk. (A) *etv4* is expressed around the margin at 6 and 7 hpf, extending along the full AP extent of the embryo at 9 hpf, and then localizing to a broad cranial area centered on the midbrain-hindbrain boundary as well as a broad posterior domain at 11 and 12 hpf. (B) *foxd3* is expressed in the dorsal ectoderm at 6 and 7 hpf, becoming cranially localized at 9 hpf and showing elevated levels in the neural plate border at 11 and 12 hpf. A small posterior expression domain is also present at 11 and 12 hpf. (C) *ap2a* is expressed at low levels in the ventral-animal gastrula up to 11 hpf, when it becomes localized primarily to the lateral aspect of the neural plate border, as also observed at 12 hpf. (D) Comparison of *foxd3* and *etv4* reveals co-labeling in the dorsal ectoderm from 6-9 hpf, as well as in the midline and a small posterior domain of *foxd3* expression. By contrast, in the cranial region *etv4* expression is at low levels in the *foxd3* expressing neural plate border domains.

including severe reduction in the jaw (Arduini, Bosse, and Henion 2009; Wang et al. 2011). Single mutants show intermediate phenotypes, suggesting that *foxd3* and *ap2a* regulate different populations and aspects of neural crest development. Loss of function in *ap2a* and *foxd3* together results in expansion of the ventrally located BMP signaling domain toward the dorsal side and reduction of chordin (a primary BMP antagonist) expression at the dorsal margin at 8 hpf (Wang et al. 2011).

I confirmed that *foxd3* and *ap2a* are expressed in opposing domains during early gastrulation (Figure 3.10 B, C), consistent with previous reports (Arduini, Bosse, and Henion 2009; Wang et al. 2011). By 9 hpf, *foxd3* is expressed bilaterally in the anterior neural plate border, consistent with the known role for *foxd3* as a pioneer transcription factor in neural crest specification (Lukoseviciute, Mayes, and Sauka-spengler 2021). *foxd3* expression expands posteriorly at 11-12 hpf and *ap2a* expression is present at the lateral aspect of the neural plate border. There was also more posterior expression of *foxd3* along the midline and in the tailbud, consistent with our previous observations (Rocha, E. Kushkowski, et al. 2021). *etv4* and *foxd3* were expressed in adjacent domains in the anterior ectoderm, with *etv4* at low levels in the bilateral *foxd3* expressing neural plate border domains and high elsewhere, such that the expression domains of these genes were complementary along the mediolateral extent of the neural plate border (Figure 3.10 D). DMSO treated carrier controls provided additional detail about expression dynamics at early stages (Figure 3.11 A). *ap2a* transcripts were more clearly present in the ventral-animal domain opposite to *etv4* at 7 and 8 hpf. *etv4* appeared to be expressed at low levels throughout the gastrula at 8 hpf, with higher expression dorsally and near the margin. At 11 hpf, *ap2a* was expressed adjacent to *foxd3* in the anterior, in a bilateral domain which extended further toward the posterior along the lateral edges of the *etv4* expression domain.

When FGF signaling was disrupted with 10 µM SU5402 at the onset of gastrulation (Figure 3.11 B), FGF signaling activity (*evt4*) appeared uniformly at low levels at 7 hpf, like

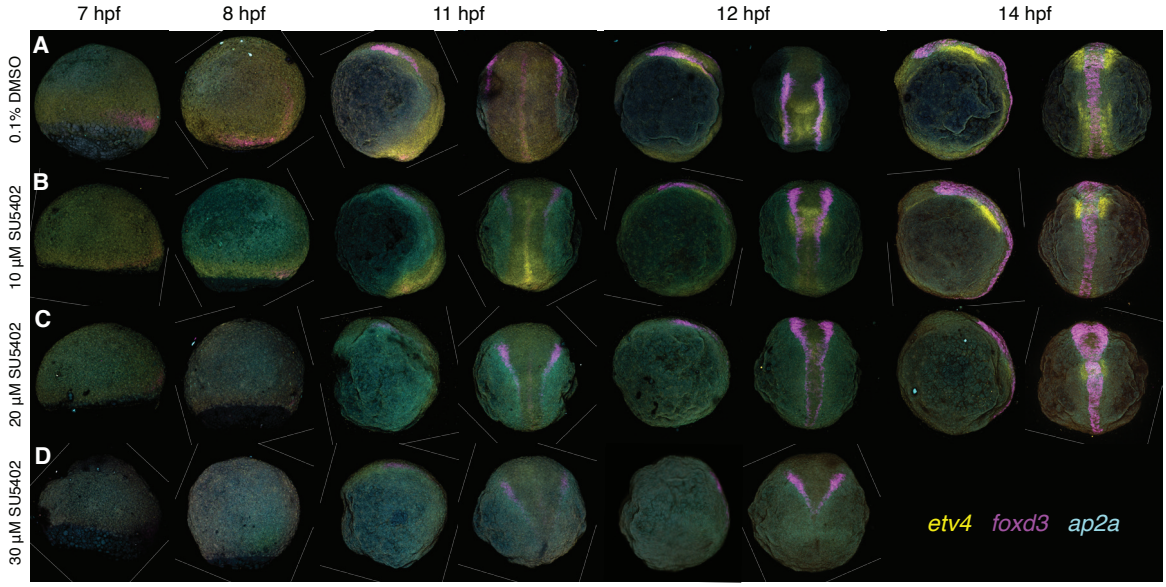

Figure 3.11: **Expression of *etv4*, *foxd3*, and *ap2a* in FGF signaling-deficient specimens.** HCR analysis of *etv4* (yellow), *foxd3* (magenta) and *ap2a* (cyan) expression in 7-14 hpf embryos treated with SU5402 to inhibit FGF signaling. (A) 0.1% DMSO carrier control treated specimens. At the 7 and 8 hpf stages, *ap2a* is expressed on the ventral side of the embryo within the ectodermal domain (towards the animal pole) in a pattern complementary to *etv4* expression, at 14 hpf there is *etv4* expression in the most recently formed somites and posterior presomitic mesoderm, data is otherwise similar to that shown in Fig. 3.10. (B) 10 µM SU5402 treated specimens. (C) 20 µM SU5402 treated specimens. (D) 30 µM SU5402 treated specimens. As expected, SU5402 treatment led to reduced or absent *etv4* expression, indicative of loss of FGF signaling, with the cranial/hindbrain expression domain being most robust to the reduction in signaling. As FGF signaling levels were reduced, the *ap2a* expression domain expanded both dorsally and marginally at 8-9 hpf, continuing to be more dorsal than in untreated specimens at later stages. Early expression of *foxd3* (at 8-9 hpf) was reduced or absent. Later bilateral expression domains within the neural plate border (at 11-14 hpf) became more medially localized as FGF signaling was reduced. In response to the most severe reduction in FGF signaling, the neural plate border fused at the midline in the posterior hindbrain.

the pattern in the DMSO treated control at 8 hpf. Higher *etv4* expression was restricted to the margin, which became even more apparent by 8 hpf. Broad dorsal and marginal expansion of lateral *ap2a* and reduction of *foxd3* to the dorsal margin was also apparent at these early stages. At 11 hpf, a band of FGF signaling activity appeared in the anterior, adjacent to the posterior extent of *foxd3* expression in the neural plate border. High FGF signaling activity was present in the posterior but was reduced compared to the control condition. The distance between the bilateral stripes of *foxd3* was reduced, whereas the lateral *ap2a* domains were expanded. Anterior FGF signaling activity increased between 11 and 14 hpf, while FGF signaling in the trunk and tailbud reduced over time compared to the controls. *foxd3* expression extended further posterior at 12 hpf, suggesting a precocious bias towards neural plate border identity in the trunk. By 14 hpf, *foxd3* was expressed in a single medial stripe that progressed toward the tailbud, and *etv4* and *ap2a* expression were present but reduced in the tailbud.

In the 20 µM SU5402 treatment group (Figure 3.11 C), lower levels of overall *etv4* expression were present at 7 hpf. Marginal FGF activity was not present at 7 or 8 hpf, and posterior FGF signaling was greatly reduced or absent from 11-14 hpf. The anterior band of FGF signaling was weakly present at 11 hpf, though signaling activity strengthened to some degree by 14 hpf in limited lateral domains. *ap2a* remained broadly expressed and was highest dorsolaterally and into the vegetal cell mass as late at 11 hpf, before reduction between 12 hpf and 14 hpf. A small dot of *foxd3* was present near the dorsal margin at 8 hpf. By 11 hpf, bilateral stripes of *foxd3* expression narrowed toward the midline and there was low expression along the midline. By 12 hpf, *foxd3* expression was even closer to the midline, further extended along the AP axis, and merged across the midline before terminating in the posterior. Lateral stripes of *foxd3* expression merged by 14 hpf and occupied a shorter AP extent than in 14 hpf control or 10 µM specimens.

In the 30 µM SU5402 treatment group (Figure 3.11 D), *etv4* was expressed at very low

levels across the blastoderm at 7 hpf, with a minimal increase in expression near the dorsolateral margin. *ap2a* was also expressed at low levels in a broad lateral domain and reduced in the far ventral gastrula compared to controls. The *etv4* and *ap2a* expression domains expanded within the dorsolateral gastrula at 8 hpf. No *foxd3* expression was observed at early stages. At 11 hpf, slight expression of *etv4* was present anterior to the *foxd3* expression domain. Anterior *foxd3* was present in bilateral stripes and diffusely at the midline. This expression appeared to merge, slightly anterior to where the blastoderm failed to close, and instead formed a small open pore to the yolk (as seen in Figure 3.8 G, H). At 12 hpf, *foxd3* expression merged at the midline, forming a "V" shape. *ap2a* was present at the midline and expanded laterally anterior to the open pore. I did not generate 14 hpf specimens for this experimental condition.

This experiment clarified the FGF signaling dynamics that occur after inhibition with SU5402 between 5.2 and 6 hpf. Based on the *etv4* expression patterns, less severe FGF signaling disruption causes the global, low-level FGF activity that normally occurs (around 8 hpf) to occur precociously (7 hpf), as shown in Figure 3.11 B and C. Higher levels of FGF signaling activity are limited to the margin and translate into a posterior FGF signaling domain by 11 hpf. However, FGF signaling is not reinforced in the posterior after gastrulation. More severe FGF signaling disruption causes failure to establish a marginal/posterior FGF signaling domain. Anterior FGF signaling at the level of the future midbrain-hindbrain boundary does arise in most SU5402-treated specimens, suggesting that later anterior FGF signaling is initiated by an independent mechanism. My interpretation of the *foxd3* and *ap2a* expression data is that FGF signaling disruption has indirect effects on formation of the neural plate and neural plate border. Less severe FGF disruption causes expansion of neural plate border identity at the expense of neural identity, as shown by abnormally medial *ap2a* expression and posterior lengthening of the *foxd3* expression domain at 11-12 hpf (Fig. 11B). Higher concentrations of SU5402 result in truncated neural structures and posterior

expansion of neural plate border genes and neural crest cells (Figure 3.11 C,D; see also Figure 3.2). These results are consistent with the increase in posterior Sox10 expression observed in Figure 4.

3.5 Discussion

In this chapter, I have provided evidence that temporally controlled inhibition of FGF signaling during a critical window in development is capable of producing dramatic phenotypic effects during gastrulation, neurulation, and segmentation. Below, I explore the possible functions of FGF at the onset of gastrulation.

3.5.1 FGF signaling controls the rate of epiboly and response to positional cues

My data support a model in which FGF signaling regulates the rate of epiboly and formation of the evacuation zone. The first morphological effect of FGF inhibition at the onset of gastrulation is precocious formation of an expanded evacuation zone and increased cell density at the margin. Data from fixed time series and live imaging both demonstrate that evacuation zone and yolk plug formation occur more rapidly in SU5402-treated embryos. However, this effect is temporary, as tailbud formation frequently occurs later than in control embryos. Quantification of epiboly rate across an SU5402 concentration gradient is needed to fully support this model.

Gene expression data in treated specimens also reveal an enlarged evacuation zone, with expansion of *ap2a* and *otx2* expression towards the animal pole, and reduced *eve1*, *hoxb1b*, and *etv4* expression at the margin, suggesting that changes in the rate of epiboly have consequences for later gene expression and cell fate specification processes. Controlling the speed of cell movements at the onset of gastrulation would also regulate the overall

timing of exposure to positional cues that pattern the blastoderm. FGF has known roles in modulating morphogen gradients through interaction with BMP, Wnt, and Nodal, as well as autoregulatory feedback loops (Zinski, Tajer, and Mullins 2018; Ota et al. 2010; Leerberg, Hopton, and B. Draper 2019; Polevoy et al. 2019). High FGF activity near the margin, in combination with Nodal, induces mesoderm development, while FGF and Wnt further from the margin regulates the position of neural plate border genes through interactions with BMP signaling. Kwon et al proposed that the lag between early expression of *ap2a* and later expression of preplacodal and neural crest markers may allow for ectodermal conditioning (Kwon et al. 2010). Recent work highlights that cell movements can play an important role in establishing patterns within the early embryo by modulating signaling dosage and cell fate specification (Tsai and Pinheiro 2025). Regulating cell movement could give cells adequate time to produce a biochemical response to overlapping positional cues and increase robustness in early embryonic patterning (Kicheva and Briscoe 2023). It is possible that axial defects and loss of placodal and pharyngeal arch neural crest are caused by loss of positional information at the onset of gastrulation.

3.5.2 Early FGF signaling influences formation of the neural plate border

Development of the preplacodal ectoderm and neural crest requires a complex interplay between major signaling pathway activity and early transcription factors to establish the neural plate border (Groves and LaBonne 2014). While later signaling events at the neural plate border have been looked at in detail, information about earlier signaling in the cranial progenitor domain of the ventral gastrula is lacking. The concurrent loss of cranial placodes and pharyngeal arch neural crest and observed increase in Sox10+ neural crest specification is particularly interesting because my ventral gastrula fate map shows that these fates arise from similar progenitor domains shown in Chapter 2 (E. E. Kushkowski and Prince 2026). I hypothesize that cranial placodes and neural crest sub-fates are particularly sensitive to

changes in signaling levels during gastrulation. Further assessment of the gastrula-stage signaling environment that generates the neural plate border will be necessary to understand the earliest influences on neural crest and cranial placode specification better. Changes in later morphology indicate that mesoderm, posterior neural tissue, placodes, and pharyngeal arch neural crest are all affected by FGF inhibition, suggesting that FGF may be broadly implicated in establishing cell fates that arise from progenitor domains within the ventral gastrula (Chapter 2, (E. E. Kushkowski and Prince 2026)). Temporally controlled manipulation of BMP, Wnt, Nodal, and FGF at the onset of gastrulation would provide insight into broader patterning requirements of different progenitor domains within the ventral gastrula.

3.5.3 Temporal effects of SU5402 treatment on FGF signaling centers

At the start of my study, the best document roles for FGF signaling were in mesoderm induction and midbrain-hindbrain boundary formation. However, the timing of how these functions were controlled was not entirely clear. Mesoderm was either reduced or entirely lost as result of FGF receptor inhibition at the onset of gastrulation. My findings support that FGF signaling is necessary to induce mesoderm within the 5.2-6 hpf treatment window in this study, likely through activation of *Fgf8* (Reifers et al. 1998; Roehl and Nüsslein-Volhard 2001). In addition to promoting mesoderm induction directly, FGF signaling activity at the onset of gastrulation is necessary for maintenance of FGF signaling in the posterior mesoderm during somitogenesis (W. Zhang et al. 2022). At lower concentrations of SU5402, I found that reduced FGF signaling activity occurs at the margin and in the early tailbud, but signaling activity is not maintained as development continues, leading to somitogenesis defects. At higher concentration of SU5402, FGF signaling activity was entirely lost in the posterior and never recovered. Unlike in the posterior, later FGF signaling activity at the midbrain-hindbrain boundary was established in most treatment conditions, suggesting that this later function is not controlled by early FGF signaling activity. Instead, reduction in FGF activity

in the anterior may be an indirect consequence of earlier axial patterning defects. It would be informative to look at specific FGF receptor expression at gastrula stages, as much of the available expression data for individual receptors focuses on later stages. This would help to disambiguate the various effects of SU5402 on patterning throughout the embryo during this critical window.

FGF signaling also has known autoregulatory effects on receptor and ligand production, meaning that inhibiting FGF receptors for a short window could have long-lasting impacts on FGF receptor patterning within the embryo during gastrulation. In the lateral line primordium, it has been reported that FGF ligand production increases when FGF receptors are inhibited (Aman and Piotrowski 2008). If this is the case, there may also be a stronger FGF signaling response once receptor function returns to normal. This could explain the precocious increase in global FGF signaling activity that I observed in response to 10 µM and 20 µM SU5402 treatment in Figure 3.11, complicating the interpretation that global low-level FGF activity is involved in increasing the rate of epiboly between 7 and 9 hpf. Further investigation of FGF receptor, ligand, and direct effector dynamics is necessary to understand better how FGF signaling functions at a molecular level during early gastrulation.

3.5.4 Posterior development phenotypes and self-organization within the vegetal extension

The vegetal extension shares a remarkable resemblance to other self-organizing cellular structures. Explants or "pescoids" elongate after detachment from the yolk, or even after dissociation and reaggregation (Schauer et al. 2020; Anlas and Trivedi 2021; Fulton, Verd, and Benjamin Steventon 2022; Cheng et al. 2023; Emig et al. 2025). In these tissues, elongation occurs in the absence of other manipulations due to stochastic self-organization or can be induced with exogenous Nodal injection. A fluid-filled lumenal cavity is also frequently observed in elongated explants, similar to a common phenotype that I observed in embryos

treated with a moderate amount of SU5402 (Figure 3.1) (Schauer et al. 2020; Fulton, Verd, and Benjamin Steventon 2022). The vegetal extension may also have some similarity to exogastrulae in *Xenopus* or mouse gastruloids (Branford and Yost 2002; Beccari et al. 2018). However, a key difference between elongated explants and the vegetal extensions is the timing during development at which they form, with explants coming from pre-gastrulation embryos and the vegetal extension forming at the end of gastrulation. One explanation for the similarities between these structures is that vegetal extensions derive from largely unpatterned ectodermal cells, similar to the largely unspecified blastoderm of the early blastula. Further investigation of the identities and organization of cells within the vegetal extension would provide insight into the molecular mechanisms that are disrupted by FGF receptor inhibition at the onset of gastrulation.

CHAPTER 4

DISCUSSION AND FUTURE DIRECTIONS

In Chapter 2, I have provided the first detailed description of the origin of zebrafish neural crest at all axial levels. My analysis of the new fate map brings into question some commonly held assumptions about neural crest specification in the zebrafish cranium, a topic I have discussed in some detail in Chapter 2. The fate map also documented the wide range of cell types that arise from the zebrafish ectomesodermal ventral gastrula: cranial placodes, spinal cord, posterior mesoderm, and possible neuromesodermal progenitors (NMPs). I identified domains of the gastrula that contribute to multiple cell fates in the pharyngula. By collecting detailed data about the resulting cell fates, including their relative abundance and contribution along the body axis, I have provided the first direct evidence for how the zebrafish gastrula contributes to the full AP extent of the body plan at 30 hpf. In Chapter 3, I have characterized the morphological effects of temporally controlled FGF inhibition and found that FGF signaling regulates the progression of gastrulation and formation of the evacuation zone, as well as patterning of the neural plate border. In addition to known posterior defects, I documented the loss of pharyngeal arch neural crest and cranial placode-derived structures in the anterior in response to FGF inhibition. These losses suggest that FGF signaling modulates patterning of the shared neural crest/cranial placode progenitor domain in the gastrula. Taken together, my dissertation findings provide novel insights that will inform future studies of the roles of signaling, morphogenesis, and cell fate specification in early development.

4.1 Development of the fate map methodology

My initial objective was to clarify the origin of the neural crest within the previously established zebrafish fate map (Dougan et al. 2003; Kimmel, Warga, and Schilling 1990; Kozlowski

et al. 1997; Melby, Warga, and Kimmel 1996; Ward, Warga, and Prince 2007; Warga, Kane, and Ho 2009; Warga and Nüsslein-Volhard 1999; K. Woo and Fraser 1995). As I developed and refined an approach for fate mapping the neural crest, the focus of the project expanded to encompass the range of cell fates that arise from the zebrafish ventral gastrula. I did not include the preliminary datasets in this thesis, but the findings I have presented in Chapter 2 encompass many of the insights gained from earlier iterations of fate mapping the neural crest. The fate map in Chapter 2 is the result of significant refinement to the fate mapping methodology, which would not have been possible without the insights I gained from collecting, analyzing, and presenting multiple preliminary fate map datasets.

The first fate map dataset that I gathered was derived from embryos that I positioned in methylcellulose and manually photoconverted by adjusting a pinhole in the lightpath of a compound microscope to select a region of interest. From this, I learned how the size and position of a photoconverted region correlated with the abundance and fate of labeled progeny at 30 hpf. While this approach was not sufficiently reproducible to allow me to confidently generate a complete dataset, observations from these initial specimens helped me to develop baseline intuition for building an informative fate map. For the next round of fate mapping, I designed embryo molds which enabled more reproducible embryo manipulation and positioning. Issues related to photoconversion size and measurement accuracy were addressed by standardizing the photoconversions using the LSM 710 confocal microscope. Each of these improvements greatly increased both the efficiency of photoconversion experiments and the analysis of early region position relative to the dorsal shield and embryo margin.

My original experimental strategy was to use the *Tg(Sox10:nEOS)* transgene marker to identify neural crest cell nuclei within photoconverted membranes in live embryos. However, after recognizing subtle pharyngeal arch and cranial morphology abnormalities in homozygous *Tg(Sox10:nEOS)* embryos, I modified my strategy to generate the fate map using *AB wildtype embryos. These specimens were fixed at 30 hpf and immunolabeled with an anti-

Sox10 antibody to identify neural crest cells. This allowed Sox10+ (neurogenic) and Sox10- (pharyngeal arch) cranial neural crest to be distinguished as separate populations at 30 hpf. As a result of this change, the published fate map provides a more nuanced characterization of neural crest sub-populations.

I initially collected fate mapping data from 30 specimens using the confocal photoconversion and Sox10 immunolabeling approach. 11/30 regions gave rise to neural crest, thus revealing the general position of the neural crest progenitor domain within the ventrolateral gastrula (data not shown). When analyzing this dataset, I divided the 30 hpf embryos into seven axial units along the AP axis and recorded basic cell type data for labeled progeny within each unit. This strategy allowed AP regionalization of cell fates at 30 hpf to be tied back to specific domains within the gastrula. These data suggested that neural crest contributions along the AP axis were not uniform. Specifically, the mapped regions produced large numbers of anterior cranial and posterior tail neural crest cells, while trunk neural crest was more sparsely labeled. This preliminary finding was ultimately confirmed by the final, published version, of my fate map. In addition, some cell fate data were recorded from the 19/30 regions that did not produce neural crest, but were not analyzed in great detail as these regions were not the focus of my initial study.

This initial, limited, fate map was important because it revealed that the region-based mapping approach could provide a wealth of information about the overall organization of the ventral gastrula. Using a region-based fate mapping approach was initially perceived as a weakness in the experimental design, but provided much more information than initially anticipated. The regions provided far more information about cell fates than a single cell labeling approach with the same number of specimens could have generated. The 30 hpf confocal imaging protocol was adjusted to include low magnification whole specimen z-stacks and high magnification 1 µm z-stacks that captured the cellular morphology of all photoconverted progeny in detail. Around this time, I switched to the new LSM 900 confocal

for photoconversions and high-resolution imaging at 30 hpf, and collected the 86 specimen dataset from which I built the final version of the fate map. These improvements in imaging parameters and data collection were essential for generating the cell fate and AP position information detailed in Chapter 2.

After optimizing the imaging and immunolabeling aspects of the fate map methodology, I further refined analysis of the fate map data. I measured and normalized the initial position of photoconverted regions at 6 hpf and plotted them on a sphere, enabling more accurate "shieldplot" depictions of region positions in the gastrula. Assessing final fates proved to be more challenging, as I wanted to collect both cell type and AP axis information that could be compared across specimens. After multiple attempts to normalize the pharyngula into equivalent axial units, I finally settled on dividing each specimen into 47 axial units based on morphology. "Spreadplots" were designed to depict cell type and axial spread data for each specimen, in rank order by relative number of photoconverted cells, providing a detailed summary of contribution to cell fates within the overall zebrafish body plan. The final fate map offers significant insight into the early organization of the ventral gastrula and raises new questions about axial patterning and the origin of key cell types during vertebrate development.

4.2 Future Directions

4.2.1 Transplants into the ventral gastrula

This project was motivated by the inability to transplant cells into a presumptive trunk neural crest domain because it had not yet been identified (Rocha, E. Kushkowski, et al. 2021). Clarification of progenitor domains in the shield stage embryo, as well as axial position and spread data will be informative to researchers interested in performing transplant experiments involving ventrally derived tissues. In addition, information about heterogene-

ity across the gastrula may inform the likelihood of successfully targeting different tissues using transplantation.

4.2.2 Lineage relationships across the neural crest progenitor domain

In the future, targeted single cell lineage tracing can be used to test hypotheses generated by the region-based fate map presented in this dissertation. Analysis of the lineage relationships between cell types across the embryonic body axes will provide much needed resolution to the individual cell fate specification trajectories that occur during embryogenesis. One of the major findings in Chapter 2 was that the pharyngeal arch and at least a subset of the Sox10+ (neurogenic) neural crest arise independently from the cranial neuroepithelium. In particular, investigating cell lineage in the cranial domain will resolve relationships between the neural crest (both mesenchymal Sox10+ and pharyngeal arch sub-populations), the various cranial placodes, and the neuroepithelium of the brain. Investigating cell potency at a single cell level will allow for careful investigation of cell fate specification mechanisms for these cranial cell types and provide insight into the developmental history of these essential cranial tissues. Further, these tissues are key to vertebrate cranial evolution, and identifying their origins and the molecular mechanisms that drive their specification may provide insight into the regulatory modules that influence cranial development across vertebrates. The zebrafish provides an accessible model in which to investigate their developmental trajectories and molecular signatures first, which could then provide hypotheses to be tested in other species for comparative studies.

Lineage analysis within the posterior domain has the potential to yield equally fruitful information about the degree to which posterior progenitor cells contribute to the range of fates during posterior elongation. I identified a small domain within the tail territory that produces the most posterior cells within the somites, spinal cord, and neural crest. I hypothesize that this small domain contains multipotent cells that may be true neuromesodermal

progenitors. These cells are hypothesized to retain multipotency after the point at which germ layer specification has occurred for the rest of the embryo, and move such that they populate the posterior aspect of the extending tail of the embryo (Martin and Benjamin Steventon 2022). The seemingly distinct, multipotent progenitor domain that I identified as producing epidermis, neural tube, neural crest, and somites at the tip of the tail warrants particular scrutiny, as this domain may contain true neuromesodermal progenitors, or be divided early into mesodermal and ectodermal lineages that move together during morphogenesis. Resolving the timing of cell fate decisions is essential to understand the unique contribution of the ventral gastrula domain to ectodermal and mesodermal components in the posterior body.

4.2.3 Morphogenesis of the cranial neural crest progenitor domain and neural plate border

In parallel with or separate from lineage tracing studies, small population or single cell tracking across the ventral domain would provide insight into domain specific morphogenetic processes that produce cranial, trunk, and tail structures. The altered gastrulation movements in the absence of FGF signaling, which were identified in Chapter 3, highlight the potential importance of early movements in cell fate specification. With information on the organization of progenitor domains in the ventral gastrula provided in the fate map, live imaging studies could be conducted to identify the migratory pathways of cells within different progenitor domains and the cell types they generate in development. In the cranial progenitor domain, tracking cell trajectories and fates from the cranial progenitor domain would clarify previously understudied aspects of cranial morphogenesis. Of particular interest for neural crest development is the early organization of the pharyngeal region and distinction between neurogenic and chondrogenic neural crest. The fate map shows that pharyngeal and Sox10+ neural crest progenitors are somewhat spatially segregated as early as 6 hpf. Previous lineage

tracing shows the organization of early neural crest in the head correlates with different fates in later development (Schilling and Kimmel 1994), however we do not know how cells from the gastrula travel to generate these structures in the 12 hpf early neurula. Live imaging of labeled cells in the cranial neural crest progenitor domain from gastrula to neurula would clarify the morphogenetic processes that produce cranial neural crest and distinguish neural crest populations of differing cell fate potential.

4.2.4 Morphogenesis of the posterior body

Tracking cell trajectories and fates from the marginal ventral domain would clarify the origin of mesodermal and ectodermal tissues in the trunk and tail. My fate mapping data suggest that there is a large territory of the ventral blastoderm that produces mesodermal tissues in the absence of neural tissues. Given that my methodology labeled cells at all layers of the blastoderm, this suggests that these mesodermal progenitors occupy the full thickness of the blastoderm. Previous studies have shown that internalization occurs later and more slowly on the ventral side of the germ ring (Keller et al. 2008). Based on these data, I hypothesize that there is a population of mesoderm progenitors that remains external and moves ventrally toward the vegetal pole, before internalizing at a later stage in gastrulation, upon tail bud formation, or via subduction movements during tailbud extension (Kanki and Ho 1997). Spreadplot data from regions that produced somites and neural tube may provide insight into the dynamics of neural and mesodermal lineages during gastrulation. Observation methods that allow for cell tracking, together with determining the depth of scatter-labeled cells within the epiblast/hypoblast/tailbud, would clarify the morphogenetic dynamics in this domain.

4.2.5 Developmental disorders of the neural crest

My findings may also be of interest to researchers who study neural crest developmental disorders, known as neurocristopathies. These disorders are linked to perturbations at different stages of neural crest development, including induction, specification, migration, and differentiation (Vega-Lopez et al. 2018). In some cases, both neural crest and placode derivatives are impacted in affected individuals. In Chapter 3, I showed that pharyngeal neural crest and placodes are both sensitive to the effects of FGF signaling inhibition at the onset of gastrulation. The fate map in Chapter 2 indicates that Sox10+ neural crest, pharyngeal arch neural crest, cranial placodes, and epidermis arise from progressively overlapping progenitor domains. Of particular interest is the overlap between pharyngeal arch neural crest and the otic placode, as these cell types are frequently both affected in neurocristopathies. The cranial neural crest and placode progenitor domain is particularly sensitive to early perturbations in signaling and morphogenesis. Future investigation of the developmental influences within this domain will be of consequence for both basic science and clinical research.

4.2.6 Uncovering the earliest influences on cell type specification

Despite ongoing interest in various aspects of later neural crest biology, the earliest developmental influences that generate the neural crest have been elusive. BMP, Wnt, and FGF all have documented early influences in neural crest specification, however their precise roles remain unclear after decades of proposing and testing hypotheses about early neural crest specification (Prasad, Charney, and García-Castro 2019). My data provide information about where to look within the gastrula for specific gene expression, signaling pathway outputs, and regulators that may be key to patterning a variety of tissues, including the neural crest. This sentiment is generally applicable to many cell fates of interest in later development. Recent advances in single cell and spatial transcriptomics offer exciting possibilities to integrate high resolution genetic and molecular data with classical embryology techniques.

Advances in imaging techniques, including automated cell tracking, 3D reconstruction of morphogenesis, and live imaging of gene expression dynamics may provide insight into key processes that pattern and rearrange the gastrula into the pharyngula. Regulation of the extracellular matrix, physical forces across tissues, metabolism, and other aspects of development may also be relevant. Approaching the earliest processes in development with all of the tools of modern developmental biology is necessary to integrate cell fate specification, morphogenesis, and signaling towards a more unified understanding of our origins.

CHAPTER 5

MATERIALS AND METHODS

5.1 Zebrafish husbandry

Wild-type zebrafish (Danio rerio) were maintained in accord with IACUC-approved protocols at the University of Chicago. Embryos were obtained from crosses of adult stocks of *AB wild-type, *Tg(His:GFP)*, and *Tg(-7.2sox10:mRFP)vu234*, referred to as *Tg(sox10:mRFP)* in the text (Kucenas et al. 2008). Embryos were maintained in E3 medium (5.0 mM NaCl, 0.17 mM KCl, 0.33 mM CaCl2, 0.33 mM MgSO4) at 28.5 °C and staged according to standard guidelines (Kimmel, Ballard, et al. 1995). Pigment synthesis was inhibited using 0.2 mM 1-phenyl 2-thiourea (PTU; Sigma) in E3 medium.

5.2 Fate Map Methods

5.2.1 Overview of fate mapping strategy

One-cell stage wild-type embryos were injected with mRNA encoding membrane-localized Kaede (Ando et al. 2002). Embryos at the 5.2-6 hpf stage were positioned in custom agarose embryo molds for photoconversion and imaging at 6 hpf (shield stage). In each specimen we labeled a small region of 60 µm diameter by photoconverting through the depth of the blastoderm. The blastoderm is approximately 3-4 cells thick at this stage and these regions included 40-50 deep layer cells. Photoconversions were targeted to domains of the embryo that had not previously been thoroughly mapped, avoiding the far dorsal side and the most marginal cells of the germ ring. Lateral and animal pole view images were acquired at the 6 hpf stage to record the position of the labeled region relative to the dorsal shield. Embryos with photoconverted regions were raised to 30 hpf, fixed, and immunolabeled with anti-Sox10 antibody to visualize Sox10+ neural crest cells. Confocal z-stacks were acquired

through entire 30 hpf specimens at low magnification (10x objective), followed by acquisition of high magnification views (40x objective) of areas containing photoconverted cells. Photoconversions were performed randomly on either the left or right side of each gastrula, but for simplicity all data have been projected onto the left side. We photoconverted a total of 97 embryos and analyzed the 86 specimens that met our inclusion criteria of photoconversion imaging performed precisely at 6 hpf, high Kaede expression levels, normal morphology at 30 hpf, and appropriate orientation during imaging to ensure accurate measurements. Our experimental approach is schematized in Figure 2.2 D-F.

5.2.2 Agarose embryo molds

We designed agarose molds to position dechorionated embryos for imaging or for manipulations, such as photoconversion, from fertilization through gastrulation stages. The molds hold 10 gastrulation-stage embryos in two rows of spherical wells, resembling an egg carton. These molds allow for rapid orientation of embryos and reproducible positioning in lateral and animal pole views.

To construct the mold block, the diameter of 6 hpf zebrafish embryos was measured in both animal pole and lateral orientation to determine parameters for the wells. Mold blocks were designed in openSCAD and rendered in MeshLab. Blocks were 3D printed with a shiny surface in acrylonitrile butadiene styrene (ABS) plastic on a Stratasys Objet500 Connex3 3D printer at the Polsky Exchange Fabrication Lab at the University of Chicago.

Imprints of the plastic mold blocks were cast in 1-1.5% agarose (Midsci) in E3 medium in 35 mm petri dishes. Petri dishes were filled halfway with heated agarose and the mold blocks were carefully inverted into the agarose to prevent air bubbles from forming. Once the agarose solidified, mold blocks were removed using forceps to reveal the mold imprint. Agarose embryo molds were used immediately or wrapped in parafilm and stored at 4°C for up to 1 week. The agarose molds were filled with E3 medium to keep the embryos submerged

during use.

5.2.3 mKaede microinjection and embryo screening

The plasmid pCS2mKaede (kindly provided by Drs. Clare Buckley and Jon Clarke) was used to transcribe mRNA encoding a CaaX-modified variant of the photoconvertible protein Kaede, which localizes specifically to cell membranes (Ando et al. 2002). Capped mRNA was generated using the MEGAscript SP6 Kit (Invitrogen). mKaede mRNA at 250ng/ml in 0.02 M KCl, supplemented with phenol red dye, was microinjected either into the cell or the top of the yolk just under the cell within 20 minutes of fertilization.

Embryos were transferred to a 28.5°C incubator for 4 hours prior to screening for fluorescence using a Leica M165FC stereo fluorescence dissecting microscope. Specimens with bright and even expression of Kaede in the blastula cell mass were selected for photoconversion. Embryos were carefully dechorionated using DuPont #5 forceps, with care taken to avoid disrupting the blastoderm. Some embryos were placed at 31.5°C or 22°C to speed up or slow down development to ensure appropriate staging during photoconversion (Kimmel, Ballard, et al. 1995).

5.2.4 Photoconversion of regions in gastrula-stage specimens

Screened 5.2-6 hpf embryos were transferred to agarose embryo molds in E3 medium and oriented to allow for direct photoconversion of a region of interest. Photoconversions were performed on an upright Zeiss LSM 900 confocal microscope using a 10X/0.3 W N-Achroplan WD 2.6 mm dipping objective, with the bleaching, time series, and region functions of the Zeiss Zen Blue software. A circular region of interest of 60 µm in diameter was selected for each individual specimen. The photoconversion was completed during 10 cycles of exposure to 405 nm light. The light passed through all layers of the blastoderm, photoconverting cells through the depth of the blastoderm, including the enveloping layer (EVL) and 2-3 layers of

deep cells over the yolk. The number of photoconverted deep cells ranged from $\tilde{4}$0-50, based on cell counts from a subset of our 6 hpf specimens.

Following photoconversion, each embryo was repositioned at 6 hpf in lateral view, with the embryonic shield localized on either the right or left side, and the margin positioned equatorially, equidistant from the animal and vegetal poles. A confocal z-stack was acquired to record the position of the photoconverted region in 3 dimensions. Each embryo was repositioned to an animal pole view and an additional z-stack acquired. After photoconversion and image acquisition was complete, embryos were transferred to E3 medium containing 200 mM 1-phenyl 2-thiourea (PTU; Sigma) to inhibit pigment formation, in a 24-well plastic plate lined with 1% agarose (Midsci) and incubated at 28.5°C.

5.2.5 Measurement of photoconverted region positions at 6 hpf

The position of the photoconverted region was measured from confocal maximum projections of the converted and unconverted mKaede signal, superimposed on a single T-PMT (transmitted light) slice that provides the location of the embryonic shield. As photoconversions were performed randomly on the right or left side of the embryo, we recorded this information prior to orienting all lateral 6 hpf images with the shield to the right and margin aligned horizontally. The center of the photoconverted region was measured in absolute distance in microns and normalized as x-y coordinates relative to the embryonic shield and ventral side (x = 1 to -1) and distance from the margin to animal pole (y = 0 to 1) from z-stacks taken after photoconversion at 6 hpf. The z coordinates were calculated from these values to determine the distance from the embryonic midline. The z coordinates were also measured as distance from the midline in animal pole view as needed and discrepancies between values from both views were resolved by comparing both 6 hpf z-stacks. We normalized these Cartesian measurements to calculate spherical coordinates on a r = 1 sphere. While there are modest inherent differences in size between embryos, this normalization approach

minimized variability in coordinate assignment between specimens, allowing for reliable comparison between specimens. Plotted positions were compared to original images to confirm their accuracy. The fate maps we provide indicate the center of each photoconverted region only, thus avoiding the complexity of depicting overlapping regions.

5.2.6 Sample fixation and immunohistochemistry

At 30 hpf, samples were fixed in 4% paraformaldehyde (Electron Microscopy Solutions) for 4 hours at room temperature or overnight at 4°C. Samples were protected from light after fixation to preserve the fluorescent signal of the photoconvertible proteins. Samples were washed in phosphate buffered saline (PBS) and into PBS with 0.1% Tween-20 (Fisher Bioreagents, PBST) before proceeding to immunohistochemistry.

Samples were washed into PBST and blocked in 10% goat serum (Sigma) with 0.1% DMSO (Sigma) in PBST (blocking solution) for 1 hour at room temperature. Samples were incubated in 1:250 anti-Sox10 primary antibody (rabbit; GeneTex, GTX128374) for at least 4 hours at room temperature, or overnight at 4°C. Samples were washed repeatedly in PBST, transferred to blocking solution for 1 hour, and incubated in 1:250 Alexa 633 secondary antibody (goat anti-rabbit; Invitrogen, A-21070) in blocking solution for at least 4 hours at room temperature, or overnight at 4°C. Samples were washed into PBS and stored for up to 1 week prior to imaging.

5.2.7 Imaging of fixed 30 hpf specimens

Fixed specimens were mounted laterally in 1% low melting point agarose (IBI Scientific) in E3 medium on glass coverslips. Tiled confocal z-stacks were acquired along the entire body axis using the 10X/0.3 W N-Achroplan WD 2.6 mm dipping objective on a Zeiss LSM 900 upright confocal microscope with 488 nm, 561 nm, and 633 nm lasers. Regions containing photoconverted cells were recorded in tiled 1 micron increment z-stacks, using the 40x/1.0

W Plan-Apochromat WD 2.5 mm dipping objective. Tiled images were fused using the stitching function in Zen Blue and saved as raw .czi files and .tif files for analysis.

5.2.8 Identification of cell fates and positions at 30 hpf

High magnification images were used to identify cell fates. Using morphological criteria, coupled with location within the specimen and Sox10 expression status (a marker of neural crest cells), we were able to confidently assign a total of 20 different cell fates (Figure 2.4). We did not map the extraembryonic periderm because it does not contribute to adult tissue; however, our qualitative observations were consistent with a previous report focused on the enveloping layer that differentiates into periderm (Kimmel and Warga 1987; Kimmel, Warga, and Schilling 1990). We elected to exclude another four cell fates (vascular tissue, pronephros, germ cells, and pectoral fin mesenchyme) from our detailed analyses because these were poorly represented, consistent with our mapping strategy focusing on regions that lie above the margin. Despite the potential for a few regions to overlap with the blood progenitor domain, we did not observe any blood cells; however, these cells may have been difficult to detect without the use of molecular markers (Warga, Kane, and Ho 2009). The remaining 15 cell types (epidermis, neural tube, retina, Sox10+ neural crest, pharyngeal arch neural crest, olfactory epithelium, lens, anterior lateral line (aLL) primordium, trigeminal (Tg) ganglion, aLL ganglion, otic vesicle, posterior lateral line (pLL) ganglion, pLL nerve, pLL primordium, and somitic mesoderm were included in all subsequent analyses. The pre-otic and post-otic cranial regions are also the sites of placodes that form cranial ganglia for sensory nerves VII, VIII, IX and X (D. W. Raible and Kruse 2000). As these ganglia are small and closely apposed at 30 hpf, it is likely that they are included within the structures we identified as anterior and posterior lateral line ganglia. A subset of cells within the aLL ganglion were Sox10+, consistent with their expected neural crest origins (Venkataraman et al. 2025).

Each 30 hpf specimen was divided into 47 equivalently sized axial units along the antero-posterior (AP) axis Fig. 3A), based on morphological landmarks and relative distance from defined morphological features, to normalize for slight differences in overall embryo length. The cranial region was divided into 12 units using the eye, otic vesicle, and posterior limit of the fin bud as reference points. The trunk was divided into 19 units, with 7 units over the yolk ball and 12 units over the hindyolk extension. The post-anal tail was divided into a further 16 units. Each unit is equivalent to the diameter of the lens and the length of the somite at the end of the hindyolk extension at 30 hpf. The anterior and posterior axial limits were recorded for each photoconverted cell type observed. In addition, we qualitatively ranked the relative contribution to each cell type labeled within a specimen. These rank ordering data are documented in our comprehensive spreadplots (Supplemental Fig. 1).

Our fate map approach is reliant on retention of photoconverted mKaede protein in all progeny cells at 30 hpf. Theoretically, Kaede protein concentrations might be diluted in rapidly dividing cells, such that they fall below detectable levels. Mindful of this issue, we excluded a small number of specimens from our analysis based on weak Kaede expression at 30 hpf. Despite these exclusions, label dilution could potentially lead to false negatives. However, the presence of labeled cells representing all the major expected cell types and at all the expected AP levels of the 30 hpf embryo (Fig. 3B) strongly suggests that the vast majority of labeled cells remain detectable.

5.2.9 Analysis and data visualization

Data analysis was performed using R and visualizations were generated using the ggplot package. To simplify data interpretation, we plotted the center of each photoconverted region on the fate maps presented. We generated lateral and animal pole orthographic projections of each embryo to depict the position of photoconverted regions. We consolidated data derived from both left and right sides onto the left-hand side for ease of visualization. Spreadplots, as

shown in Supplemental Fig. 1, were generated as tile plots indicating the presence or absence of cell types in each axial unit, for each specimen. These presence or absence data do not, however, provide information on the varied number of labeled cells present within each axial unit. Each spreadplot indicates the specific region of the gastrula labeled, summarizes the axial distribution of the resultant 30 hpf labeled cell types, and presents the cell types in rank order with the most abundant cell type shown at the top. In addition, we gathered qualitative information about the abundance of each cell type (high, medium, low, or sparse), allowing for comparison across specimens (Supplementary Figure 2).

5.3 FGF Signaling Methods

5.3.1 Pharmacological manipulation

Embryos from the same clutch were collected within a 10-15 minute time window and transferred to a 28.5°C incubator. Embryos were divided into treatment groups in a 24-well plate prior to 5.2 hpf. All embryo medium was removed and replaced with 990 mL of E3. Appropriate volumes of 10 mM SU5402 stock solution in DMSO and DMSO were added to the medium to a final volume of 1 mL. Final concentrations were 0.1% DMS0 and 5-30 µM SU5402. Embryos were incubated at 28.5°C for 45 minutes, washed >3 times with excess E3, and transferred to a new well plate. For time series experiments, treatment groups were divided into individual wells by fixation time point and returned to the incubator.

5.3.2 Timelapse microscopy

Tg(His:GFP) embryos were transferred into agarose embryo molds for live imaging using the 10X/0.3 W N-Achroplan WD 2.6 mm dipping objective on a Zeiss LSM 900 upright confocal microscope with 488 nm, 561 nm, and 633 nm lasers. Experiments were performed with a heated stage, however temperature variations in the microscope facility did cause slightly

delayed development compared to incubator-raised siblings. Confocal z-stacks were acquired every 5 or 10 minutes to generate timelapse datasets.

5.3.3 Hybridization chain reaction

Hybridization chain reaction was performed as described in Choi et al., 2018 and Ibarra-Garcia-Padilla et al., 2021 (H. M. T. Choi et al. 2018; Ibarra-García-Padilla et al. 2021).

5.3.4 Immunolabeling

Fixed samples were washed into PBST and blocked in 10% goat serum (Sigma) with 0.1% DMSO (Sigma) in PBST (blocking solution) for 1 hour at room temperature. Samples were incubated in 1:250 anti-Sox10 primary antibody (rabbit; GeneTex, GTX128374) and 1:250 anti-Myhc primary antibody (mouse; Millipore, 2880709) for at least 4 hours at room temperature, or overnight at 4°C. Samples were washed repeatedly in PBST, transferred to blocking solution for 1 hour, and incubated in 1:250 Alexa 633 secondary antibody (goat anti-rabbit; Invitrogen, A-21070) and 1:250 Alexa 488 secondary antibody (goat anti-mouse; Invitrogen, 1069546) in blocking solution for at least 4 hours at room temperature, or overnight at 4°C. Samples were washed into PBS and stored for up to 1 week prior to imaging.

BIBLIOGRAPHY

Agathon, Antoine, Christine Thisse, and Bernard Thisse (2003). "The molecular nature of the zebrafish tail organizer". In: *Nature* 424.6947. ISBN: 0028-0836, pp. 448–452. DOI: 10.1038/nature01822.

Aman, Andy and Tatjana Piotrowski (Nov. 2008). "Wnt/-Catenin and Fgf Signaling Control Collective Cell Migration by Restricting Chemokine Receptor Expression". In: *Developmental Cell* 15.5, pp. 749–761. DOI: 10.1016/j.devcel.2008.10.002.

Ando, Ryoko et al. (2002). "An optical marker based on the UV-induced green-to-red photoconversion of a fluorescent protein". In: *Proceedings of the National Academy of Sciences of the United States of America* 99.20, pp. 12651–12656. DOI: 10.1073/pnas.202320599.

Anlas, Kerim and Vikas Trivedi (Aug. 31, 2021). "Studying evolution of the primary body axis in vivo and in vitro". In: *eLife* 10, e69066. DOI: 10.7554/eLife.69066.

Arduini, Brigitte L., Kevin M. Bosse, and Paul D. Henion (June 15, 2009). "Genetic ablation of neural crest cell diversification". In: *Development* 136.12, pp. 1987–1994. DOI: 10.1242/dev.033209.

Attardi, Andrea et al. (Jan. 15, 2019). "Neuromesodermal progenitors are a conserved source of spinal cord with divergent growth dynamics". In: *Development* 146.2, dev175620. DOI: 10.1242/dev.175620.

Baggiolini, Arianna et al. (Mar. 2015). "Premigratory and Migratory Neural Crest Cells Are Multipotent In Vivo". In: *Cell Stem Cell* 16.3, pp. 314–322. DOI: 10.1016/j.stem.2015.02.017.

Barone, Vanessa et al. (2017). "An Effective Feedback Loop between Cell-Cell Contact Duration and Morphogen Signaling Determines Cell Fate". In: *Developmental Cell* 43.2, 198–211.e12. DOI: 10.1016/j.devcel.2017.09.014.

Beccari, Leonardo et al. (Oct. 2018). "Multi-axial self-organization properties of mouse embryonic stem cells into gastruloids". In: *Nature* 562.7726, pp. 272–276. DOI: 10.1038/s41586-018-0578-0.

Bhattacharya, Dipanjan et al. (2021). "Strain maps characterize the symmetry of convergence and extension patterns during zebrafish gastrulation". In: *Scientific Reports* 11.1. ISBN: 0123456789, pp. 1–12. DOI: 10.1038/s41598-021-98233-z.

Bökel, Christian and Michael Brand (Aug. 2013). "Generation and interpretation of FGF morphogen gradients in vertebrates". In: *Current Opinion in Genetics & Development* 23.4, pp. 415–422. DOI: 10.1016/j.gde.2013.03.002.

Branford, William W. and H. Joseph Yost (Dec. 2002). "Lefty-Dependent Inhibition of Nodal- and Wnt-Responsive Organizer Gene Expression Is Essential for Normal Gastrulation". In: *Current Biology* 12.24, pp. 2136–2141. DOI: 10.1016/S0960-9822(02)01360-X.

Bronner-Fraser, Marianne and Scott E. Fraser (Sept. 1988). "Cell lineage analysis reveals multipotency of some avian neural crest cells". In: *Nature* 335.6186, pp. 161–164. DOI: 10.1038/335161a0.

Cheng, Tao et al. (Apr. 2023). "Nodal coordinates the anterior-posterior patterning of germ layers and induces head formation in zebrafish explants". In: *Cell Reports* 42.4, p. 112351. DOI: 10.1016/j.celrep.2023.112351.

Cho, Gun-Sik, Sun-Cheol Choi, and Jin-Kwan Han (May 2013). "BMP signal attenuates FGF pathway in anteroposterior neural patterning". In: *Biochemical and Biophysical Research Communications* 434.3, pp. 509–515. DOI: 10.1016/j.bbrc.2013.03.105.

Choi, Harry M. T. et al. (June 15, 2018). "Third-generation in situ hybridization chain reaction: multiplexed, quantitative, sensitive, versatile, robust". In: *Development* 145.12, dev165753. DOI: 10.1242/dev.165753.

Concha, Miguel L. (Oct. 1, 2025). "Zebrafish Gastrulation". In: *Annual Review of Cell and Developmental Biology* 41.1, pp. 89–134. DOI: 10.1146/annurev-cellbio-012125-115503.

Conklin, Edwin G. (May 1905). "Mosaic development in ascidian eggs". In: *Journal of Experimental Zoology* 2.2, pp. 145–223. DOI: 10.1002/jez.1400020202.

Cooper, Emma J. and Steffen Scholpp (2024). "Transport and gradient formation of Wnt and Fgf in the early zebrafish gastrula". In: *Current Topics in Developmental Biology*. Vol. 157. Elsevier, pp. 125–153. DOI: 10.1016/bs.ctdb.2023.12.003.

Couly, Gerard F. and Nicole M. Le Douarin (1985). "Mapping of the early neural primordium in quail-chick chimeras: I. Developmental relationships between placodes, facial ectoderm and prosencephalon". In: *Developmental Biology* 110. DOI: 10.1016/0012-1606(85)90101-0.

Cruz, Carlos et al. (Feb. 23, 2010). "Induction and patterning of trunk and tail neural ectoderm by the homeobox gene eve1 in zebrafish embryos". In: *Proceedings of the National Academy of Sciences* 107.8, pp. 3564–3569. DOI: 10.1073/pnas.1000389107.

D'Amico, Leonard A. and Mark S. Cooper (Dec. 2001). "Morphogenetic domains in the yolk syncytial layer of axiating zebrafish embryos". In: *Developmental Dynamics* 222.4, pp. 611–624. DOI: 10.1002/dvdy.1216.

Dal-Pra, Sophie et al. (2006). "Noggin1 and Follistatin-like2 function redundantly to Chordin to antagonize BMP activity". In: *Developmental Biology* 298.2, pp. 514–526. DOI: 10.1016/j.ydbio.2006.07.002.

Dale, L. and J. M. W. Slack (Apr. 1, 1987). "Fate map for the 32-cell stage of *Xenopus laevis*". In: *Development* 99.4, pp. 527–551. DOI: 10.1242/dev.99.4.527.

Delaune, Emilie, Patrick Lemaire, and Laurent Kodjabachian (Jan. 15, 2005). "Neural induction in *Xenopus* requires early FGF signalling in addition to BMP inhibition". In: *Development* 132.2, pp. 299–310. DOI: 10.1242/dev.01582.

Dougan, Scott T. et al. (2003). "The role of the zebrafish nodal-related genes squint and cyclops in patterning of mesendoderm". In: *Development* 130.9, pp. 1837–1851. DOI: 10.1242/dev.00400.

Draper, Bruce W., David W. Stock, and Charles B. Kimmel (Oct. 1, 2003). "*Zebrafish fgf24* functions with *fgf8* to promote posterior mesodermal development". In: *Development* 130.19, pp. 4639–4654. DOI: 10.1242/dev.00671.

Dubrulle, Julien et al. (2015). "Response to Nodal morphogen gradient is determined by the kinetics of target gene induction". In: *eLife* 4, pp. 1–27. DOI: 10.7554/eLife.05042.

Edens, Brittany M. and Marianne E. Bronner (2024). "Making developmental sense of the senses, their origin and function". In: *Current Topics in Developmental Biology*. Vol. 159. Elsevier, pp. 132–167. DOI: 10.1016/bs.ctdb.2024.01.015.

Emig, Alyssa A. et al. (May 1, 2025). "Temporal dynamics of BMP/Nodal ratio drive tissue-specific gastrulation morphogenesis". In: *Development* 152.9. DOI: 10.1242/dev.202931.

Esmaeli, Mojtaba et al. (July 9, 2024). "Molecular signaling directing neural plate border formation". In: *The International Journal of Developmental Biology* 68.2, pp. 65–78. DOI: 10.1387/ijdb.230231me.

Ezin, Akouavi M., Scott E. Fraser, and Marianne Bronner-Fraser (June 2009). "Fate map and morphogenesis of presumptive neural crest and dorsal neural tube". In: *Developmental Biology* 330.2, pp. 221–236. DOI: 10.1016/j.ydbio.2009.03.018.

Farrell, Jeffrey A. et al. (2018). "Single-cell reconstruction of developmental trajectories during zebrafish embryogenesis". In: *Science* 360.6392. ISBN: 0036-8075, eaar3131. DOI: 10.1126/science.aar3131.

Fauny, Jean-Daniel, Bernard Thisse, and Christine Thisse (2009). "The entire zebrafish blastula-gastrula margin acts as an organizer dependent on the ratio of Nodal to BMP activity". In: *Development* 136.22. ISBN: 0950-1991, pp. 3811–3819. DOI: 10.1242/dev.039693.

Fuentes, Ricardo et al. (2020). "The maternal coordinate system: Molecular-genetics of embryonic axis formation and patterning in the zebrafish". In: *Current Topics in Developmental Biology*. Vol. 140. Elsevier, pp. 341–389. DOI: 10.1016/bs.ctdb.2020.05.002.

Fulton, Timothy, Berta Verd, and Benjamin Steventon (2022). "The unappreciated generative role of cell movements in pattern formation". In: *Royal Society Open Science* 9.4. DOI: 10.1098/rsos.211293.

Fürthauer, Maximilian et al. (June 15, 2004). "Fgf signalling controls the dorsoventral patterning of the zebrafish embryo". In: *Development* 131.12, pp. 2853–2864. DOI: 10.1242/dev.01156.

Garnett, Aaron T., Tyler A. Square, and Daniel M. Medeiros (Nov. 15, 2012). "BMP, Wnt and FGF signals are integrated through evolutionarily conserved enhancers to achieve robust expression of Pax3 and Zic genes at the zebrafish neural plate border". In: *Development* 139.22, pp. 4220–4231. DOI: 10.1242/dev.081497.

Griffin, Kevin, Roger Patient, and Nigel Holder (1995). "Analysis of FGF function in normal and no tail zebrafish embryos reveals separate mechanisms for formation of the trunk and the tail". In: *Development* 121.9, pp. 2983–2994.

Griffin, Kevin J. P. and David Kimelman (Dec. 2003). "Interplay between FGF, one-eyed pinhead, and T-box transcription factors during zebrafish posterior development". In: *Developmental Biology* 264.2, pp. 456–466. DOI: 10.1016/j.ydbio.2003.09.008.

Gritsman, Kira, William S. Talbot, and Alexander F. Schier (2000). "Nodal signaling patterns the organizer". In: *Development* 127.5, p. 921.

Gritsman, Kira, Jiaojiao Zhang, et al. (1999). "The EGF-CFC protein one-eyed pinhead is essential for nodal signaling". In: *Cell* 97.1, pp. 121–132. DOI: 10.1016/S0092-8674(00)80720-5.

Groves, Andrew K. and Carole LaBonne (May 2014). "Setting appropriate boundaries: Fate, patterning and competence at the neural plate border". In: *Developmental Biology* 389.1, pp. 2–12. DOI: 10.1016/j.ydbio.2013.11.027.

Harish, Rohit Krishnan et al. (Oct. 1, 2023). "Real-time monitoring of an endogenous Fgf8a gradient attests to its role as a morphogen during zebrafish gastrulation". In: *Development* 150.19, dev201559. DOI: 10.1242/dev.201559.

Hatada, Yohko and Claudio D. Stern (Oct. 1, 1994). "A fate map of the epiblast of the early chick embryo". In: *Development* 120.10, pp. 2879–2889. DOI: 10.1242/dev.120.10.2879.

Hino, Hiromu et al. (2018). "Roles of maternal wnt8a transcripts in axis formation in zebrafish". In: *Developmental Biology* 434.1, pp. 96–107. DOI: 10.1016/j.ydbio.2017.11.016.

Ho, Robert K. and Charles B. Kimmel (1993). "Commitment of Cell Fate in the Early Zebrafish Embryo". In: *Science* 261.5117, pp. 109–111.

Ibarra-García-Padilla, Rodrigo et al. (Sept. 2021). "A protocol for whole-mount immunocoupled hybridization chain reaction (WICHCR) in zebrafish embryos and larvae". In: *STAR Protocols* 2.3, p. 100709. DOI: 10.1016/j.xpro.2021.100709.

Joly, Jean-Stéphane et al. (Dec. 1, 1993). "The ventral and posterior expression of the zebrafish homeobox gene *eve1* is perturbed in dorsalized and mutant embryos". In: *Development* 119.4, pp. 1261–1275. DOI: 10.1242/dev.119.4.1261.

Kane, Donald A. and Rachel M. Warga (1994). "Domains of movement in the zebrafish gastrula". In: *Seminars in Developmental Biology* 5, pp. 101–109. DOI: 10.1006/sedb.1994.1014.

Kanki, John P. and Robert K. Ho (1997). "The development of the posterior body in zebrafish". In: *Development* 124.4, p. 881. DOI: https://doi.org/10.1242/dev.124.4.881.

Keller, Philipp J. et al. (Nov. 14, 2008). "Reconstruction of Zebrafish Early Embryonic Development by Scanned Light Sheet Microscopy". In: *Science* 322.5904, pp. 1065–1069. DOI: 10.1126/science.1162493.

Kicheva, Anna and James Briscoe (Oct. 16, 2023). "Control of Tissue Development by Morphogens". In: *Annual Review of Cell and Developmental Biology* 39.1, pp. 91–121. DOI: 10.1146/annurev-cellbio-020823-011522.

Kimmel, Charles B., William W. Ballard, et al. (1995). "Stages of embryonic development of the zebrafish". In: *Developmental Dynamics* 203.3, pp. 253–310. DOI: 10.1002/aja.1002030302.

Kimmel, Charles B. and Rachel M. Warga (1987). "Indeterminate cell lineage of the Zebrafish embryo". In: *Developmental Biology* 124, pp. 269–280. DOI: 10.1016/0012-1606(87)90478-7.

Kimmel, Charles B., Rachel M. Warga, and Donald A. Kane (Feb. 1, 1994). "Cell cycles and clonal strings during formation of the zebrafish central nervous system". In: *Development* 120.2, pp. 265–276. DOI: 10.1242/dev.120.2.265.

Kimmel, Charles B., Rachel M. Warga, and Thomas F. Schilling (1990). "Origin and organization of the zebrafish fate map". In: *Development* 108.4, pp. 581–594. DOI: https://doi.org/10.1242/dev.108.4.581.

Koos, David S. and Robert K. Ho (1998). "The nieuwkoid gene characterizes and mediates a Nieuwkoop-center-like activity in the zebrafish". In: *Current Biology* 8.22, pp. 1199–1206. DOI: 10.1016/S0960-9822(07)00509-X.

Koos, David S. and Robert K. Ho (1999). "The nieuwkoid/dharma homeobox gene is essential for bmp2b repression in the zebrafish pregastrula". In: *Developmental Biology* 215.2, pp. 190–207. DOI: 10.1006/dbio.1999.9479.

Kozlowski, David J. et al. (1997). "Regional cell movement and tissue patterning in the zebrafish embryo revealed by fate mapping with caged fluorescein". In: 75.5. ISBN: 1208-6002, pp. 551–562. DOI: 10.1139/bcb-75-5-551.

Kucenas, Sarah et al. (2008). "CNS-derived glia ensheath peripheral nerves and mediate motor root development". In: *Nature Neuroscience* 11.2, pp. 143–151. DOI: 10.1038/nn2025.

Kudoh, Tetsuhiro, Miguel L. Concha, et al. (Aug. 1, 2004). "Combinatorial Fgf and Bmp signalling patterns the gastrula ectoderm into prospective neural and epidermal domains". In: *Development* 131.15, pp. 3581–3592. DOI: 10.1242/dev.01227.

Kudoh, Tetsuhiro, Stephen W. Wilson, and Igor B. Dawid (Sept. 15, 2002). "Distinct roles for Fgf, Wnt and retinoic acid in posteriorizing the neural ectoderm". In: *Development* 129.18, pp. 4335–4346. DOI: 10.1242/dev.129.18.4335.

Kushkowski, Elaine E. and Victoria E. Prince (2026). "Zebrafish ventral gastrula fate map reveals neural crest progenitor domain". In: *Developmental Dynamics*, pp. 1–25. DOI: doi:10.1002/dvdy.70174.

Kwon, Hye-Joo et al. (Sept. 23, 2010). "Identification of Early Requirements for Preplacodal Ectoderm and Sensory Organ Development". In: *PLoS Genetics* 6.9. Ed. by Mary C. Mullins, e1001133. DOI: 10.1371/journal.pgen.1001133.

Langdon, Yvette G. and Mary C. Mullins (2011). "Maternal and zygotic control of zebrafish dorsoventral axial patterning". In: *Annual Review of Genetics* 45, pp. 357–377. DOI: 10.1146/annurev-genet-110410-132517.

Lecaudey, Virginie et al. (Aug. 15, 2008). "Dynamic Fgf signaling couples morphogenesis and migration in the zebrafish lateral line primordium". In: *Development* 135.16, pp. 2695–2705. DOI: 10.1242/dev.025981.

Leerberg, Dena, Rachel E. Hopton, and Bruce Draper (2019). "Fibroblast Growth Factor Receptors Function Redundantly During Zebrafish Embryonic Development". In: Artwork Size: 12689829 Bytes, 12689829 Bytes. DOI: 10.25386/GENETICS.8162003.

Levin, Michal et al. (Mar. 31, 2016). "The mid-developmental transition and the evolution of animal body plans". In: *Nature* 531.7596, pp. 637–641. DOI: 10.1038/nature16994.

Lin, Cheng-Yung et al. (Dec. 2013). "Normal Function of Myf5 During Gastrulation Is Required for Pharyngeal Arch Cartilage Development in Zebrafish Embryos". In: *Zebrafish* 10.4, pp. 486–499. DOI: 10.1089/zeb.2013.0903.

Lister, James A. et al. (Feb. 2006). "Zebrafish Foxd3 is required for development of a subset of neural crest derivatives". In: *Developmental Biology* 290.1, pp. 92–104. DOI: 10.1016/j.ydbio.2005.11.014.

Liu, Zairan, Stephanie Woo, and Orion D. Weiner (2018). "Nodal signaling has dual roles in fate specification and directed migration during germ layer segregation in zebrafish". In: *Development (Cambridge)* 145.17, pp. 1–12. DOI: 10.1242/dev.163535.

Logan, Catriona Y. and David R. McClay (1999). "4 - Lineages That Give Rise to Endoderm and Mesoderm in the Sea Urchin Embryo". In: *Cell Lineage and Fate Determination*. Academic Press. DOI: 10.1002/dvg.23096.

Londin, Eric R., Jack Niemiec, and Howard I. Sirotkin (Mar. 2005). "Chordin, FGF signaling, and mesodermal factors cooperate in zebrafish neural induction". In: *Developmental Biology* 279.1, pp. 1–19. DOI: 10.1016/j.ydbio.2004.11.016.

Lu, Fu I., Christine Thisse, and Bernard Thisse (2011). "Identification and mechanism of regulation of the zebrafish dorsal determinant". In: *Proceedings of the National Academy of Sciences of the United States of America* 108.38, pp. 15876–15880. DOI: 10.1073/pnas.1106801108.

Lukoseviciute, Martyna, Sarah Mayes, and Tatjana Sauka-spengler (2021). "Neuromesodermal progenitor origin of trunk neural crest in vivo". In.

Lyons, David A. et al. (Mar. 2005). "erbb3 and erbb2 Are Essential for Schwann Cell Migration and Myelination in Zebrafish". In: *Current Biology* 15.6, pp. 513–524. DOI: 10.1016/j.cub.2005.02.030.

Maier, Esther C. and Tanya T. Whitfield (Dec. 4, 2014). "RA and FGF Signalling Are Required in the Zebrafish Otic Vesicle to Pattern and Maintain Ventral Otic Identities". In: *PLoS Genetics* 10.12. Ed. by Mary C. Mullins, e1004858. DOI: 10.1371/journal.pgen.1004858.

Martik, Megan L. and Marianne E. Bronner (Oct. 2021). "Riding the crest to get a head: neural crest evolution in vertebrates". In: *Nature Reviews Neuroscience* 22.10, pp. 616–626. DOI: 10.1038/s41583-021-00503-2.

Martik, Megan L., Shashank Gandhi, et al. (2019). "Evolution of the new head by gradual acquisition of neural crest regulatory circuits". In: *Nature* 574.7780. ISBN: 0028-0836, pp. 675–678. DOI: 10.1038/s41586-019-1691-4.

Martin, Benjamin L. and Benjamin Steventon (July 2022). "A fishy tail: Insights into the cell and molecular biology of neuromesodermal cells from zebrafish embryos". In: *Developmental Biology* 487, pp. 67–73. DOI: 10.1016/j.ydbio.2022.04.010.

McClintock, James M. et al. (July 1, 2001). "Consequences of Hox gene duplication in the vertebrates: an investigation of the zebrafish Hox paralogue group 1 genes". In: *Development* 128.13, pp. 2471–2484. DOI: 10.1242/dev.128.13.2471.

McLaren, Susannah B. P. and Benjamin J. Steventon (2021). "Anterior expansion and posterior addition to the notochord mechanically coordinate zebrafish embryo axis elongation". In: *Development (Cambridge)* 148.18. DOI: 10.1242/DEV.199459.

Melby, Anna E., Chris Beach, et al. (2000). "Patterning the early zebrafish by the opposing actions of bozozok and vox/vent". In: *Developmental Biology* 224.2, pp. 275–285. DOI: 10.1006/dbio.2000.9780.

Melby, Anna E., Rachel M. Warga, and Charles B. Kimmel (1996). "Specification of cell fates at the dorsal margin of the zebrafish gastrula". In: *Development (Cambridge, England)* 122, pp. 2225–2237. DOI: https://doi.org/10.1242/dev.122.7.2225.

Mohammadi, Moosa et al. (May 9, 1997). "Structures of the Tyrosine Kinase Domain of Fibroblast Growth Factor Receptor in Complex with Inhibitors". In: *Science* 276.5314, pp. 955–960. DOI: 10.1126/science.276.5314.955.

Moody, Sally A. (1987a). “Fates of the Blastomeres of the 16-Cell Stage Xenopus Embryo”. In.

— (1987b). “Fates of the Blastomeres of the 32-Cell-Stage Xenopus Embryo”. In.

Moreno-Ayala, Roberto et al. (Jan. 2021). “Variability of an Early Developmental Cell Population Underlies Stochastic Laterality Defects”. In: *Cell Reports* 34.2, p. 108606. DOI: 10.1016/j.celrep.2020.108606.

Myers, Dina C., Diane S. Sepich, and Lilianna Solnica-Krezel (2002). “Bmp activity gradient regulates convergent extension during zebrafish gastrulation”. In: *Developmental Biology* 243.1, pp. 81–98. DOI: 10.1006/dbio.2001.0523.

Nájera, Guillermo Serrano and Cornelis J. Weijer (Apr. 1, 2023). “The evolution of gastrulation morphologies”. In: *Development* 150.7, dev200885. DOI: 10.1242/dev.200885.

Neaverson, Alexandra and Benjamin Steventon (Dec. 2025). “Coordinating tissue development to build body and brain: Lessons from the gastrula organiser and its derivatives”. In: *Cells & Development* 184, p. 204042. DOI: 10.1016/j.cdev.2025.204042.

Ota, Satoshi et al. (Dec. 2010). “FGF receptor gene expression and its regulation by FGF signaling during early zebrafish development”. In: *genesis* 48.12, pp. 707–716. DOI: 10.1002/dvg.20682.

Pera, Edgar M., Atsushi Ikeda, and Edward Eivers (2003). “Integration of IGF, FGF, and anti-BMP signals via Smad1 phosphorylation in neural induction”. In: *Genes & Development* 17, pp. 3023–3028. DOI: 10.1101/gad.1153603.

Polevoy, Hanna et al. (June 2019). “New roles for Wnt and BMP signaling in neural anteroposterior patterning”. In: *EMBO reports* 20.6, e45842. DOI: 10.15252/embr.201845842.

Prasad, Maneeshi S., Rebekah M. Charney, and Martín I. García-Castro (Jan. 2019). “Specification and formation of the neural crest: Perspectives on lineage segregation”. In: *genesis* 57.1, e23276. DOI: 10.1002/dvg.23276.

Pshennikova, Elena S., Maria B. Tereshina, and Anna S. Voronina (2017). “Expression of vox and vent mRNAs and encoded proteins in zebrafish embryos”. In: *Stem Cell Investigation* 4.7, pp. 60–60. DOI: 10.21037/sci.2017.06.05.

Raible, David W. and Judith S. Eisen (1994). “Restriction of neural crest cell fate in the trunk of the embryonic zebrafish”. In: *Development* 120.3, p. 495. DOI: https://doi.org/10.1242/dev.120.3.495.

Raible, David W. and Gregory J. Kruse (May 29, 2000). “Organization of the lateral line system in embryonic zebrafish”. In: *The Journal of Comparative Neurology* 421.2, pp. 189–198. DOI: 10.1002/(SICI)1096-9861(20000529)421:2<189::AID-CNE5>3.0.CO;2-K.

Raible, David W., Andrew Wood, et al. (1992). “Segregation and early dispersal of neural crest cells in the embryonic zebrafish”. In: *Developmental Dynamics* 195.1. ISBN: 1058-8388, pp. 29–42. DOI: 10.1002/aja.1001950104.

Raible, Florian and Michael Brand (2001). “Tight transcriptional control of the ETS domain factors Erm and Pea3 by Fgf signaling during early zebra®sh development”. In: *Mechanisms of Development*.

Reifers, Frank et al. (1998). "Fgf8 is mutated in zebrafish acerebellar (ace) mutants and is required for maintenance of midbrain-hindbrain boundary development and somitogenesis". In: *Development*.

Rocha, Manuel, Anastasia Beiriger, et al. (Oct. 15, 2020). "From head to tail: regionalization of the neural crest". In: *Development* 147.20, dev193888. DOI: 10.1242/dev.193888.

Rocha, Manuel, Elaine Kushkowski, et al. (Dec. 2021). "Zebrafish Cdx4 regulates neural crest cell specification and migratory behaviors in the posterior body". In: *Developmental Biology* 480, pp. 25–38. DOI: 10.1016/j.ydbio.2021.08.002.

Rocha, Manuel, Noor Singh, et al. (Jan. 2020). "Neural crest development: insights from the zebrafish". In: *Developmental Dynamics* 249.1, pp. 88–111. DOI: 10.1002/dvdy.122.

Roehl, Henry and Christiane Nüsslein-Volhard (Apr. 2001). "Zebrafish pea3 and erm are general targets of FGF8 signaling". In: *Current Biology* 11.7, pp. 503–507. DOI: 10.1016/S0960-9822(01)00143-9.

Rohde, Laurel A. and Carl-Philipp Heisenberg (2007). "Zebrafish Gastrulation: Cell Movements, Signals, and Mechanisms". In: *International Review of Cytology*. Vol. 261. Elsevier, pp. 159–192. DOI: 10.1016/S0074-7696(07)61004-3.

Sambasivan, Ramkumar and Benjamin Steventon (2021). "Neuromesodermal Progenitors: A Basis for Robust Axial Patterning in Development and Evolution". In: *Frontiers in Cell and Developmental Biology* 8 (January), pp. 1–9. DOI: 10.3389/fcell.2020.607516.

Saude, Leonor et al. (2000). "Axis-inducing activities and cell fates of the zebrafish organizer". In: *Development* 127.16, pp. 3407–3417.

Schauer, Alexandra et al. (Apr. 6, 2020). "Zebrafish embryonic explants undergo genetically encoded self-assembly". In: *eLife* 9, e55190. DOI: 10.7554/eLife.55190.

Schier, Alexander F. et al. (1997). "The one-eyed pinhead gene functions in mesoderm and endoderm formation in zebrafish and interacts with no tail". In: *Development* 124.2, pp. 327–342. DOI: 10.1242/dev.124.2.327.

Schilling, Thomas F. and Charles B. Kimmel (1994). "Segment and cell type lineage restrictions during pharyngeal arch development in the zebrafish embryo". In: *Development* 120.3, p. 483. DOI: https://doi.org/10.1242/dev.120.3.483.

Schlosser, Gerhard (2010). "Making Senses". In: *International Review of Cell and Molecular Biology*. Vol. 283. Elsevier, pp. 129–234. DOI: 10.1016/S1937-6448(10)83004-7.

— (Sept. 2014). "Early embryonic specification of vertebrate cranial placodes". In: *WIREs Developmental Biology* 3.5, pp. 349–363. DOI: 10.1002/wdev.142.

Schneider, Stephan et al. (1996). "-Catenin Translocation Into Nuclei Demarcates the Dorsalizing Centers in Frog and Fish Embryos". In: *Mechanisms of Development* 57.2, pp. 191–198. DOI: 10.1016/0925-4773(96)00546-1.

Shah, Gopi et al. (Dec. 17, 2019). "Multi-scale imaging and analysis identify pan-embryo cell dynamics of germlayer formation in zebrafish". In: *Nature Communications* 10.1, p. 5753. DOI: 10.1038/s41467-019-13625-0.

Shimizu, Takashi, Young-Ki Bae, and Masahiko Hibi (Dec. 1, 2006). "Cdx-Hox code controls competence for responding to Fgfs and retinoic acid in zebrafish neural tissue". In: *Development* 133.23, pp. 4709–4719. DOI: 10.1242/dev.02660.

Smith, Natalie L. and David Kimelman (2020). "Establishing The Body Plan". In: *The Zebrafish in Biomedical Research*. Elsevier, pp. 81–88. DOI: 10.1016/B978-0-12-81243 1-4.00007-5.

Solnica-Krezel, Lila and Diane S. Sepich (2012). "Gastrulation: Making and Shaping Germ Layers". In: *Annual Review of Cell and Developmental Biology* 28.1, pp. 687–717. DOI: 10.1146/annurev-cellbio-092910-154043.

Stachel, Scott E., David J. Grunwald, and Paul Z. Myers (1993). "Lithium perturbation and goosecoid expression identify a dorsal specification pathway in the pregastrula zebrafish". In: *Development* 117.4, pp. 1261–1274. DOI: 10.1242/dev.117.4.1261.

Steventon, Ben, Claudio Araya, et al. (Mar. 1, 2009). "Differential requirements of BMP and Wnt signalling during gastrulation and neurulation define two steps in neural crest induction". In: *Development* 136.5, pp. 771–779. DOI: 10.1242/dev.029017.

Steventon, Ben, Fernando Duarte, et al. (2016). "Species-specific contribution of volumetric growth and tissue convergence to posterior body elongation in vertebrates". In: *Development (Cambridge)* 143.10, pp. 1732–1741. DOI: 10.1242/dev.126375.

Stooke-Vaughan, Georgina A. et al. (Feb. 21, 2025). "The physical roles of different posterior tissues in zebrafish axis elongation". In: *Nature Communications* 16.1, p. 1839. DOI: 10 .1038/s41467-025-56334-7.

Streit, Andrea (July 2025). "The neural plate border: multipotent progenitors or cells of mixed identity?" In: *Developmental Biology* 523, pp. 51–58. DOI: 10.1016/j.ydbio.202 5.04.002.

Stundl, Jan and Marianne E. Bronner (Feb. 2025). "Tempting fate: Neural crest induction along the body axis". In: *Cells & Development*, p. 204000. DOI: 10.1016/j.cdev.2025 .204000.

Sulston, J.E. et al. (Nov. 1983). "The embryonic cell lineage of the nematode Caenorhabditis elegans". In: *Developmental Biology* 100.1, pp. 64–119. DOI: 10.1016/0012-1606(83)90 201-4.

Tam, P. P. L. and R. S. P. Beddington (Jan. 1, 1987). "The formation of mesodermal tissues in the mouse embryo during gastrulation and early organogenesis". In: *Development* 99.1, pp. 109–126. DOI: 10.1242/dev.99.1.109.

Thawani, Ankita and Andrew K. Groves (Dec. 7, 2020). "Building the Border: Development of the Chordate Neural Plate Border Region and Its Derivatives". In: *Frontiers in Physiology* 11, p. 608880. DOI: 10.3389/fphys.2020.608880.

Thiery, Alexandre P. et al. (Aug. 2, 2023). "scRNA-sequencing in chick suggests a probabilistic model for cell fate allocation at the neural plate border". In: *eLife* 12, e82717. DOI: 10.7554/eLife.82717.

Thisse, Bernard and Christine Thisse (2015). "Formation of the vertebrate embryo: Moving beyond the Spemann organizer". In: 42. ISBN: 1084-9521, pp. 94–102. DOI: 10.1016/j .semcdb.2015.05.007.

Tsai, Tony Yu-Chen and Diana Pinheiro (Sept. 2025). "Coping with uncertainty: Challenges for robust pattern formation in dynamical tissues". In: *Seminars in Cell & Developmental Biology* 173, p. 103629. DOI: 10.1016/j.semcdb.2025.103629.

Tuazon, Francesca B. and Mary C. Mullins (2015). "Temporally coordinated signals progressively pattern the anteroposterior and dorsoventral body axes". In: 42. ISBN: 1084-9521, pp. 118–133. DOI: 10.1016/j.semcdb.2015.06.003.

Vega-Lopez, Guillermo A. et al. (Dec. 2018). "Neurocristopathies: New insights 150 years after the neural crest discovery". In: *Developmental Biology* 444, S110–S143. DOI: 10.1016/j.ydbio.2018.05.013.

Venkataraman, Vishruth et al. (Feb. 11, 2025). *Development of the zebrafish anterior lateral line system is influenced by underlying cranial neural crest*. DOI: 10.1016/j.ydbio.2025.05.025.

Vogt, Walther (1925). "Gestaltungsanalyse am Amphibienkeim mit örtlicher Vitalfiirbung. Vorwort über Wege and Ziele. I. Teil. Methodik und Wirkungsweise der ortlichen Vitalfârbung mit Agar als Fârbträger". In: *W. Roux' Archiv f. Entwicklungsmechanik* 106, pp. 542–610. DOI: https://doi.org/10.1007/BF02079545.

— (1929). "Gestaltungsanalyse am Amphibienkeim mit Örtlicher Vitalfärbung.II. Teil. Gastrulation und Mesodermbildung bei Urodelen und Anuren." In: *W. Roux' Archiv f. Entwicklungsmechanik* 120, pp. 384–706. DOI: https://doi.org/10.1007/BF02109667.

Wan, Yinan et al. (Mar. 12, 2026). "Whole-embryo spatial transcriptomics at subcellular resolution from gastrulation to organogenesis". In: *Science* 391.6790, eadt3439. DOI: 10.1126/science.adt3439.

Wang, Wen Der et al. (2011). "Tfap2a and Foxd3 regulate early steps in the development of the neural crest progenitor population". In: *Developmental Biology* 360.1, pp. 173–185. DOI: 10.1016/j.ydbio.2011.09.019.

Ward, Andrea B., Rachel M. Warga, and Victoria E. Prince (June 2007). "Origin of the zebrafish endocrine and exocrine pancreas". In: *Developmental Dynamics* 236.6, pp. 1558–1569. DOI: 10.1002/dvdy.21168.

Warga, Rachel M., Donald A. Kane, and Robert K. Ho (May 2009). "Fate Mapping Embryonic Blood in Zebrafish: Multi- and Unipotential Lineages Are Segregated at Gastrulation". In: *Developmental Cell* 16.5, pp. 744–755. DOI: 10.1016/j.devcel.2009.04.007.

Warga, Rachel M. and Charles B. Kimmel (1990). "Cell movements during epiboly and gastrulation in zebrafish". In: *Development* 108.4, p. 569.

Warga, Rachel M. and Christiane Nüsslein-Volhard (Feb. 15, 1999). "Origin and development of the zebrafish endoderm". In: *Development* 126.4, pp. 827–838. DOI: 10.1242/dev.126.4.827.

Weston, James A. and Jean Paul Thiery (May 2015). "Pentimento: Neural Crest and the origin of mesectoderm". In: *Developmental Biology* 401.1, pp. 37–61. DOI: 10.1016/j.ydbio.2014.12.035.

Weston, James A., Hisahiro Yoshida, et al. (Jan. 2004). "Neural crest and the origin of ectomesenchyme: Neural fold heterogeneity suggests an alternative hypothesis". In: *Developmental Dynamics* 229.1, pp. 118–130. DOI: 10.1002/dvdy.10478.

Williams, Margot L. K. and Lilianna Solnica-Krezel (2020). *Cellular and molecular mechanisms of convergence and extension in zebrafish*. 1st ed. Vol. 136. Publication Title: Current Topics in Developmental Biology. Elsevier Inc. 377–407. DOI: 10.1016/bs.ctdb.2019.08.001.

Williams, Ruth M et al. (Jan. 28, 2022). "Single-cell atlas of early chick development reveals gradual segregation of neural crest lineage from the neural plate border during neurulation". In: *eLife* 11, e74464. DOI: 10.7554/eLife.74464.

Woo, Katherine and Scott E. Fraser (1995). "Order and coherence in the fate map of the zebrafish nervous system". In: *Development* 121.8, p. 2595. DOI: https://doi.org/10.1242/dev.121.8.2595.

Wymeersch, Filip J. et al. (2016). "Position-dependent plasticity of distinct progenitor types in the primitive streak". In: *eLife* 5 (JANUARY2016), pp. 1–28. DOI: 10.7554/eLife.10042.

Xia, Chenglong et al. (Sept. 24, 2019). "Spatial transcriptome profiling by MERFISH reveals subcellular RNA compartmentalization and cell cycle-dependent gene expression". In: *Proceedings of the National Academy of Sciences* 116.39, pp. 19490–19499. DOI: 10.1073/pnas.1912459116.

Yamanaka, Yojiro et al. (1998). "A novel homeobox gene, dharma, can induce the organizer in a non-cell- autonomous manner". In: *Genes and Development* 12.15. ISBN: 8168793889, pp. 2345–2353. DOI: 10.1101/gad.12.15.2345.

Yan, Lu et al. (2018). "Maternal Huluwa dictates the embryonic body axis through b-catenin in vertebrates". In: *Science* 362.6417. DOI: 10.1126/science.aat1045.

Yu, Hung-Hsiang and Cecilia B. Moens (Apr. 2005). "Semaphorin signaling guides cranial neural crest cell migration in zebrafish". In: *Developmental Biology* 280.2, pp. 373–385. DOI: 10.1016/j.ydbio.2005.01.029.

Yu, Shuizi Rachel et al. (Sept. 2009). "Fgf8 morphogen gradient forms by a source-sink mechanism with freely diffusing molecules". In: *Nature* 461.7263, pp. 533–536. DOI: 10.1038/nature08391.

Zhang, Weiting et al. (Feb. 7, 2022). "Fgf8 dynamics and critical slowing down may account for the temperature independence of somitogenesis". In: *Communications Biology* 5.1, p. 113. DOI: 10.1038/s42003-022-03053-0.

Zinski, Joseph, Benjamin Tajer, and Mary C. Mullins (June 2018). "TGF- Family Signaling in Early Vertebrate Development". In: *Cold Spring Harbor Perspectives in Biology* 10.6, a033274. DOI: 10.1101/cshperspect.a033274.